Agreement No. CE 43/2010(HY)

Central Kowloon Route
中九龍幹線

Cogent and Convincing Materials for Temporary Reclamation at Kowloon Bay

February 2013

中九龍幹線 Central Kowloon Route

路政署 Highways Department

Highways Department

Agreement No. CE 43/2010 (HY)
Central Kowloon Route – Design and Construction

Cogent and Convincing Materials for Temporary Reclamation in Kowloon Bay

217722-REP-044-02

Revised Final | February 2013

Arup-Mott MacDonald Joint Venture
Level 5 Festival Walk
80 Tat Chee Avenue
Kowloon Tong
Kowloon
Hong Kong
www.arup.com

Job number 217722

Arup-Mott MacDonald Joint Venture

Contents

Appendices

1 INTRODUCTION

Background

1.1 Central Kowloon Route (CKR) is a 4.7 km long dual 3-lane trunk road across central Kowloon linking West Kowloon at Yau Ma Tei Interchange with the Kai Tak Development and road network at Kowloon Bay in East Kowloon. **Figure 1-1** shows the layout plan and longitudinal section of CKR.

1.2 In the investigation and preliminary design stage in 2007 to 2009, we reviewed over 40 alignment options in the previous CKR studies. The present alignment was selected after comparing the impacts of the various options on buildings/community facilities, environment, land and transport and making reference to public comments collected in the public engagement exercise. The selected alignment was generally supported by Legislative Council, Yau Tsim Mong, Kowloon City and Kwun Tong District Councils.

Underwater Tunnel in Kowloon Bay

1.3 A 370 m long section of the CKR tunnel between the Kowloon City Ferry Pier to the Kai Tak Development Area will pass through the seabed of Kowloon Bay. Due to various site constraints, it will have to be constructed using the temporary reclamation method.

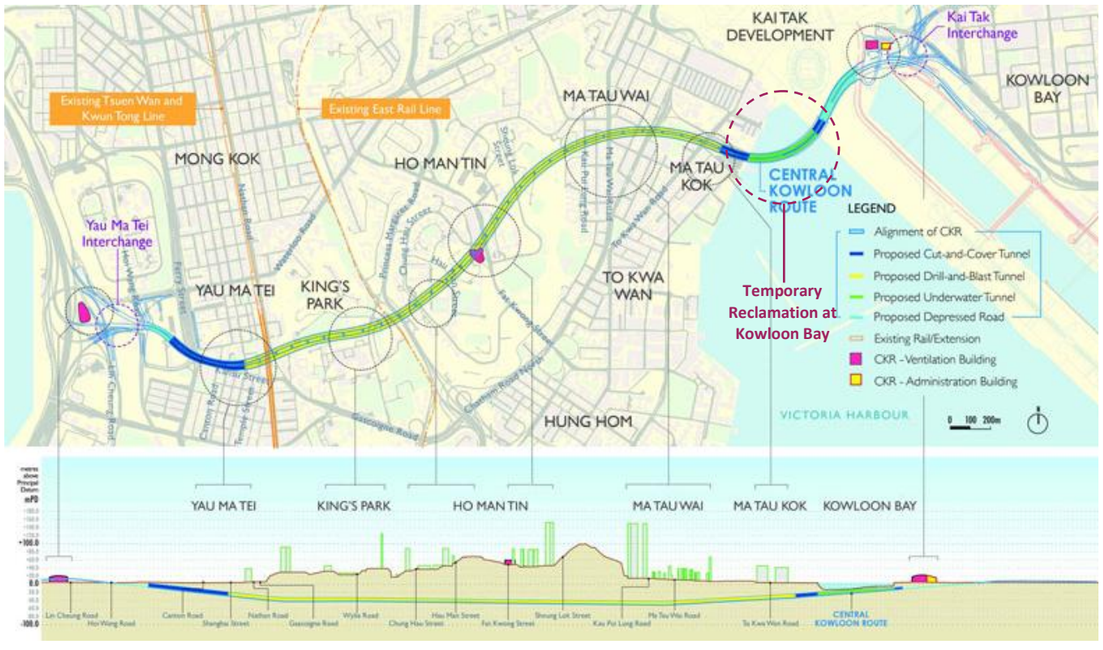

Figure 1-1 – Alignment of CKR

Protection of the Harbour Ordinance (PHO)

Presumption against Reclamation

1.4 The PHO originally resulted from a private member's bill proposed in 1996 by the Society for Protection of the Harbour. The bill was first enacted as the original Ordinance in June 1997 and was then modified in the course of the legislative process. The PHO provides protection and preservation of the harbour by establishing a presumption against reclamation. In December 1999, the Ordinance was further amended to its present form by expanding its scope to cover the whole of Victoria Harbour.

1.5 Section 3 of the Ordinance states:

(1) The harbour is to be protected and preserved as a special public asset and a natural heritage of Hong Kong people and for that purpose there shall be a presumption against reclamation in the harbour. [Section 3(1)]

(2) All public officers and public bodies shall have regard to the principle stated in subsection (1) for guidance in the exercise of any powers vested in them. [Section 3(2)]

1.6 The PHO specifically defines the term "reclamation" as "any work carried out or intended to be carried out for the purpose of forming land from the sea-bed or foreshore". The definition of "reclamation" in the PHO is specific to the formation of land, implying works that exceed the sea level. It is considered that even smallscale reclamation required for the construction of piers, landing steps, etc. should also comply with the PHO.

Judgment of Court of Final Appeal (CFA) in Town Planning Board v Society for Protection of the Harbour Ltd. (on 9 January 2004)

1.7 The Town Planning Board made decisions on the Draft Wan Chai North Outline Zoning Plan (OZP) (No. S/H25/1), in December 2002 and February 2003, that included proposals for reclamation within Victoria Harbour. This was challenged in the legal system by the Society for Protection of the Harbour on the grounds that the Town Planning Board made decisions that were unlawful and/or unreasonable and irrational.

1.8 The appeal was dismissed in the judgment of the CFA handed down on 9 January 2004. The CFA held that –

(a) in order to implement the strong and vigorous statutory principle of protection and preservation, the presumption against reclamation must be interpreted in such a way that it can only be rebutted by establishing an overriding public need for reclamation. This can conveniently be referred to as "the overriding public need test";

(b) where there is a reasonable alternative to reclamation, an overriding need for reclamation would not be made out. There would be no such overriding need since the need could be met by the alternative means; and

(c) the extent of the proposed reclamation should not go beyond the minimum of that which is required by the overriding need.

1.9 Public needs would be community needs. They would include the economic, environmental and social needs of the community. A need should only be regarded as overriding if it is a compelling and present need. The need has to be compelling so that it has the requisite force to prevail over the strong public need for protection and preservation. The need has to be a present need in the sense that taking into account the time scale of planning exercises, the need would arise within a definite and reasonable timeframe. If the need would not arise over such a timeframe, it would not have the strength to displace the presumption. A compelling and present need goes far beyond something which is "nice to have", desirable, preferable or beneficial. But on the other hand it is not a last resort or something that the public "cannot do without". A present need takes into account the timescale of planning exercises, and the need would arise within a definite and reasonable time frame.

1.10 The judgment further states that where there is a reasonable alternative to reclamation, an overriding need for reclamation would not be made. All circumstances should be considered including the economic, environmental and social implications of each alternative. The cost as well as the time and delay involved would be relevant. The extent of the proposed reclamation should not go beyond the minimum of that which is required by the overriding need. Each area proposed to be reclaimed must be justified.

1.11 In order to enable a public officer or body to be satisfied that the overriding public need test has been met, the materials in the case in question must be cogent and convincing.

Court of First Instance Judgment in Society for Protection of the Harbour v Secretary for Justice (on 20 March 2008)

1.12 Government proposed to construct the Central-Wan Chai Bypass (CWB) along the north shore of Hong Kong Island to relieve the traffic congestion along the existing east-west corridor. The cut-and-cover tunnel of CWB in the ex-Public Cargo Working Area in Wan Chai and the Causeway Bay Typhoon Shelter would be constructed using temporary reclamation. The temporary reclamation works were expected to last about six years. Upon completion of construction, the temporary reclamation would be removed and the sea-bed would be reinstated. Government considered that the temporary reclamation would not be subject to the requirements of the PHO.

1.13 The Society for Protection of the Harbour applied to the High Court on the grounds that the PHO did not differentiate in specific terms between reclamation that is intended to result in permanent land formation and temporary reclamation. The Society for Protection of the Harbour sought a declaration that even reclamation works that are intended to be transitory, or even intended to avoid the very need for permanent reclamation, are nevertheless subject to the presumption against reclamation and may not lawfully be carried out unless it can be demonstrated that they are necessary by meeting the "overriding public need test".

1.14 The Court of First Instance ruled in favour of the Society and declared that the PHO and the presumption against reclamation do apply to the proposed temporary reclamation for CWB.

Report Structure

1.15 This Report includes the CCM for demonstrating that the proposed temporary reclamation in Kowloon Bay for constructing the underwater tunnel of CKR complies with the requirements of the PHO. It has been prepared in accordance with Housing, Planning and Lands Bureau Technical Circular No. 1/04 issued by the then Housing, Planning and Lands Bureau on 19 August 2004 to provide guidance for public officers and public bodies in considering and approving reclamation proposals including information on the public consultation process for such proposals.

1.16 The contents of the subsequent chapters of this Report are as follows –

(a) **Chapter 2** presents information and assessment supporting the overriding public need for the CKR project;

(b) **Chapter 3** shows that there are no reasonable alternatives to the proposed temporary reclamation in Kowloon Bay;

(c) **Chapter 4** shows that the extent of the proposed temporary reclamation will be the minimum;

(d) **Chapter 5** describes the public consultation conducted on the temporary reclamation and summarizes the feedback from the public; and

(e) **Chapter 6** provides the conclusion on the temporary reclamation and describes the recommended scheme.

2 OVERRIDING PUBLIC NEED

Introduction

2.1 The guidelines provided in HPLB TC No. 1/04 have been referred to with regard to the approach taken for assessing the overriding public need for the project. The Technical Circular states that the first step is to establish if there is a compelling and present public need for the project. The term "public needs" is defined as economic, environmental and social needs of the community. It is taken that community refers to the greater need of the public rather than meeting the special needs or interests of a few.

2.2 The term "compelling" is defined in HPLB TC 1/04 as having the requisite force to prevail over the strong public need for protection and preservation of the harbour. This is required to be supported by cogent and convincing materials (such as findings of studies, forecasts, costs and benefit analysis, etc.) that support the overriding need for reclamation aspects of the project.

2.3 The term "present need" is defined as time scale requirements and demonstrating that the need would arise within a definite and reasonable time frame. To satisfy this, there must be a concrete programme of implementation and firm commitment from the concerned government departments, with endorsement by relevant authorities, as applicable.

2.4 The following describes the compelling and present public need for the CKR and the benefit it will provide to the community of Hong Kong.

Traffic Justifications

(A) Overview

2.5 The traffic on existing major east-west link in Kowloon, including Lung Cheung Road, Boundary Street, Prince Edward Road West, Argyle Street, Waterloo Road, Gascoigne Road Flyover and Chatham Road North is nearing saturation and traffic congestion frequently occurs. The Government has implemented local traffic management and improvement measures. However, since the areas on both sides of the existing east-west corridors are highly developed, there is little or no room for improvement. As a result, these measures can only alleviate local traffic problems in the short term.

2.6 CKR is a proposed dual 3-lane trunk road across central Kowloon linking the West Kowloon in the west and the proposed Kai Tak Development in the east. Its western end at West Kowloon would connect to Yau Ma Tei Interchange and via the interchange traffic could access to Western Harbour Crossing, Tsim Sha Tsui, West Kowloon Cultural District, West Kowloon Highway, Route 8, and Route 3 respectively. Its eastern end at Kai Tak area, would connect to Kowloon Bay, Kowloon East, Kwun Tong Bypass, Tseung Kwan O Tunnel, T2, and Tseung Kwan O Lam Tin Tunnel respectively. CKR together with T2 and Tseung Kwan O Lam Tin Tunnel would form a strategic highway link, namely Route 6, connecting West Kowloon and TKO.

2.7 With the substantial developments in West Kowloon Cultural District and Kai Tak Development at the west and east ends of CKR respectively, the completion of these developments in stages, their traffic impacts to the strategic east-west link roads and the critical junctions within Kowloon area would be significant.

2.8 The need for a direct traffic route linking West and East Kowloon was identified two decades ago under numerous studies to cater for the cross-Kowloon traffic demand and to relieve the congestion on the existing traffic routes in central Kowloon. In the intervening years, traffic volume has grown and cross-Kowloon traffic demands have increased as a result of developments in West Kowloon, Kowloon Bay and Tseung Kwan O. The need to provide a relieving west-east route has become a priority to road users and the public at large and the provision of CKR should meet the need. In addition, the proposed developments at Kai Tak, Anderson Road and the West Kowloon Cultural District as shown in **Figure 2-1** will no doubt further increase the demand for such a link.

Figure 2-1 – Proposed Development in Kowloon East and West

2.9 The road traffic between West and East Kowloon is currently served by Lung Cheung Road, Boundary Street, Prince Edward Road, Argyle Street, Waterloo Road and Chatham Road North. Apart from Lung Cheung Road and Gascoigne Road Flyover, these existing east-west road links have capacities constrained by frequent frontage access and signal controlled junctions, which are constraining the traffic flows. Based on the comprehensive traffic surveys conducted in 2011, a baseline review on the performance of existing junctions and road as well as the existing traffic issues have been summarised. It is also noted in the 2011 Annual Traffic Census that over 60% of vehicular traffic travelling between east and west of Kowloon (crossing the Screenline A-A in **Figure 2-2**) are commercial vehicles (i.e. taxi, public light buses, goods vehicles, coaches and buses).

Figure 2-2 – Level of Services of Existing Routes in Kowloon

2.10 It was determined that, the existing major east-west running road corridors (Lung Cheung Road, Prince Edward Road West and Boundary Street) in Kowloon have long been plagued by the problem of inadequate traffic capacities. It can be partly attributed to the increase in property developments on both the western part (e.g. West Kowloon Reclamation, Lantau) and the eastern part (e.g. Tseung Kwan O) of the Kowloon Peninsula and the New Territories in recent years, without an upgrade in west-east traffic capacity of a comparable scale. Some examples of traffic congestion are shown in **Figure 2-3**.

Figure 2-3 – Existing Traffic Conditions at Central and West Kowloon

2.11 Many of these road corridors have already reached their traffic-carrying capacities during peak travel hours. For example, the traffic flows of Prince Edward Road West and Boundary Street during peak hours in a single direction can reach volume-to-capacity ratios of 0.8 and 1.1 respectively, indicating that they are already operating close to or above capacity. The volume-to-capacity ratio between West Kowloon and East Kowloon, for year 2011, is summarised in **Table 2-1** below.

Table 2-1 Performance of Critical East-West Kowloon Roads in 2011

Road	Direction	V/C Ratio 2011 (Existing)	
		AM	PM
Lung Cheung Rd (from Lion Rock Tunnel Rd to Chuk Yuen Rd)	EB	0.9	0.8
	WB	0.9	0.9
	WB (slip road from Chuk Yuen Road)	0.9	0.6
Boundary St (from Tai Hang Tung Rd to Embankment Rd)	EB	**1.0**	**1.1**
Prince Edward Rd West (from Embankment Rd to Kadoorie Ave)	WB	0.8	0.7
Argyle St & FO (from Gullane Rd to Tin Kwong Rd))	EB	0.8	0.9
	WB	0.8	0.8
Waterloo Road (from Pitt Street to Dundas Street)	NB	0.9	1.0
	SB	0.9	0.7
Gascoigne Road Flyover (Eastern side of Nathan Road)	EB	0.8	**>1.3**
	WB	**1.2**	**1.1**

Road	Direction	V/C Ratio 2011 (Existing)	
		AM	**PM**
Chatham Road North (from Wuhu St to Ping Chi Street)	EB	**1.1**	**1.1**
	WB	0.8	1.2
	WB (farside free flow lane)	**1.3**	0.4
East Kowloon Corridor (from Ma Tau Kok Rd to Chatham Rd North)	EB	1.0	**1.1**
	WB	0.8	0.6

Note:
Volume to capacity (v/c) ratio is an indicator which reflects the performance of a road. A v/c ratio equal to or less than 1.0 means that a road has sufficient capacity to cope with the volume of vehicular traffic under consideration and the resultant traffic will flow smoothly. A v/c ratio above 1.0 indicates the onset of congestion; that above 1.2 indicates more serious congestion with traffic speeds deteriorating progressively with further increase in traffic.

2.12 CKR will provide an alternative route for the traffic to bypass the congested road network thus significantly reducing the journey time. For example, it is estimated that during the peak hours in 2021, the journey time between west and east Kowloon via CKR would take around only 5 minutes, compared to 30-35 minutes without CKR. CKR will also substantially reduce the traffic volumes around major east-west corridors and relieving their traffic congestion. The improved traffic conditions will also benefit the adjacent areas including Wong Tai Sin, Ho Man Tin and Kowloon City.

2.13 CKR will also connect with the high speed roadways on both sides of Kowloon to form the key component of a strategic road network. In this regard, the Kai Tak Interchange on the eastern side will connect CKR with the road network in Kowloon Bay, Kwun Tong and Kai Tak Development thus enhancing the convenience of travelling between these areas and West Kowloon and providing the transport infrastructure for supporting the Energizing Kowloon East initiative introduced by the Government. CKR together with the proposed Trunk Road T2 at Kai Tak Development and Tseung Kwan O – Lam Tin Tunnel will form Route 6 with a total length of 12.5 km that will directly link up West Kowloon and Tseung Kwan O.

2.14 The Yau Ma Tei Interchange located on the western side will provide comprehensive slip roads connecting West Kowloon Highway and Lin Cheung Road. Vehicles can use West Kowloon Highway to access Hong Kong Island in the south, Kwai Tsing Container Terminal and Hong Kong International Airport in the west as well as Northwest New Territories in the north. Vehicles can also access the West Kowloon Development Area, West Kowloon Terminus of Guangzhou-Shenzhen-Hong Kong Express Rail Link (XRL) and West Kowloon Cultural District through Lin Cheung Road.

2.15 The following summarises traffic issues within East, West and Central Kowloon.

(B) Traffic Situation in West Kowloon

2.16 The total traffic flows observed at the junctions (e.g. Austin Road West / Austin Road / Canton Road, Lin Cheung Road / Jordan Road and Canton Road / Wui Cheung Road) within West Kowloon area are generally more critical during the weekday peak periods due to the traffic to/from newly residential and office developments. At the more critical junctions, some of the queues are mainly extended from the downstream junction, e.g. the traffic queue at Jordan Road eastbound at Jordan Road/ Ferry Street/ Canton Road junction has extended to Lin Cheung Road/ Jordan Road junction during Saturday Noon peak period.

2.17 From the result of road link capacity assessment at Gascoigne Road, the long traffic queue at both Gascoigne Road Flyover eastbound and westbound has also affected the actual demand of vehicles that can pass through that section of road. From the observation, the maximum queue at Gascoigne Road Flyover eastbound and westbound would be up to Waterloo Road and Fat Kwong Street, respectively.

(C) Traffic Situation in Central Kowloon

2.18 The road network in the Central part of Kowloon Peninsula is characterised by essentially a grid format made up of east-west and north-south running roads. Of particular concern in the current study are the roads higher in the road hierarchy system, i.e. trunk roads, primary distributors and district distributors, which have the important role of providing high throughput capacity for cross-district traffic.

2.19 While some of the above roads are classified as primary distributors with the planning intention of serving mostly cross-district traffic, in reality a significant portion of traffic on these roads is local district traffic.

2.20 Most of the junctions within the Central Kowloon district are generally more critical during the weekday peak periods (e.g. J/O Austin Road / Chatham Road South / Cheong Wan Road, J/O Argyle Street / Nathan Road, J/O Argyle Street / Waterloo Road / Princess Margaret Road, J/O Argyle Street / Sai Yee Street and J/O Chatham Road North / Wuhu Street). The queue length results also indicated that most of the critical east-west road arms such as Prince Edward Road West and Boundary Street would have longer queue length than weekend peak periods.

2.21 Long traffic queue was also observed at the J/O Argyle Street/ Sai Yee Street and the J/O Argyle Street/ Yim Po Fong Street. Based on the observation, traffic queue at Sai Yee Street northbound at the J/O Sai Yee Street/ Mong Kok Road would affect the actual demand of vehicles that can pass through the junction at Sai Yee Street northbound at the J/O Argyle Street/ Sai Yee Street during weekday and weekend periods. With the effect of the traffic queue, the calculated R.C. at this junction during weekend period is higher than weekday period. With similar situation at the J/O Argyle Street/ Yim Po Fong Street, the traffic queue at Argyle Street westbound at the J/O Argyle Street/ Sai Yee Street would also affect the actual demand of vehicles that can pass through the junction at Argyle Street westbound at the J/O Argyle Street/ Yim Po Fong Street. The short distance of carriageway of Argyle Street between Sai Yee Street and Yim Po Fong Street is also one of the constraints in the road network that exacerbate the issue with traffic queue.

2.22 The results of journey time survey have also indicated that the average speed along the critical roads (i.e. Boundary Street, Prince Edward Road West, and Jordan Road) at Central Kowloon area were travelling slower than other critical road links during both AM and PM peak periods. This is mainly affected by junction stoppages (e.g. J/O Ferry Street / Waterloo Road and J/O Argyle Street / Tong Mi Road) and frontage accesses.

(D) Traffic Situation in East Kowloon

2.23 The road network in East Kowloon is characterised by a series of major road corridors closely spaced apart running in a northwest-southeast orientation (Kai Tak Tunnel-Kai Fuk Road corridor, Kwun Tong Bypass, Prince Edward Road East-Kwun Tong Road corridor, and Clear Water Bay Road) intersected more-or-less perpendicularly by three strategic links, namely Lung Cheung Road, Tseung Kwan O Tunnel and Eastern Harbour Crossing, and a number of roads lower in the road hierarchy. Of particular relevance to the current study of Trunk Road T2 are the aforementioned northwest-southeast

major road corridors, as T2 is running in the same orientation and could possibly offer traffic relief impacts on these roads. Separately, roads and junctions within Kowloon Bay will be of relevance to the study of roads and development at the Kai Tak South Apron as these would be the immediate connecting links between the South Apron and the areas outside Kai Tak.

2.24 The junctions within the East Kowloon area are mainly critical during the weekday peak hour periods due to the traffic from the industrial and office developments. However, as indicated in the junction capacity assessment results, these critical junctions would still operate at an acceptable level of operation during weekday peak periods except the J/O of Wai Yip Street / Wai Fat Road are likely to perform with overloaded reserve capacity due to the heavy traffic flow from Kwun Tong Bypass access through this junction toward Kwun Tong and Lam Tin area during weekday peak periods.

(E) Network Reliability

2.25 There was a major incident of scaffolding collapse at Prince Edward Road East shown in **Figure 2-4**, which is one of the most important West and East corridors, on 9 May 2005 that led to severe traffic congestion in the whole Kowloon area.

Figure 2-4 – Scaffolding Collapse at Prince Edward Road East on 9 May 2005

2.26 The proposed CKR can serve as an emergency corridor for eastbound and westbound traffic in Central Kowloon. As discussed in the "Report of the Task Force on Emergency Transport Coordination" in June 2005, the eastbound and westbound traffic in Central Kowloon was severely affected due to inclement weather condition. The task force also commented that the north-south bound traffic in Kowloon is more developed yet the east-west bound roads are inadequate. They considered that there is a need to increase the capacity for east-west bound traffic.

(F) Traffic Management Schemes

2.27 The Government has implemented local traffic management and improvement measures. However, since the areas on both sides of the existing east-west corridors are highly developed, there is little or no room for improvement. As a result, these measures can only alleviate local traffic problems in the short term. To effectively resolve the east-west traffic problems in Central Kowloon, CKR should be commissioned as soon as possible to provide an alternative route to bypass congested road sections and increase the capacity for east-west movement.

(G) Traffic Forecasts

2.28 Traffic studies have long predicted the consequences of continued traffic growth along the major east-west corridors without the implementation of CKR. The traffic forecast for year 2021 have also confirmed the need for the trunk road after taking into account the latest land use planning assumptions and population projections, to ensure that traffic forecasts are in line with the current strategic and local planning intentions. The Third Comprehensive Transport Study (CTS 3), Base District Transport Model (BDTM) as well as Territorial Population and Employment Data Matrices (TPEDM) have been referenced to examine the traffic conditions at the strategic and local levels, for the cases with and without the implementation of CKR.

2.29 The future traffic condition, as shown in **Figure 2-5**, is expected to be worsening in 2021 without CKR in place. **Table 2-2** below summarises the road link performance for the scenario with and without CKR in 2021.

Figure 2-5 – Year 2021 Traffic Conditions in East and West Kowloon

Table 2-2 Performance of Critical East-West Kowloon Roads in 2021

Road	Direction	V/C Ratio			
		2021 Without CKR		2021 With CKR	
		AM	PM	AM	PM
Lung Cheung Rd (from Lion Rock Tunnel Rd to Chuk Yuen Rd)	EB	**1.2**	**1.1**	0.9	1.0
	WB	1.0	1.0	0.9	0.8
	WB (slip road from Chuk Yuen Road)	**1.1**	0.6	0.9	0.5

Road	Direction	V/C Ratio			
		2021 Without CKR		2021 With CKR	
		AM	PM	AM	PM
Boundary St (from Tai Hang Tung Rd to Embankment Rd)	EB	**1.2**	**1.3**	0.9	0.9
Prince Edward Rd West (from Embankment Rd to Kadoorie Ave)	WB	**1.1**	0.8	0.9	0.7
Argyle St & FO (from Gullane Rd to Tin Kwong Rd))	EB	**1.1**	1.0	0.7	0.7
	WB	**1.1**	0.9	0.7	0.8
Waterloo Road (from Pitt Street to Dundas Street)	NB	1.0	0.9	1.0	0.9
	SB	**1.2**	0.8	**1.1**	0.7
Gascoigne Road Flyover (Eastern side of Nathan Road)	EB	**1.3**	**>1.3**	**1.1**	**1.2**
	WB	**1.3**	**1.3**	**1.1**	**1.2**
Chatham Road North (from Wuhu St to Ping Chi Street)	EB	**1.3**	**1.2**	**1.1**	1.0
	WB	1.0	**1.2**	1.0	0.7
	WB (farside free flow lane)	**1.3**	0.9	**1.1**	**1.1**
East Kowloon Corridor (from Ma Tau Kok Rd to Chatham Rd North)	EB	**1.3**	**1.3**	**1.1**	**1.1**
	WB	0.7	0.7	**1.1**	1.0
Central Kowloon Route	EB	-	-	0.6	0.7
	WB	-	-	0.7	0.6

Note:
Volume to capacity (v/c) ratio is an indicator which reflects the performance of a road. A v/c ratio equal to or less than 1.0 means that a road has sufficient capacity to cope with the volume of vehicular traffic under consideration and the resultant traffic will flow smoothly. A v/c ratio above 1.0 indicates the onset of congestion; that above 1.2 indicates more serious congestion with traffic speeds deteriorating progressively with further increase in traffic.

2.30 In general, it is expected that the level of service of those existing main routes is “F”, i.e. “Crawling Travel Speed” if there is no CKR in 2021 whereas the level of service will be improved to “D”, ie. “Reduced Travel Speed” as shown in **Figure 2-2**.

2.31 For Reserve / Capacity ratio (R/C) at major junctions, **Table 2-3** below and **Figure 2-6** summarises the performance for the existing, with and without CKR scenario in 2021.

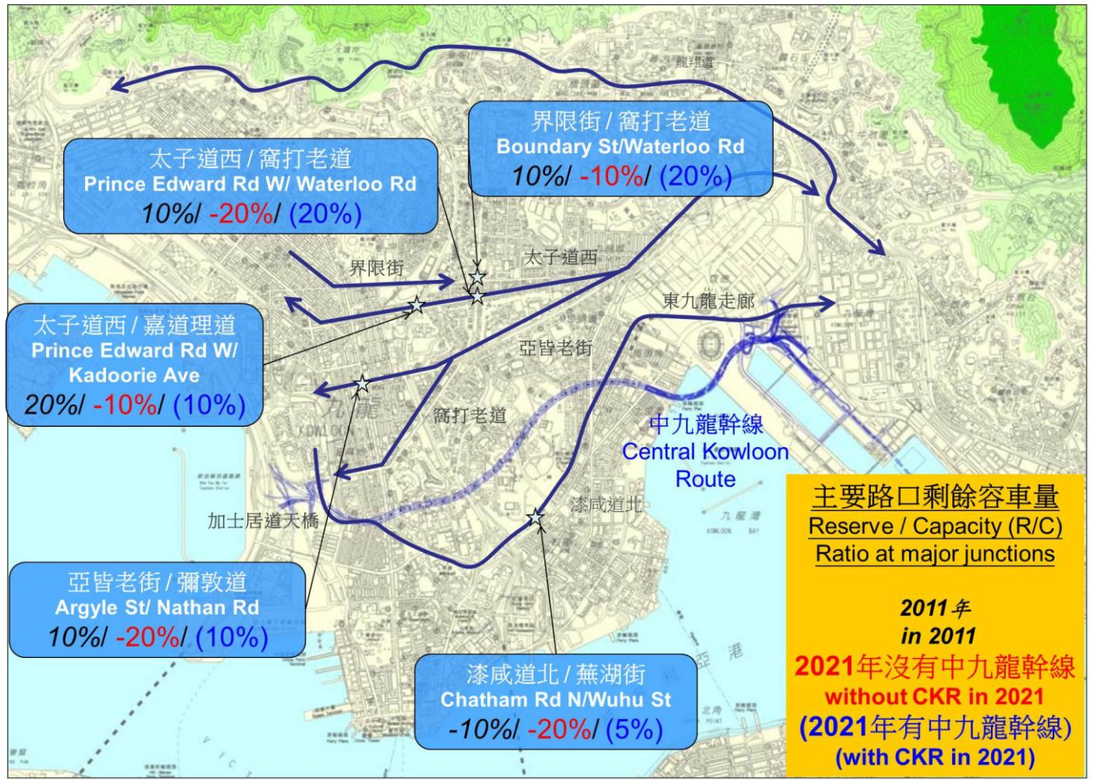

Figure 2-6 – Reserve / Capacity (R/C) Ratio at Major Junctions in Kowloon

Table 2-3 Performance of Critical Junctions

Road Junction	At 2011	At 2021 without CKR	At 2021 with CKR
Boundary Street / Waterloo Rd	10%	-10%	20%
Prince Edward Road West / Waterloo Road	10%	-20%	20%
Prince Edward Road West / Kadoorie Ave.	20%	-10%	10%
Argle Street / Nathan Road	10%	-20%	10%
Chatham Road North / Wuhu Street	-10%	-20%	5%

2.32 It is observed that all R/C ratio become negative values if there is without CKR at 2021. It means the junctions do not have reserve capacity that implies the situation of traffic congestion is worsen.

(H) Conclusions

2.33 The existing east-west corridors serving Kowloon Central, East and West are operating beyond their capacity, as can be observed on site. Previous and recent strategic transport studies have predicted further increase in traffic demand along the east-west corridor, and confirmed the need for an additional east-west trunk road to avoid more extensive and frequent traffic congestion, and even gridlock, on the road network.

2.34 The traffic forecast for year 2021 has also confirmed that a dual 3-lane trunk road (such as CKR), together with connecting roads, is required to divert traffic away from the existing east-west corridor to provide adequate relief to the corridor and the local road network.

2.35 CKR is the strategic road network of Kowloon and will provide the essential east-west linkage between Kowloon East and Kowloon West. The implementation of CKR will relieve the existing congested east-west corridors of Kowloon. The anticipated travel time between Kowloon East and West is estimated to decrease from the ~30-35 minutes to ~5 minutes in 2021 with CKR.

2.36 The need for CKR has been clearly established through traffic and transport studies. The findings of the traffic and studies demonstrate conclusively the compelling and present need for CKR.

Benefits of the Project

(A) Economic Returns

2.37 Savings resulting from travel distance and travel time are the primary source of economic benefits from CKR. Direct benefits accrue to travellers to/from East-West Kowloon who enjoy both more direct and quicker journeys. Indirect benefits accrue to Central Kowloon traffic (for example across Waterloo Road) that enjoys higher travel speeds, and therefore reduced travel time, as traffic diverts from congested routes such as Argyle Street, Waterloo Road and Jordan Road onto the new CKR corridor. Although bus vehicle travel time savings are relatively smaller, the higher vehicle occupancy means that public transport travel time savings are a significant component of the overall time savings.

2.38 It is estimated that the journey time between West Kowloon and Kowloon Bay in the morning peak in 2021 would only take about 5 minutes resulting in a saving of 25 to 30 minutes as compared to that without CKR. CKR is more important if there is any serious traffic congestion resulting from blockage of any east-west corridor.

2.39 Time savings are converted into monetary values by multiplying the respective time savings in hours for each passenger group by that group's value of time (VOT). VOT therefore reflects the willingness to pay for an hour of time savings. The VOT for each passenger group is assessed based on Travel Characteristics Survey 2002 and inflated to current prices. It is estimated that by 2030, the daily travel time savings will reach 120 thousands passenger hours bringing an economic value of $2.6 billion per annum.

2.40 Accident benefits will arise as travellers are diverted to use tunnel from local roads. According to the accident statistics provided by the Transport Department, the accident rate per veh-km for tunnels is 85% lower than local road during 2006 – 2010.

2.41 Based on an assessment period of 48 years covering construction and operational periods and assuming the real discount rate, the CKR project is estimated to produce a positive Net Present Value (NPV) of $ 19,503 million with Economic Internal Rate of Return (EIRR) of 7.5% and Benefit Cost Ratio (BCR) of 1.8. It is clear from the analysis that the economic benefits from the development of CKR are sufficient to cover the economic costs and the CKR project is economically viable.

(B) Environmental Benefits

2.42 Some of the key east-west corridors in Kowloon are approaching or have exceeded their design capacities, resulting in traffic congestion and long traffic queues. The main objective of the proposed CKR is to relieve traffic congestion at peak hours on the existing east-west corridors, including the Lung Cheung Road, Boundary Street, Prince Edward Road West, Argyle Street, Waterloo Road, Gascoigne Road Flyover and Chatham Road North.

2.43 As the traffic on the existing major routes across Kowloon could be diverted by CKR, the traffic volume on at-grade corridors will be reduced. Pollution resulted from traffic congestion could therefore be alleviated and the environment would be improved.

2.44 With CKR in place, the traffic conditions (e.g. in terms of average travelling speed) along these key east-west corridors would be improved and this would lead to a reduction in the substances such as CO_2, NO_x and RSP released from vehicles.

2.45 Through the adoption of advanced technology like Air Purification System (APS), exhaust concentrations from the 3 ventilation buildings along CKR are largely decreased by the Electro-Static Precipitator (ESP) and NO_2 removal system.

2.46 The Year 2021 traffic forecast for the key east-west corridors has been input to EPD's latest EmFAC-HK v2.1 which has been implemented with the latest emission control measures. The same EmFAC model has been adopted in the CKR Environmental Impact Assessment (EIA). The EmFAC-HK model would consider a number of factors including traffic flow, travel speed, territory-wide Vehicle-Kilometre-Travelled (VKT), vehicular mix etc and estimate the total annual emissions of CO_2, NO_x and RSP from the road sections concerned. The following **Table 2-4** summarises the results.

Table 2-4 Estimation of Annual Emission for Key East-West Corridors

Substances from Vehicular Emission	Reduction by CKR at 2021[1], Ton / year
CO_2	Approx 20,000
NOx	Approx 18
RSP	Approx 2

[1] Considering key East-West Corridors ONLY

(C) Social Benefits

2.47 In the future when CKR is completed, there will be a reduction in journey time, which will improve the connection between districts supporting the social developments.

Conclusions

2.48 Since there is an urgent need for the construction of CKR to alleviate the existing traffic congestions, and since CKR can also improve the environment as well as yield economic and social benefits, there is an overriding public need for constructing CKR.

3 NO REASONABLE ALTERNATIVES TO RECLAMATION

Introduction

3.1 This chapter examines whether there are reasonable alternatives to the proposed temporary reclamation in Kowloon Bay for the construction of the underwater tunnel of CKR. We will first consider if the underwater tunnel for the selected alignment can be constructed using reasonable alternative methods that will not require temporary reclamation. We will then consider if there are alternative alignments that will not involve reclamation.

Constraints in Design and Construction Arrangements

Layout at Eastern End

3.2 As shown in **Figure 1-1**, the drill-and-blast tunnel of CKR starting from Yau Ma Tei and running through King's Park, Ho Man Tin and Ma Tau Wai will be constructed in bed rock about 40 m to 140 m below ground level to ensure that the construction and operation of CKR will not affect the structural integrity and normal use of the buildings along the tunnel alignment. As CKR will have to connect to the road network in Kowloon Bay and Kai Tak Development area, the vertical alignment will rise at 4% starting from the eastern side of Ma Tau Wai Road. The vertical profile of CKR beneath Kowloon Bay can be seen in **Figure 3-1**.

3.3 As the length of the section on 4% gradient exceeds 500 m, a climbing lane is provided for the eastbound carriageway starting at Lucky Building in accordance with relevant design standards for use by heavy vehicles. Furthermore, as the horizontal alignment of the section in Kowloon Bay is on a circular curve of 330 m radius, both the east bound and west bound carriageways have to be widened to a maximum of 3 m to provide adequate sight distances in accordance with design standards, which is the minimum requirement, and to ensure traffic safety.

3.4 With these geometric functional requirements and geological conditions, the need for a very deep and unusually wide tunnel section (approximately 47m to 58m) complicates the engineering design of the underwater tunnel and demands a very robust design scheme.

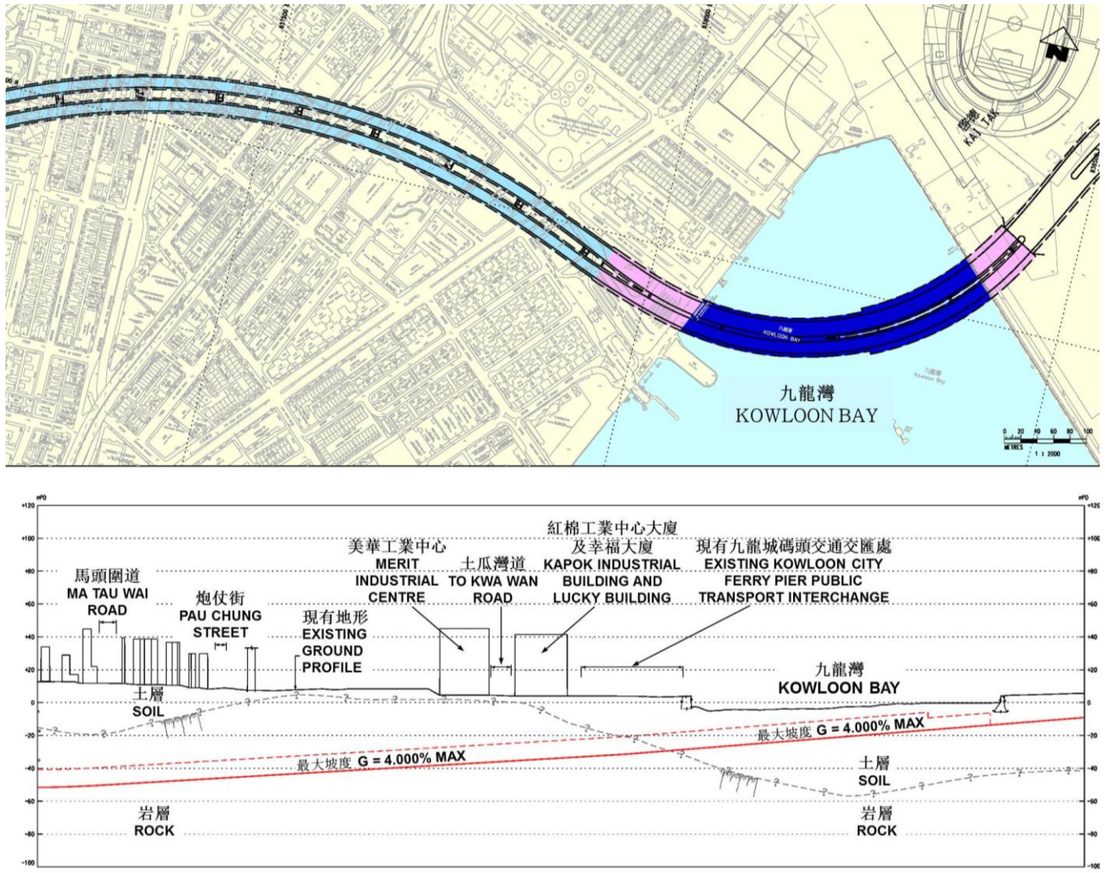

Figure 3-1 – Layout at Eastern End

Kowloon City Ferry Pier

3.5 The pier is currently used for the passenger ferry service between Kowloon City and North Point. Construction works will be carried out on the northern side of the pier. Suitable arrangements will be implemented so that normal ferry operation can continue during construction stage.

Ma Tau Kok Public Pier

3.6 The Ma Tau Kok Public Pier will have to be demolished to facilitate the construction of the underwater tunnel. The public pier will be re-provided temporarily at the waterfront promenade near King Wan Street during the construction period and reinstated upon the completion of the construction works.

Hong Kong & China Gas Company (HKCG) Naphtha Jetty

3.7 The jetty is currently used for off-loading naphtha delivered by ships and delivery to the nearby HKCG Ma Tau Kok Plant. According to HKCG, 36 shipments of naphtha are currently delivered each year. Marine access will have to be maintained during construction stage to continue normal shipment.

Construction Methods Not Involving Reclamation

3.8 We have considered whether the underwater tunnel can be constructed using the following methods that would not involve temporary reclamation –

(a) Immersed Tube Tunnel (IMT); and

(b) Tunnel Boring Machine (TBM).

(A) Immersed Tube Tunnel (IMT)

3.9 Under this method, a trench of about 220 m and 30 m deep will be excavated in the seabed along the tunnel alignment by dredging of marine mud as shown in **Figure 3-2**. The tunnel units (about 47 m to 58 m wide, and 16.5 m high) will be cast off site and floated to the tunnel site for sinking into pre-determined locations on the trench. The tunnel units will be joined. Upon the completion of jointing, the trench will be backfilled to the original seabed level. An IMT typical section and backfilling arrangement are shown in **Figure 3-3** and **Figure 3-4** respectively.

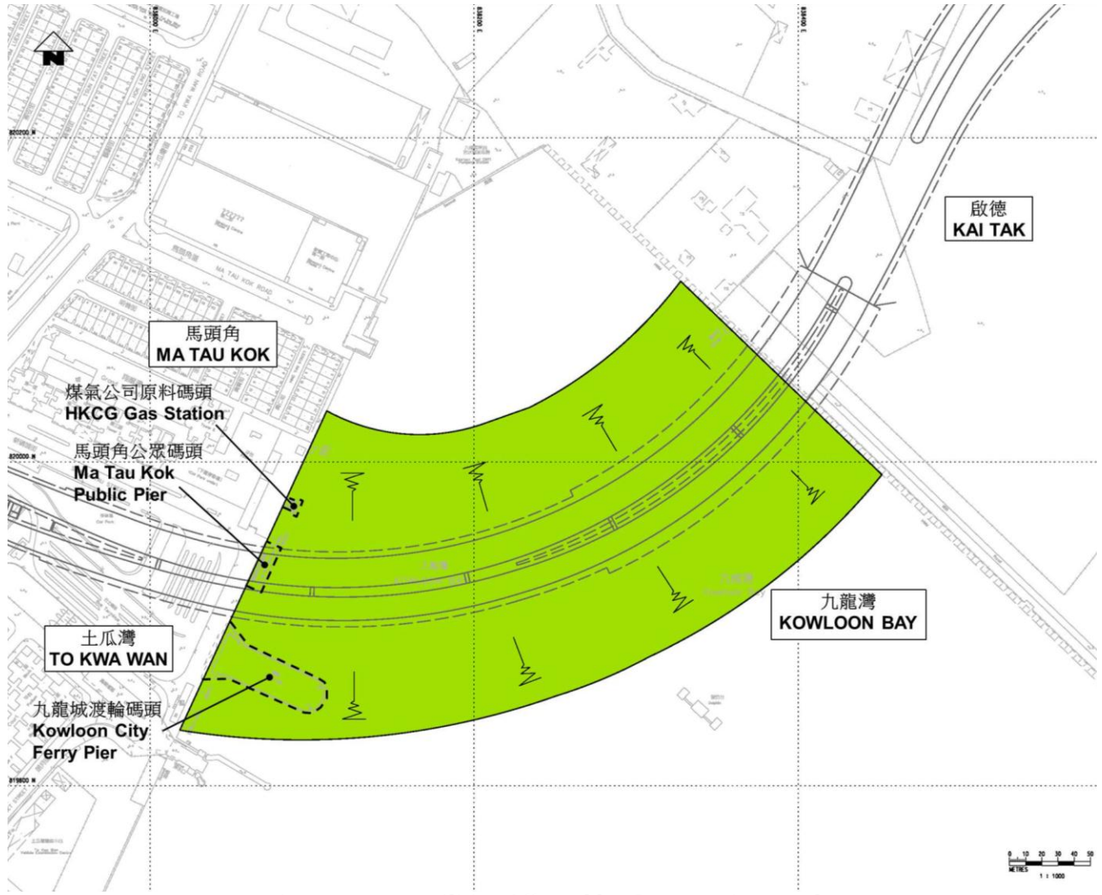

Figure 3-2 – Facilities Affected by Construction Works

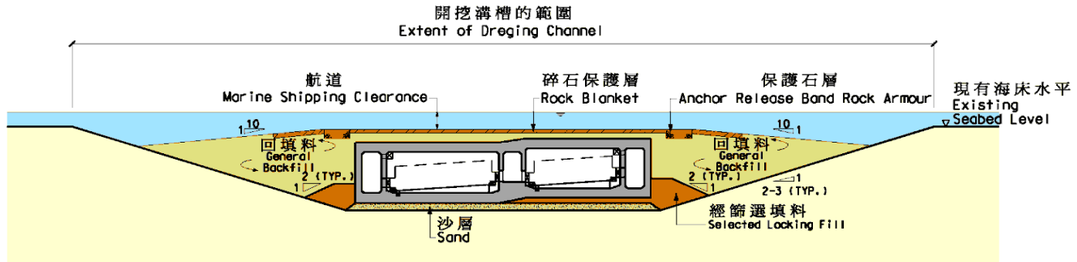

Figure 3-3 – Typical Section through Immersed Tube Tunnel (IMT)

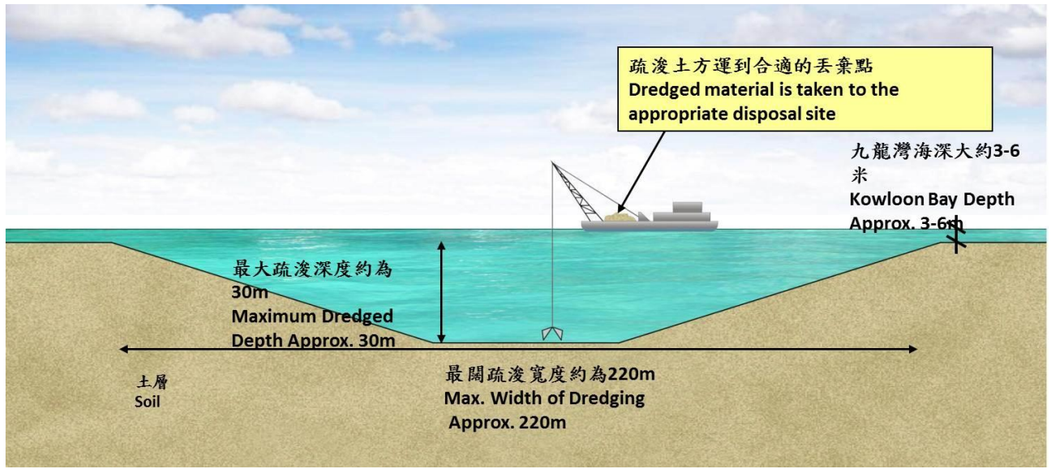

Figure 3-4 (a) Step 1 – Extensive Dredging of Existing Marine Sea Bed

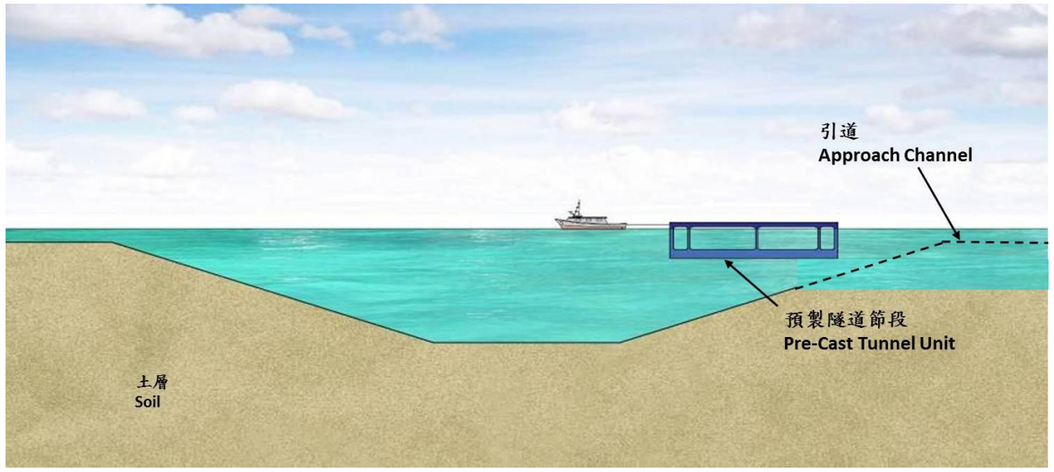

Figure 3-4 (b) Step 2 – Float Pre-Cast Tunnel Unit into Position

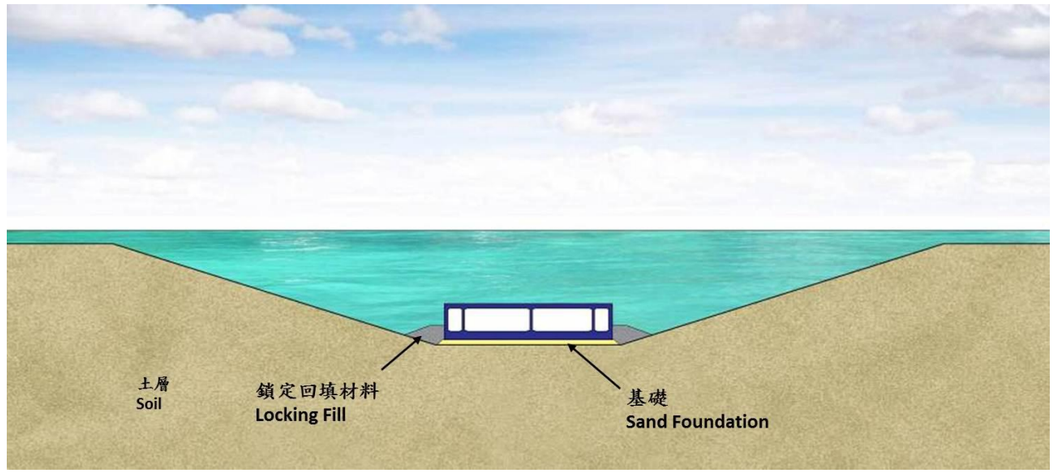

Figure 3-4 (c) Step 3 – Sink and Merge Pre-Cast Tunnel Units and Place Locking Fill

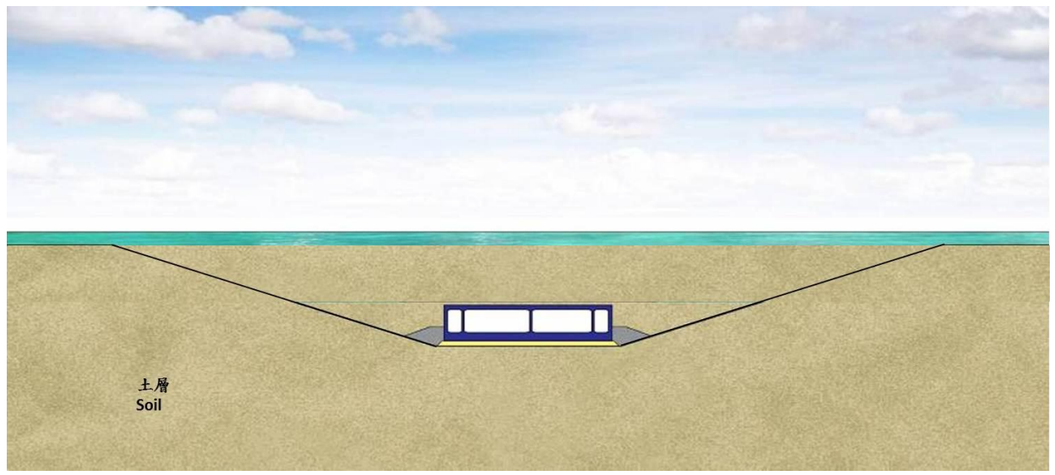

Figure 3-4 (d) Step 4 – Backfill Pre-Cast Units and Restore Sea Bed to Previous Conditions

3.10 An example of floating the immersed tunnel tube precast unit is shown in **Figure 3-5** for information.

Figure 3-5 – Example of Immersed Tube Tunnel (IMT)

3.11 The dredging of the trench for placement of IMT box will involve the removal and disposal of approximately 0.75 million m^3 of marine mud. Furthermore, as the sea in Kowloon Bay is only about 6m to 8m deep, an approach channel of about 1,300 m long, 150 m wide and 12 m deep will have to be formed adjacent to the tunnel site to provide sufficient draft for floating the precast units thus resulting in the dredging and disposal of approximately 1.8 million m^3 of marine mud in total, as shown in **Figure 3-6**.

Figure 3-6 – Dredged Trench and Approach Channel for IMT

3.12 The trench will also affect the structural integrity of the existing Ma Tau Kok and Kai Tak seawalls, and foundation of the private buildings adjacent to the seawall as shown in **Figure 3-7**. The jetty of Hong Kong China Gas Co for transporting raw materials and the Kowloon City Ferry Pier would also have to be relocated during the construction period.

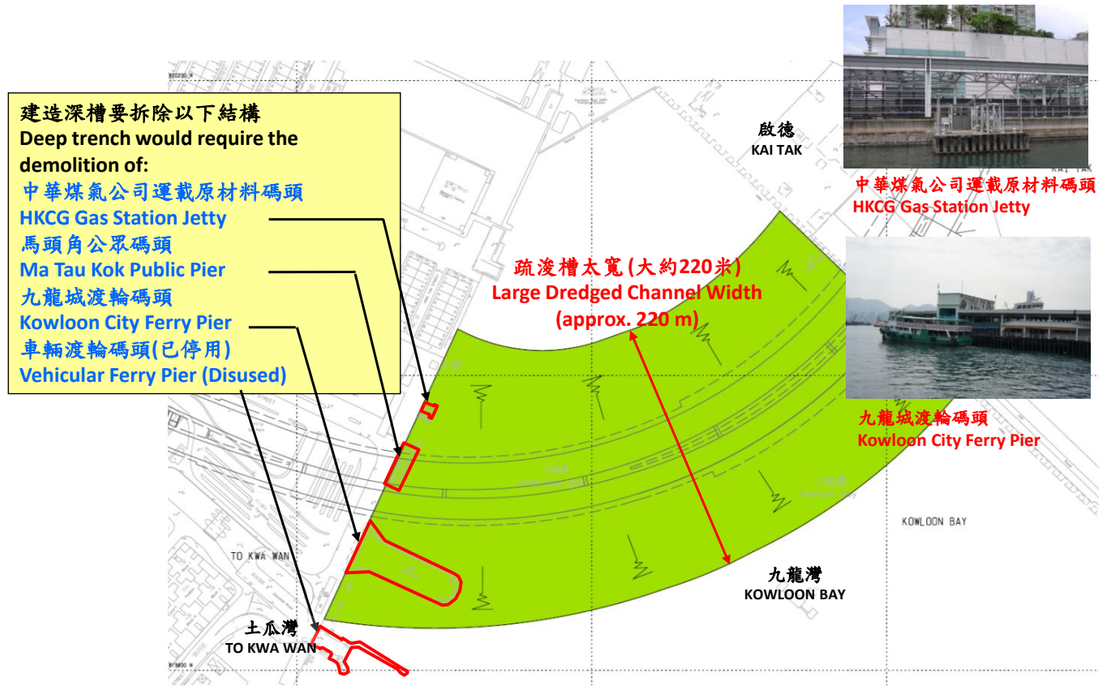

Figure 3-7 – Structure to be Affected by Trench Excavation for IMT

3.13 Given the large volume of marine mud that will have to be dredged to form the trench for placing the immersed tube units; the equally large volume of marine mud to be dredged for forming the approach channel for floating these units; and the impacts on the seawall, the adjacent private buildings, the HKCG jetty and operation of passenger ferry, IMT is therefore not a reasonable alternative.

(B) Tunnel Boring Machine

3.14 This method involves boring of circular tunnel section using Tunnel Boring Machine (TBM) through the stratum along the tunnel alignment. The bored tunnel surface will then be protected with concrete lining. An example of TBM is shown in **Figure 3-8** for reference.

Figure 3-8 – Tunnel Boring Machine (TBM)

3.15 Before the construction of the concrete lining, air pressure about 300 kPa to 500 kPa (or three to five times the atmospheric pressure) will have to be applied inside the tunnel to uphold the excavated face of the tunnel and to prevent the seepage of water into the tunnel. As such, sufficient soil cover will be required for containing the pressure inside the tunnel. The amount of cover required will depend on the ground conditions. Given the relatively low strength (undrained shear strength down to about 4kPa) of the soil in the seabed of Kowloon Bay the cover required will be about 1.5 times the diameter of the tunnel as illustrated in **Figure 3-9**. The diameter of the eastbound tunnel (with three traffic lanes and one climbing lane) will be 20.5 m. The diameter of the westbound tunnel (with three traffic lanes) will be 17 m. The cover required will be about 30.75 m and 25.5 m respectively.

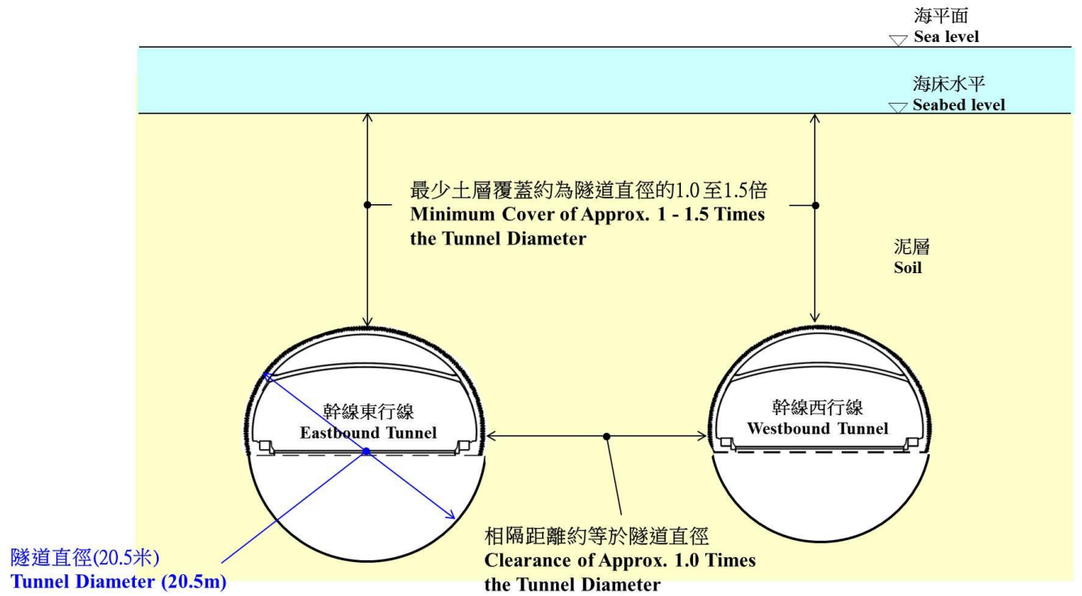

Figure 3-9 – Required Soil Cover for Tunnel Boring Machine

3.16 As the tunnel will have to gradually rise to ground level to connect to the road network in Kowloon Bay and KTD, the maximum soil cover will only be 17 m at the western end and the minimum soil cover will only be 2 m at the eastern end as illustrated in **Figure 3-10**. This will be less than 1.5 times the diameter of the tunnel.

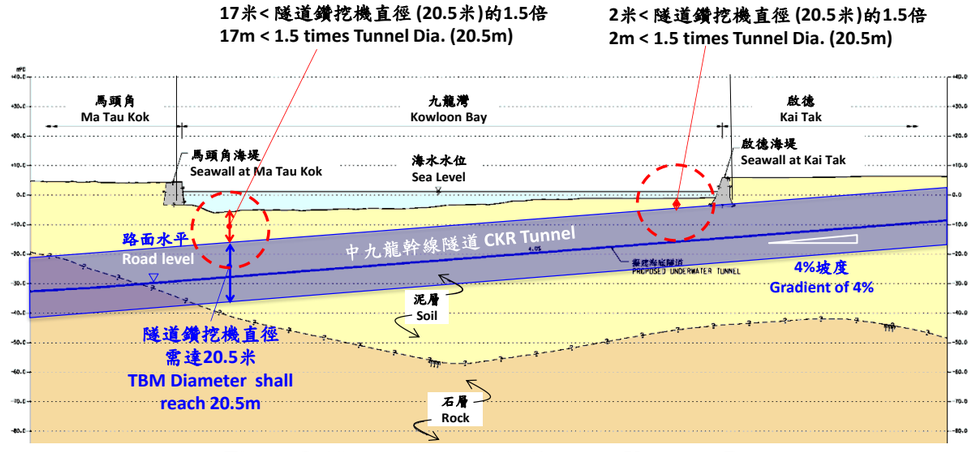

Figure 3-10 – Available Soil Cover at Kowloon Bay

3.17 The available soil cover would be inadequate for containing the air pressure that would be required for upholding the excavated tunnel face and preventing the seepage of ground water thus leading to blow out failure as illustrated in **Figure 3-11**.

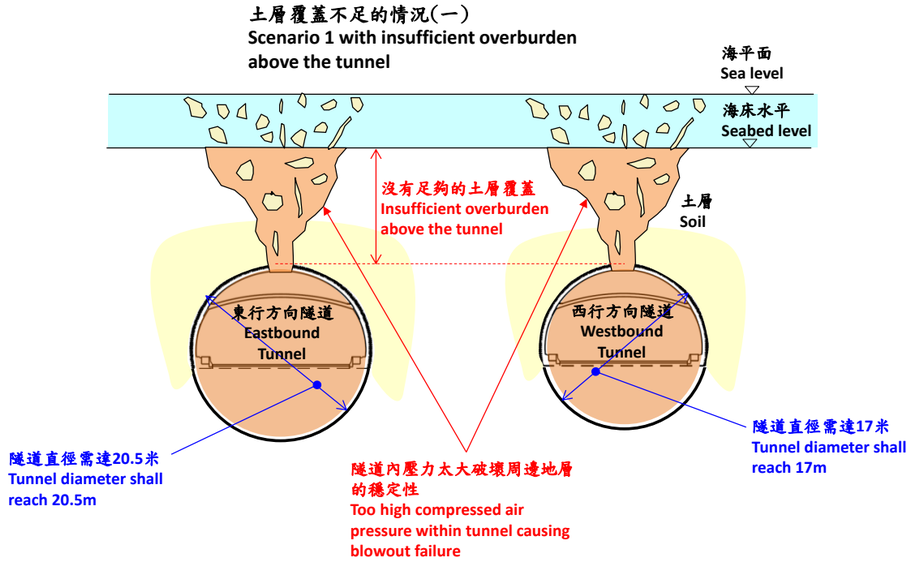

Figure 3-11 – Blow-out Failure Scenario

3.18 On the other hand, if the air pressure were reduced, the pressure would be insufficient for upholding the excavated sections and for preventing the seepage of ground water. As such, the tunnel could also fail because of the collapse of the excavated face and excessive seepage of ground water as illustrated in **Figure 3-12**.

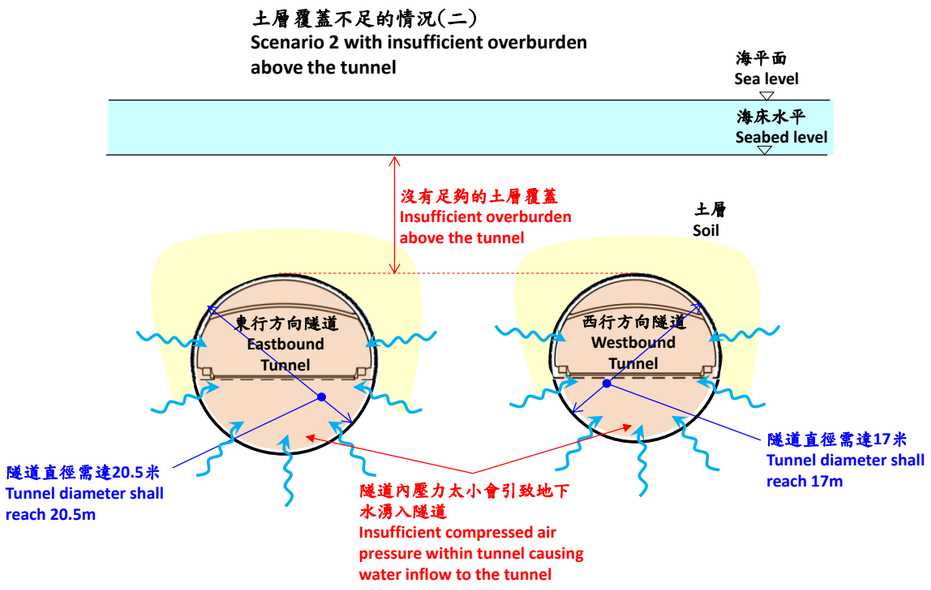

Figure 3-12 – Seepage Failure Scenario

3.19 For the foregoing reasons, the use of TBM for constructing the underwater tunnel would be unsafe both for construction personnel and the public. TBM is therefore not a reasonable alternative.

(C) Construction Method Involving Reclamation

3.20 Since both the IMT and TBM methods are not reasonable alternatives, we have considered whether the underwater tunnel can be constructed on temporary reclamation using the cut-and-cover method as shown in **Figure 3-13**.

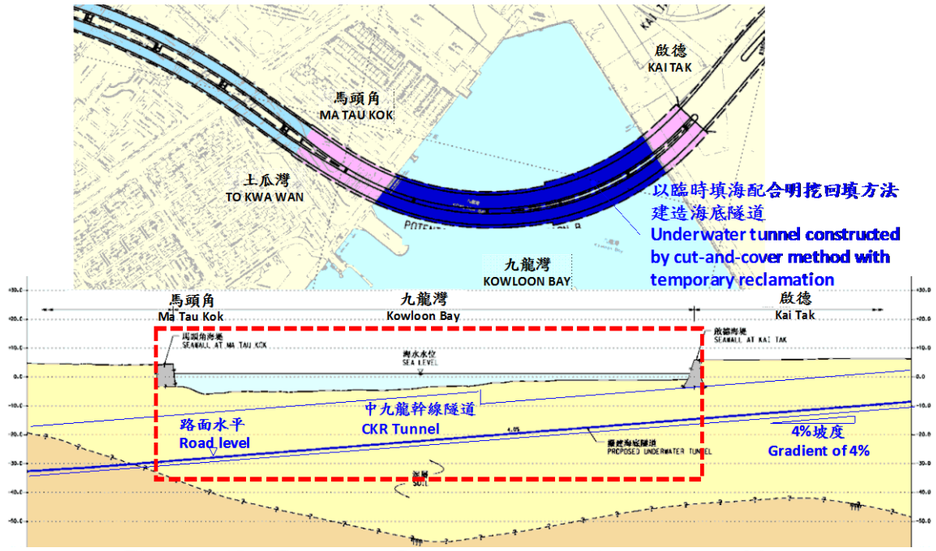

Figure 3-13 – Temporary Reclamation with Cut-and-cover Method

3.21 The construction of tunnel using cut-and-cover tunnel method has been widely adopted in Hong Kong for many different building, railway and infrastructure projects. For the construction of underwater tunnel or depressed road connecting underwater tunnel, the combination of temporary reclamation to provide a dry working platform and cut-and-cover method for tunnel construction has also been widely adopted and considered as the one of the most practical and effective method. An example of construction of tunnel by cut-and-cover method within temporary reclamation is shown in **Figure 3-14**.

Figure 3-14 – Example of Temporary Reclamation with Cut-and-cover Method

3.22 Under this method, temporary seawall will be constructed using large pipe-piles along the underwater tunnel alignment. The space enclosed by the temporary seawall will then be reclaimed to form a working platform. Diaphragm walls will be constructed on this platform to form a cofferdam. Excavation work will be carried out within the cofferdam to facilitate the construction of the tunnel structure. The temporary reclamation and seawall will be removed after the completion of the tunnel, and the seabed will be reinstated to its original levels. An illustrative construction sequence is shown in **Figure 3-15** for reference.

3.23 After the formation of the working platform by temporary reclamation, temporary retaining structure will be installed for the subsequent bulk excavation. Type of temporary retaining structure is dictated by depth of excavation, water level and ground condition. For underwater tunnel with more than 20m deep excavation required, high water level up to over +2.0mPD (sea level) and presence of up to around 9m soft marine deposits, the temporary retaining wall is expected to retain large pressure from adjacent ground and sea. Diaphragm wall is hence considered as the preferred type of retaining structure in view of its large structure capacity to resist the soil and water pressure. The diaphragm will need to penetrate sufficient depth or even into bedrock (if the rockhead level is not deep) to provide overturning stability and water cut-off.

3.24 Bulk excavation together with installation of lateral support will hence be carried out after diaphragm wall installation to provide a dry working platform for the in-situ construction of the tunnel structure. After the construction of tunnel structure, backfill will be carried out up to the seabed level and the remaining temporary reclamation will be removed. At last, the seabed will be restored back to the original seabed profile.

Figure 3-15 (a) - Cut-and-Cover Method with Temporary Reclamation - Step 1

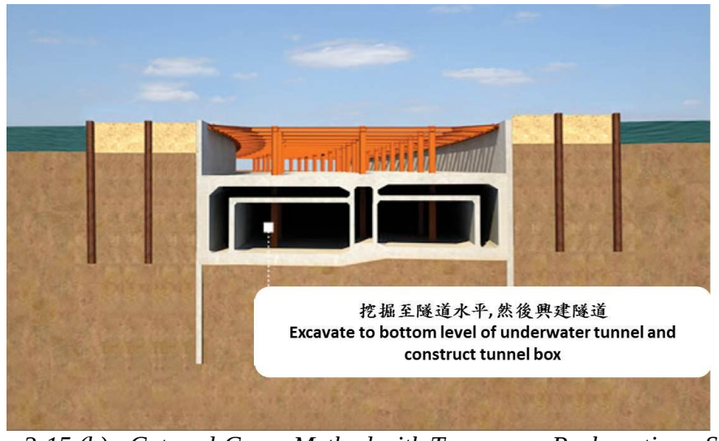

Figure 3-15 (b) - Cut-and-Cover Method with Temporary Reclamation - Step 2

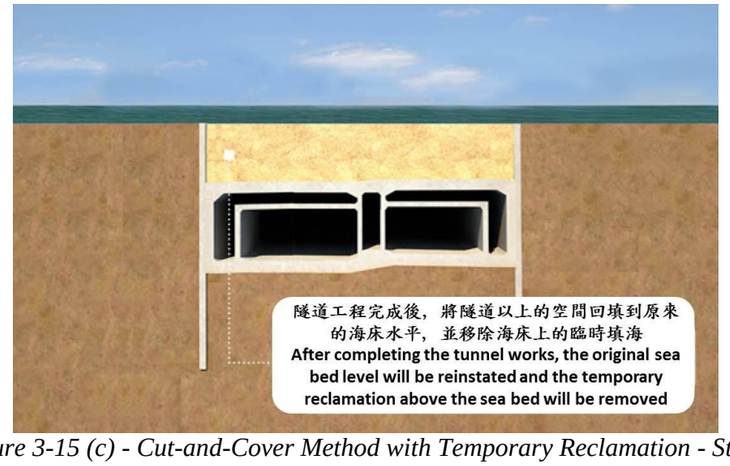

Figure 3-15 (c) - Cut-and-Cover Method with Temporary Reclamation - Step 3

3.25 The temporary reclamation would be implemented in two stages so as to maintain marine access to HKCG naphtha jetty and avoid affecting the discharge of an existing stormwater box culvert, which is between the ex-airport runway and Ma Tau Kok, into Kowloon Bay. Stage 1 will proceed in the Kowloon Bay sea area near the Kai Tak Development Area to reclaim an approximately 1.8 hectares site for the construction of a 180 m long section of the tunnel which will take about 26 months to complete and reinstate the seabed to its original level. Stage 2 will proceed in the sea area fronting Kowloon City Ferry Pier to reclaim an approximately 2.0 hectares site for the construction of a tunnel of about a 190 m long section of the tunnel which will also take about 26 months to complete and reinstate the seabed to its original level. Normal operation of the passenger ferry service on Kowloon City Ferry Pier will be maintained during the construction period. This two stage temporary reclamation arrangement is illustrated in **Figure 3-16** and **Figure 3-17**.

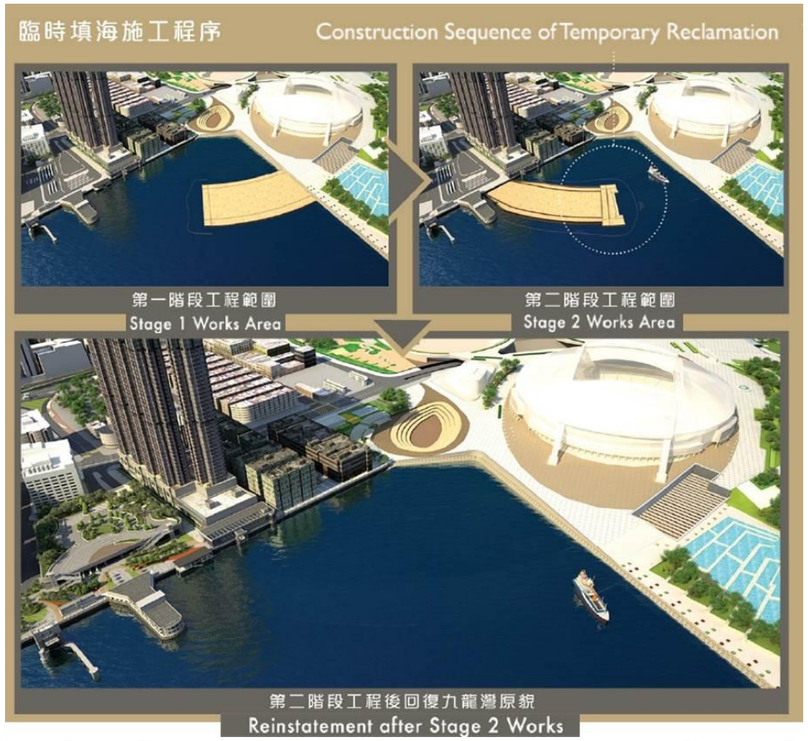

Figure 3-16 – Two Stage Temporary Reclamation Arrangement in Kowloon Bay

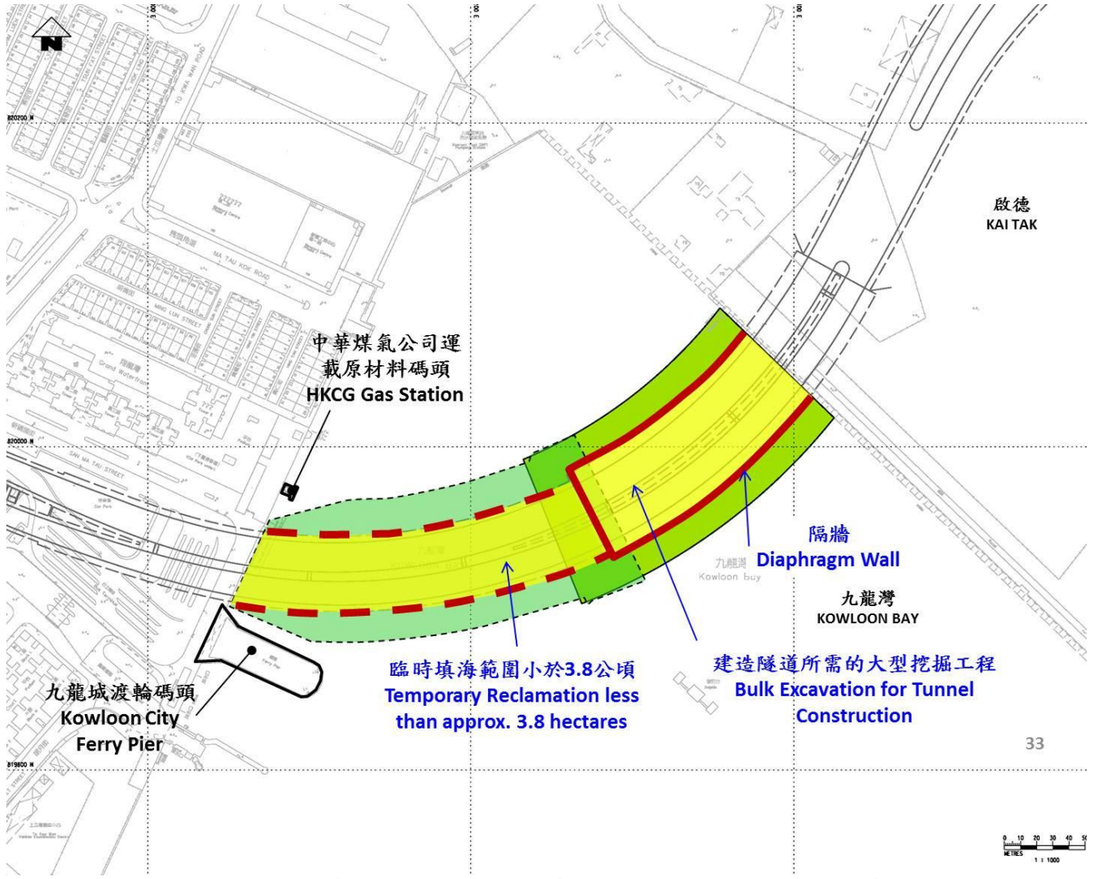

Figure 3-17 – Two Stage Temporary Reclamation Arrangement in Kowloon Bay

3.26 For the foregoing reasons, the construction of the underwater tunnel using the cut-and-cover method on temporary reclamation is feasible and is indeed the only safe and practical construction method.

(D) Alternative Alignments

3.27 In the Investigation and Preliminary Design stage between 2007 and 2009, we explored if there were other alternative alignments, including Alignments A, C to E, and the present Alignment (Alignment B) as shown in **Figure 3-18**.

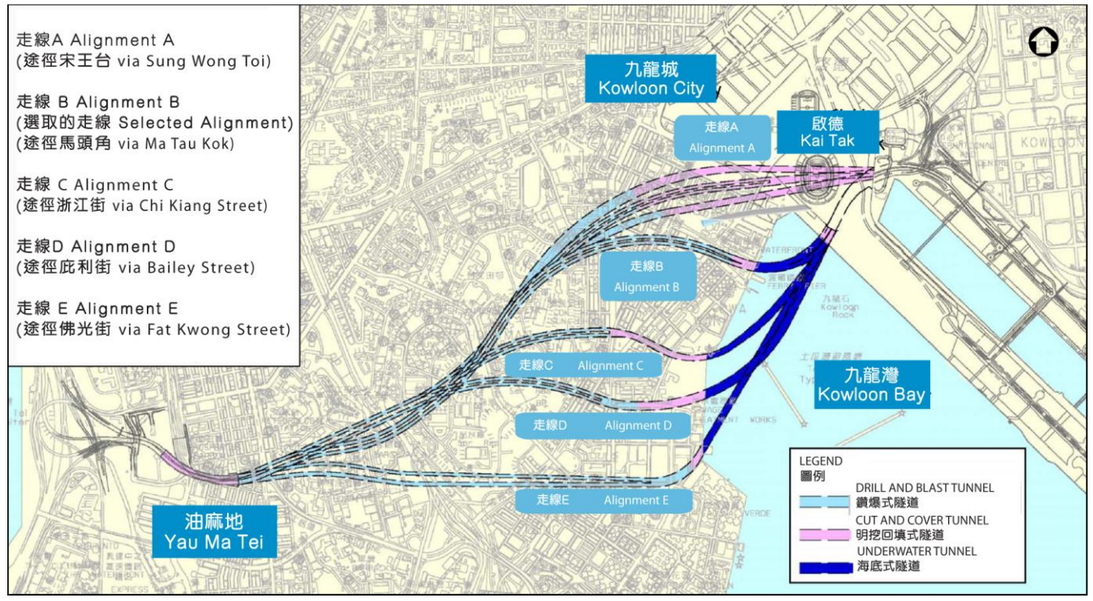

Figure 3-18 – Alternative Alignment in Investigation and Preliminary Design Stage

3.28 Alignment A is an inland option which does not involve reclamation. However, it includes a 600 m long tunnel which passes under tens of private buildings along Mok Cheong Street in To Kwa Wan. The affected private buildings would have to be resumed and demolished to implement the project. Alignment A is therefore not a reasonable alternative.

3.29 While Alignments C to E pass through existing roads and undeveloped areas along seashore and then across the sea to connect with Kai Tak Interchange, they also involve resumption and demolition of private buildings, and larger extent of temporary reclamation when compared with Alignment B. Therefore, Alignments C to E are also not reasonable alternatives. On the other hand, Alignment B only requires use of the Kowloon City Ferry Pier Public Transport Interchange for construction works but does not involve resumption and demolition of private properties, and the extent of temporary reclamation is the minimum.

4 MINIMUM EXTENT OF TEMPORARY RECLAMATION

Introduction

4.1 This chapter examines the factors related to the extent of temporary reclamation required for construction of the underwater tunnel in Kowloon Bay and identifies a scheme involving the minimum extent of temporary reclamation.

Length of Reclamation

4.2 As shown in **Figure 4-1** below, the underwater tunnel is on a circular curve with a radius of 330 m at the centreline. It is the shortest reverse curve alignment in minimum desirable radius between the locations of Kowloon City Ferry Pier Public Transport Interchange and Kai Tak River. The length of the underwater tunnel and hence the length of the temporary reclamation are also the minimum required.

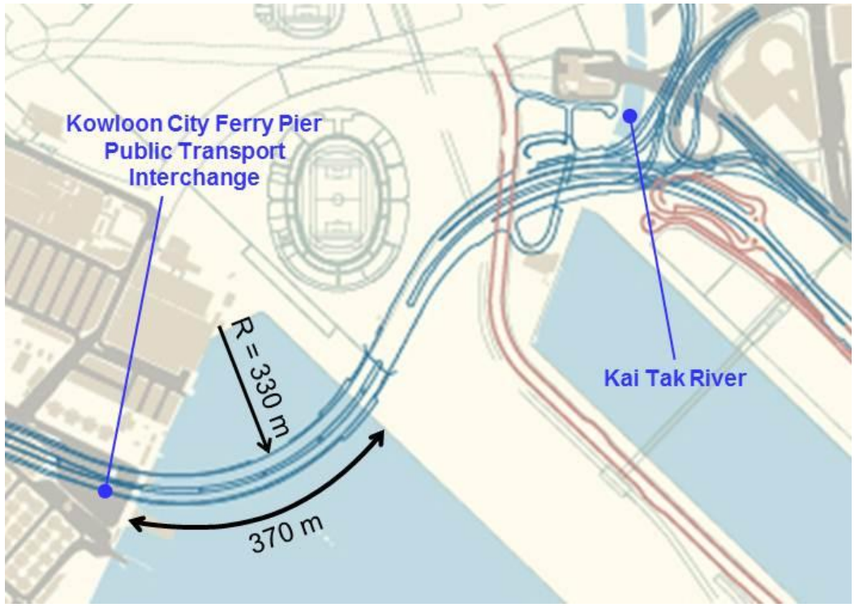

Figure 4-1 – Length of Reclamation

Width of Reclamation

4.3 The width of the tunnel is governed by the curve radius of 330 m. As shown in Figure 4-2, this is the minimum radius for providing the sight distance required under Volume 2, Section 3.3.5 of TPDM for ensuring traffic safety with adequate forward visibility.

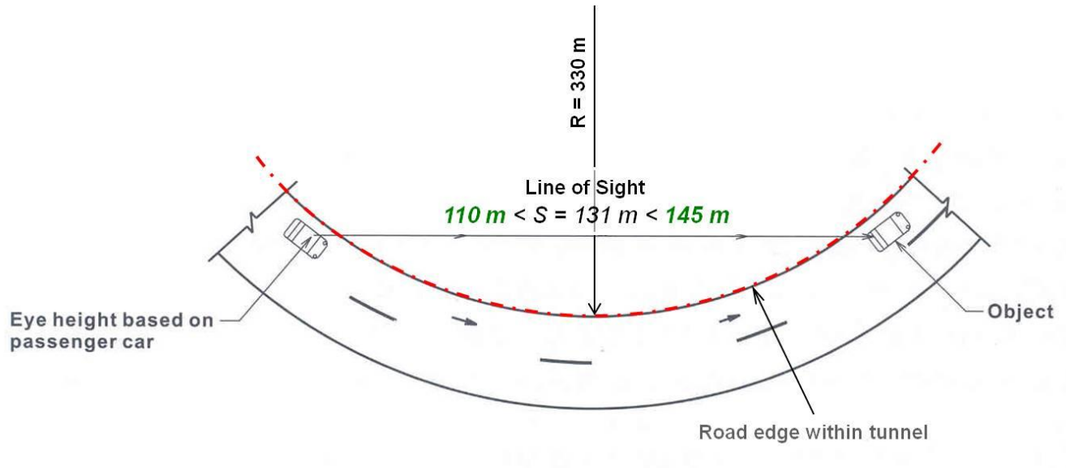

Figure 4-2 – Sight Distance Requirement

4.4 As shown in **Figure 4-3** below, the width of the temporary reclamation varies from 87 m to 98 m and is made up as follows –

(a) the width of the cofferdam formed by the diaphragm walls which varies from 47 m to 58 m; and

(b) a working platform 20 m wide on each side of the diaphragm wall.

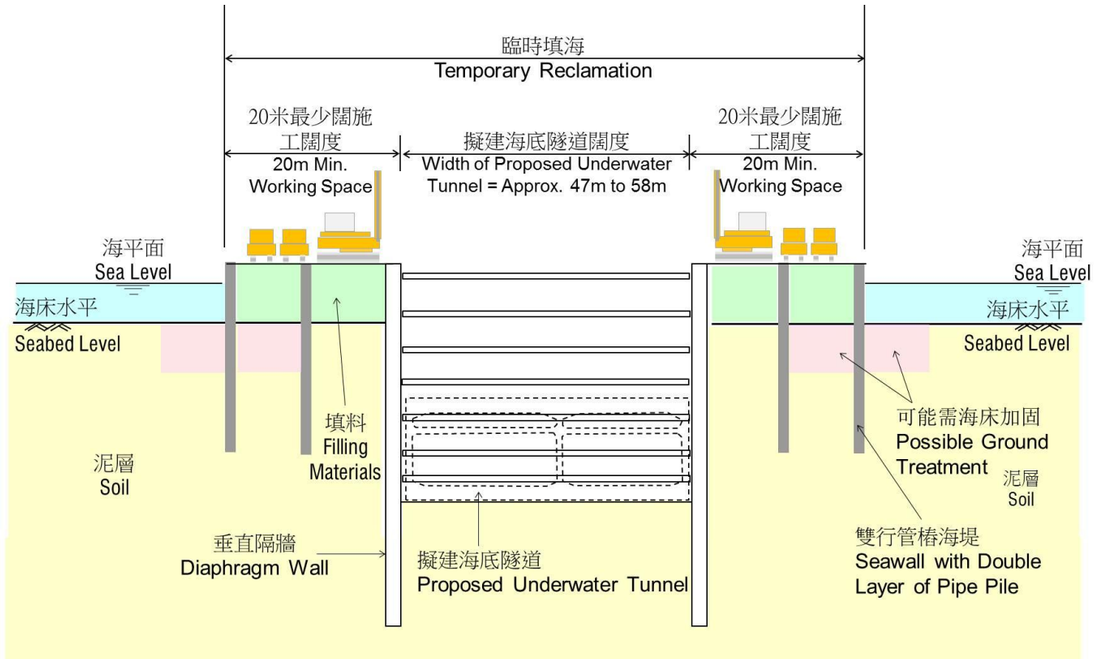

Figure 4-3 – Typical Cross Section of Temporary Reclamation

4.5 The width of the underwater tunnel and hence the width of the temporary reclamation are also the minimum required.

4.6 Regarding paragraph 4.4(a), as explained in paragraph 3.25 of Chapter 3, the tunnel will be constructed in two stages as follows –

(a) Stage 1 will proceed in the Kowloon Bay sea area near the Kai Tak Development Area to reclaim an approximately 1.8 hectares site for the construction of a 180 m long section of the tunnel which will take about 26 months to complete and reinstate the seabed to its original level; and

(b) Stage 2 will proceed in the sea area fronting Kowloon City Ferry Pier to reclaim an approximately 2.0 hectares site for the construction of a tunnel of about a 190 m long section of the tunnel which will also take about 26 months to complete and reinstate the seabed to its original level.

4.7 For the section of the tunnel to be constructed in Stage 1, the ventilation duct is located on both sides of the tunnel given the limited headroom under the vertical seawall along KTD. The width of this section is therefore about 58 m. For the section of the tunnel to be constructed in Stage 2, as more headroom is available, the ventilation duct is located on top of the tunnel to minimize the extent of reclamation. The width of this section is therefore about 47 m.

4.8 Regarding paragraph 4.4(b), the working platform will be required to provide working space for construction plant (such as cranes, dump trucks, excavators and etc.), loading and unloading of materials delivered by barges and circulation of construction traffic. According to the experience of construction of underwater tunnel by similar method in Central-Wan Chai Bypass, this 20 m width is just adequate for these uses. As such, the width of the proposed temporary reclamation is also the minimum as illustrated in the photographs in **Figures 4-4** and **4-5**.

Duration of Temporary Reclamation

4.9 The total duration for temporary reclamation will take approximately 52 months. Stone column construction, seawall construction, diaphragm wall construction, excavation and tunnel box construction will each take 5 to 6 months to complete, while reclamation filling, backfilling and reclamation removal and restoration will take 1 to 2.5 months to finish. As some of these tasks can be carried out in parallel, each of the two stages of reclamation will take approximately 26 months to complete.

Summary of Minimum Reclamation Requirements

4.10 Detailed examination of the engineering requirements in respect to the construction of the underwater tunnel, reclamation, seawalls, and re-provisioning of affected facilities has been conducted to accurately define the minimum extent of required temporary reclamation.

4.11 Each of the two stages of the reclamation will last less than approximately 26 months, starting from early-2015 to mid/late-2019 tentatively.

4.12 It is concluded that the area of temporary reclamation has been minimized. The total area of temporary reclamation does not exceed 3.8 ha, with a maximum of 2.0 ha at any given time.

Figure 4-4 – Temporary Reclamation of Central-Wan Chai Bypass

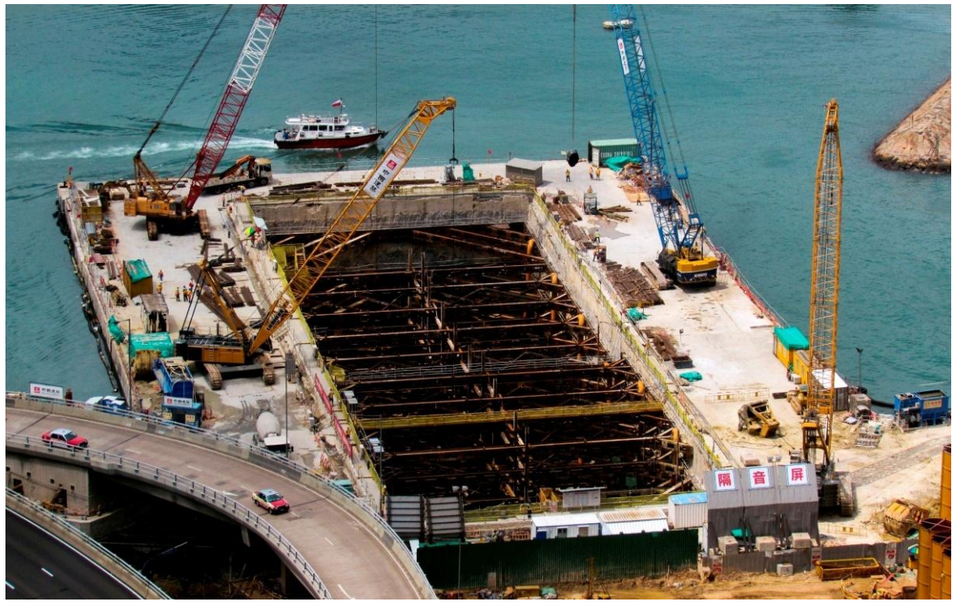

Figure 4-5 – Temporary Reclamation of Central-Wan Chai Bypass

5 PUBLIC CONSULTATION

Public Engagement in Previous Stage of Study

5.1 Highways Department (HyD) commissioned the Investigation and Preliminary Design (I&PD) of CKR in 2007. Since the project would have significant impacts on traffic, land use and environment, a comprehensive public engagement strategy was adopted by organizing public forums, focus group meetings, outreach activities, interviews, questionnaire survey, site visits and planning competition to collect public views on major key issues. Through these activities, good communication was established with various stakeholders, including residents, owners' committees, community organizations, business operators and District Councils. We have also consulted Yau Tsim Mong, Kowloon City and Kwun Tong District Councils as well as the Legislative Council Panel on Transport about CKR.

5.2 One of the major tasks of the I&PD study was to select a preferred alignment. We have reviewed more than 40 options that were formulated under previous CKR studies and 14 new options were developed. The present alignment was selected after comparing the impacts of the options on reprovisioning of community facilities, environment, land and transport and making reference to comments collected during the public engagement process. The alignment was generally supported by Legislative Council Panel on Transport, Yau Tsim Mong, Kowloon City and Kwun Tong District Councils.

5.3 Through the public engagement activities, we understood that the public generally supported the construction of CKR. The public also expected that CKR would effectively connect to the road networks in East Kowloon and West Kowloon in order to alleviate traffic congestion and would properly preserve the Yau Ma Tei Police Station, Temple Street Night Market, Tin Hau Temple and Yung Shu Tau culture at the same time.

Public Forum on 18 July 2009

5.4 The proposal of temporary reclamation was discussed at length with residents at the east end of the proposed CKR alignment. The general consensus was without objection to the proposed temporary reclamation, but it was wholly agreed that environmental concerns should be addressed and that the reclamation should only be carried out if no reasonable alternative exists.

5.5 Several members of the public in fact opined desire for minor permanent reclamation of Kowloon Bay with the aim of providing new community facilities such as parks, libraries, sitting out areas and an opportunity to provide a continuous promenade linking Ma Tau Kok with Kai Tak Development. It was also suggested by the public that minor permanent reclamation would provide opportunity for mitigating concerns over Kowloon Bay odour problems.

5.6 The proposals received from the public regarding minor permanent reclamation were noted by the design team, but it is well understood that the proposal will be acceptable only if the three tests as laid down by the High Court with regard to the presumption against reclamation under section 3 of the Protection of the Harbour Ordinance can be satisfied. This should be considered separately as no such permanent reclamation is required under the CKR proposal.

Focus Group Meeting on 20 June 2009

5.7 Attendees were introduced to the history of the project. Recent developments of the alignment options were discussed along with likely project impacts to public facilities and the environment.

5.8 Attending parties included Society for Protection of the Harbour, Friends of the Harbour, the Hong Kong Institute of Engineers, the Hong Kong Institute of Architects, Hong Kong Institution of Surveyors and members of the Kowloon City District Council.

5.9 It has been suggested that the proposed demolition of Ma Tau Kok Public Pier and the associated re-provisioning of the other ferry piers will provide opportunity to enhance the Harbour front and renew public facilities in the area.

Conclusions from Previous Stage Public Engagement

5.10 The members of the public, with Yau Tsim Mong, Kowloon City and Kwun Tong District Councils as well as the Panel on Transport of the Legislative Council have been consulted in the previous stage of study on the CKR preferred alignment and proposed works.

5.11 Overall, most members of the public and their appointed representatives have shown support for the preferred alignment with no significant opposition expressed to the proposed temporary reclamation.

Public Engagement in Current Stage of Study

5.12 Phase 2 Public Engagement for CKR was launched on 5 December 2012 to collect public views on the detailed design and construction arrangement of CKR.

5.13 Various public engagement activities including focus group meetings and briefing sessions with residents along the proposed alignment of CKR, public forums, focus group meetings with green groups and professional institutes, jade market operators and briefing sessions to District Councils and Harbourfront Commission were carried out throughout the 3-month consultation period.

5.14 Since temporary reclamation at Victoria Harbour would be required for the construction of CKR Kowloon Bay section, the project proponent is required to establish an overriding public need for the proposed reclamation work under the Protection of the Harbour Ordinance. In this regard, the cogent and convincing materials supporting and justifying the overriding public need for reclamation were reviewed with the public through various public engagement activities. Consultation with Harbourfront Commission, a professional forum on temporary reclamation at Kowloon Bay and a public forum on temporary reclamation in Kowloon Bay were carried out.

5.15 To facilitate public discussion, Phase 2 Public Engagement Digest, in both Chinese and English and bilingual newsletters (Issue No. 26 and 27) covering the key issues, including introduction of detailed design of Central Kowloon Route, benefit of Central Kowloon Route, greening and landscaping opportunities, preservation of cultural heritage, reprovisioning arrangement of public facilities affected by CKR, environmental impact of CKR and the mitigation measures, and construction arrangement of CKR including temporary reclamation at Kowloon Bay section, were prepared and widely distributed. Roving exhibitions with physical model and Virtual Reality model in various locations in Yau Ma Tei, Kwun Tong, Kowloon City and Ho Man Tin were also carried out.

5.16 Around 50,000 invitations were sent to residential units, schools, local organisations and commercial buildings along and near the alignment of CKR, district councillors, members of area committees, professional institutes and green groups to invite them to participate in the public engagement activities. Advertisements of the public forum were posted on two Chinese newspapers,

Oriental Daily (東方日報) and HK Headline (頭條日報), and one English newspaper, The Standard on 4th, 11th, 18th, 25th January and 1st February 2013 respectively to reach out the general public as much as possible and invite the general public to the public forums. Stakeholders with different backgrounds, knowledge and views were brought together to discuss on various issues related to the detailed design of CKR.

5.17 The public engagement activities carried out are summarized in **Table 5-1** below.

Table 5-1 – Summary of Stakeholder Engagement Activities in Current Stage of Study

Date	Public Engagement Activities
11 Dec 2012	Meeting with Residents of Prosperous Gardens
12 Dec 2012	Focus Group Meeting with Residents in King's Park Constituency
13 Dec 2012	Consultation with Yau Tsim Mong District Council
13 Dec 2012	Focus Group Meeting with Residents in Ma Hang Chung Constituency
14 Dec 2012	Focus Group Meeting with Residents in Ma Tau Kok Constituency
15 Dec 2012	Focus Group Meeting with Residents in Jordan West Constituency
15 Dec 2012	Focus Group Meeting with Residents in Yau Ma Tei Constituency
16 Dec 2012	Meeting with Residents of Grand Waterfront
17 Dec 2012	Focus Group Meeting with Residents in Lok Man Constituency
18 Dec 2012	Focus Group Meeting with Residents in Hoi Sham Constituency
19 Dec 2012	Focus Group Meeting with Residents in Sheung Lok Constituency
19 Dec 2012	Focus Group Meeting with Residents in Oi Chun Constituency
20 Dec 2012	Focus Group Meeting with Residents in Oi Man Constituency
2 Jan 2013	Focus group meeting with Jade Hawkers
4 Jan 2013	Focus group meeting with Green Groups
7 Jan 2013	Consultation with Harbourfront Commission
8 Jan 2013	Consultation with Kwun Tong District Council
8 Jan 2013	Consultation with Wong Tai Sin District Council
10 Jan 2013	Professional Forum on Temporary Reclamation at Kowloon Bay
12 Jan 2013	Public Forum in Yau Tsim Mong District
17 Jan 2013	Consultation with Traffic and Transport Committee, Yau Tsim Mong District Council
17 Jan 2013	Consultation with Kowloon City District Council
18 Jan 2013	Meeting with Residents of Wyler Gardens
19 Jan 2013	Public Forum in Kowloon City District
22 Jan 2013	Meeting with Hong Kong Institute of Architects
26 Jan 2013	Meeting with Residents in King's Park
1 Feb 2013	Consultation with Community Building Committee, Yau Tsim Mong District Council
2 Feb 2013	Public Forum on Temporary Reclamation in Kowloon Bay
4 Feb 2013	Meeting with Hong Kong Institute of Planners, Hong Kong Institute of Urban Design and Hong Kong Institute of Landscape Architects

Public Views on Temporary Reclamation in Current Stage of Study

5.18 This section outlines the major comments from the public and other stakeholders received in Phase 2 Public Engagement regarding temporary reclamation at Kowloon Bay for the construction of CKR.

5.19 The general public and local residents along or near the alignment of CKR generally agreed that CKR could improve the east-west traffic in Kowloon and relieve the congestion in existing east-west corridors. Many requested early implementation of the project. However, some individual green groups and members of the public raised that the solution for traffic congestion should be traffic demand management rather than building more roads. This concern was subsequently reviewed by independent expert who considered that the car ownership in Hong Kong was relatively low and very high percentage of road users was in fact commercial vehicles, and there was need for the construction of CKR.

5.20 Vast majority of participants, which included local residents and the general public, did not have strong view on the proposed temporary reclamation at Kowloon Bay for the construction of CKR. Some members of the public even suggested the government to carry out permanent reclamation at that corner of the Harbour at Kowloon City Ferry Pier to solve the odour problem and provide pedestrian linkage to Kai Tak Development.

Briefing Sessions and Consultations with District Councils

5.21 Yau Tsim Mong, Kowloon City, Wong Tai Sin, and Kwun Tong District Councils, agreed that CKR could improve the east-west traffic in Kowloon and relieve the congestion in existing east-west corridors. They urged the Government to implement the CKR construction as soon as possible. Many district councillors considered that diverting traffic into CKR could reduce the number of vehicles on road in areas of Yau Ma Tei, Ho Man Tin and Kowloon City, so it would improve the traffic condition and the environment.

5.22 Some district councillors expressed their support to the temporary reclamation and they agreed with the professional judgement on the need for reclamation. Some Kowloon City district councillors further proposed to consider suitable mitigation measures to prevent the worsening of odour problems in the area.

Consultation with Harbourfront Commission

5.23 The cogent and convincing materials required to support and justify the overriding public need for reclamation, as well as the detail design and construction arrangement of CKR, were presented to Harbourfront Commission.

5.24 Harbourfront Commission in general agreed on the strategic need, its alignment and recognised the need for the proposed temporary reclamation works required for the construction of CKR.

Professional Forum on Temporary Reclamation at Kowloon Bay

5.25 In order to establish an overriding public need for the reclamation work under the Protection of the Harbour Ordinance, the cogent and convincing materials required to support and justify the overriding public need for reclamation were presented to professionals and academics in the professional forum. After the presentation from the consultant, two independent experts were invited to review the cogent and convincing materials presented by the consultant.

5.26 The professionals and academics did not have disagreement to the justifications of the need of CKR presented by the consultant and reviewed by two independent experts.

5.27 The professionals and academics generally agreed that there were no alternative construction and alignment options that did not require reclamation. They considered that tunnel boring machine (TBM) and immersed tube tunnel (IMT) were not reasonable construction methods for the underwater tunnel at Kowloon Bay.

5.28 The professionals and academics generally considered that the proposed temporary reclamation construction method with cut-and-cover would involve less dredging and disturbance to the seabed, when compared to other construction methods. The proposed arrangements were considered reasonable.

Public Forum on Temporary Reclamation at Kowloon Bay

5.29 A Public Forum on Temporary Reclamation in Kowloon Bay was held to establish an overriding public need for the reclamation work under the Protection of the Harbour Ordinance with the general public. The forum was conducted to discuss: (1) whether there is an overriding need for the project; (2) whether there is alternative to reclamation; and (3) whether the extent of reclamation is the minimum. After the presentation from the consultant, two independent experts were invited to review the cogent and convincing materials presented by the consultant.

5.30 Members of the public agreed that there was an urgent need to resolve the traffic congestion, and there was overriding public need for the construction of CKR. It was also agreed that there was no safe, reliable and reasonable alternative method to the proposed reclamation method and that the current proposed extent of reclamation is the minimum.

6 CONCLUSIONS

Whether There is an Overriding Public Need for Reclamation

6.1 Yau Tsim Mong, Kowloon City, Wong Tai Sin, and Kwun Tong District Councils, local residents along or near the alignment of CKR and the general public agreed that CKR could improve the east-west traffic in Kowloon and relieve the congestion in existing east-west corridors. They urged the Government to implement the construction of CKR as soon as possible. Harbourfront Commission also stated their acceptance on the strategic need of CKR. Various professional institutes did not challenge the need for CKR.

6.2 Many district councillors and local residents considered that diverting traffic into CKR could reduce the number of vehicles on road in areas like Yau Ma Tei, Ho Man Tin and Kowloon City, so that it would improve the overall traffic condition and the environment.

6.3 In the Public Forum on Temporary reclamation in Kowloon Bay, the public agreed that there was urgent need to resolve the traffic congestion in the East-west traffic, and there was overriding public need for the construction of CKR.

6.4 Therefore, it was agreed with the public that there is an overriding public need for the construction of CKR.

No Reasonable Alternative to Reclamation

6.5 Harbourfront Commission stated that they would not challenge the justifications for the temporary reclamation required for the construction of CKR which were presented by the consultant and reviewed by two independent experts. These included the justifications on no reasonable alignment that did not require reclamation and no reasonable construction methods that did not require reclamation.

6.6 In the Professional Forum, professionals and academics generally agreed that there were no alternative construction and alignment options that did not require reclamation. They considered that tunnel boring machine (TBM) and immersed tube tunnel (IMT) were not reasonable construction methods for the underwater tunnel at Kowloon Bay.

6.7 In the Public Forum on Temporary reclamation in Kowloon Bay, the public agreed that there were no safe and reliable alternative construction and alignment options that did not require reclamation.

6.8 Therefore, it was agreed with the public that there was no reasonable alternative to reclamation.

Minimum Extent of Reclamation

6.9 Harbourfront Commission stated that they would not challenge the justifications for the temporary reclamation required for the construction of CKR which were presented by the

consultant and reviewed by two independent experts. These included the justifications on the proposed construction arrangement would involve minimal impairment to the Harbour.

6.10 In the Professional Forum, professionals and academics generally considered that the proposed temporary reclamation construction method would involve minimal impairment to the Harbour.

6.11 In the Public Forum on Temporary reclamation in Kowloon Bay, the public agreed that the extent of reclamation is the minimum.

6.12 Therefore, it was agreed with the public that the proposed extent of temporary reclamation is the minimum.

Phase 2 Public Engagement Exercise

6.13 We started the Phase 2 Public Engagement for CKR in early December 2012 to gather public views on the detailed design and construction arrangements of the project. A series of public engagement activities were carried out as scheduled, including over 10 focus group meetings with residents along the alignment of CKR, green groups, professional institutes and other stakeholders and five rounds of roving exhibitions at various locations in Yau Ma Tei, Ho Man Tin, To Kwa Wan and Kwun Tong.

6.14 We have also consulted Yau Tsim Mong, Kowloon City, Wong Tai Sin and Kwun Tong District Councils, as well as the Harbourfront Commission. We have also conducted three public forums on 12, 19 January 2013 and 2 February 2013 in Yau Tsim Mong District and Kowloon City District respectively to collect views from the general public on CKR. We would like to express our gratitude to different sectors of the community for their active participation and valuable comments.

Independent Expert Review

6.15 In the interest of the Protection of the Harbour Ordinance and as part of the public engagement activities associated with this report, two independent expert reviewers, Professor William H.K. LAM and Professor Charles W.W. NG, had been appointed to:

a) Provide a critical review of this report with consideration to the need for reclamation of Kowloon Bay for CKR.

b) Confirm that the argument for the proposed temporary reclamation is cogent and convincing.

c) Ascertain that the “overriding public need test” has been satisfied.

d) Confirm that there is no reasonable alternative to the reclamation.

e) Confirm that the proposed extent is the minimum requirement.

6.16 The Independent Expert Review Reports by Professor William H.K. LAM and Professor Charles W.W. NG are attached in **Appendix A** and **Appendix B** respectively.

Compliance with the PHO

6.17 In conclusion, it is clear that the three tests in rebutting the presumption against the reclamation as set out in the PHO have been satisfied:

- In facilitating the construction of the CKR and therefore in meeting the overriding public need for the route, there is consequently a compelling and present need for the reclamation in Kowloon Bay. All of the reclamation is temporary and will be removed upon completion of construction, with the seabed reinstated to the original level.

- No reasonable alternative to temporary reclamation is found for constructing the Underwater Tunnel Section of the CKR.

- The extent of reclamation has been determined to be the minimum required.

Appendix A

Independent Expert Review of Cogent and Convincing Materials Report for Temporary Reclamation at Kowloon Bay by Professor William H.K. LAM

PolyU Technology & Consultancy Company Ltd
理大科技及顧問有限公司

Traffic justification for the need of Central Kowloon Route –Independent Expert Review (Quotation Ref. Hy(S)Q/062/2012)

Project Ref. No.: **P12-0276**

William H.K. LAM
18 February 2013

1. Introduction

On 28th December 2012, Highways Department (HyD) of the Government of the Hong Kong Special Administrative Region appointed Ir Prof. William H.K. Lam of PolyU Technology & Consultancy Company Limited (PTeC), under Agreement No. Hy(S)Q/062/2012, to provide independent EXPERT review services in respect of traffic justification for the need of the Central Kowloon Route (CKR).

THE EXPERT has also been asked to comment on the minimum extent of temporary reclamation in relation to the length of the preferred alignment of CKR being the shortest and complying with the relevant highway design standards.

2. Description of the Project

CKR is a proposed dual 3-lane trunk road (including a tunnel section with 3.9km) across Central Kowloon linking the West Kowloon in the west and the proposed Kai Tak development in the east. Its western end at West Kowloon would connect to Yau Ma Tei Interchange and via the interchange traffic could access to Western Harbour Crossing, Tsim Sha Tsui, West Kowloon Reclamation Development Area, West Kowloon Highway, Route 8, and Route 3 respectively. Its eastern end at Kai Tak area, would connect to Kowloon Bay, Kowloon East, Kwun Tong Bypass, Tseung Kwan O (TKO) Tunnel, T2, and TKO-LTT respectively. CKR together with T2 and TKO-LTT would form a strategic highway link, namely Route 6, connecting West Kowloon and TKO new town.

The construction of CKR was previously targeted for completion in 2016. The current target is to start construction of CKR in early 2015 for completion and commissioning in end 2020.

3. Traffic Review

The following review was based on the draft updated traffic impact assessment (TIA) report for the Central Kowloon Route – Design and Construction (Ref: REP-081-00), the final

香港九龍紅磡理工大學 QR 棟 6 樓 QR603 室
QR603, 6/F, QR Core, The Hong Kong Polytechnic University, Hunghom, Kowloon, Hong Kong.
電子郵編 E-mail: ptec@inet.polyu.edu.hk 電話 Tel: (852) 3400 2704 / 3400 2714 傳真 Fax: (852) 2356 7583

report of supplementary traffic study for Central Kowloon Route (Ref. HMW 1/2010 (TT)), the revised draft report on updated economic assessment (Ref. REP-077-01), and the supplementary documents provided by THE CONSULTANT of Highways Department (HyD), Arup-Mott MacDonald Joint Venture.

3.1 Existing Road Network

The Central Kowloon area is currently served by the east-west Corridor ("the Corridor") comprising of major roads such as Lung Cheung Road, Boundary Street, Prince Edward Road West, Argyle Street & Flyover, Chatham Road North, East Kowloon Corridor, Gascoigne Road Flyover. This Corridor is primarily serving as a key east-west link with the responsibility of carrying the long-haul traffic between east and west of Kowloon peninsula.

At the same time, the Corridor also serves as a major link providing north-south connections to various local districts and providing key accesses to its adjacent areas with very short connecting roads. Unfortunately, the numerous junctions with side roads as well as underpasses and flyovers integrated with the Corridor create substantial weaving and merging movements. As a result, the Corridor is over-saturated and too heavily used by local traffic accessing its adjacent areas such that it is unable to perform its intended function for serving the long-haul east-west traffic. Traffic queues from any bottlenecks along the Corridor's side roads or its main section usually result in blockage of other movements and rapid deterioration of traffic condition.

A minor accident or incident occurs along or at the vicinity of the Corridor often results in serious congestion and delay in the road network, and in some more serious cases, gridlock of the whole Central Kowloon area and complete blockage of the Corridor (e.g. the serious incident at Prince Edward Road East on 9 May 2005). These are clear indications that the stability and reliability of both the strategic road network and the Central Kowloon local road network are in an unsatisfactory state.

3.2 Existing Traffic Pattern

PolyU Technology & Consultancy
Company Limited 理大科技及顧問有限公司

The existing Corridor is already operating beyond its design capacity. Regular traffic queues along the Corridor are found at major road junctions in the Corridor. The maximum queue length of these major road junctions are observed up to 200m long or above. These critical east-west approach arms of junction include:

- Lai Cheung Road EB of Hoi Wang Road / Lai Cheung Road junction;
- Ma Tau Chung Road SB of Ma Tau Chung Road / Sung Wong Toi Road junction;
- Austin Road WB of Austin Road West / Austin Road / Canton Road junction;
- Jordan Road EB of Jordan Road / Ferry Street / Canton Road junction;
- Jordan Road EB of Jordan Road / Nathan Road junction;
- Boundary Street EB of Boundary Street / Waterloo Road junction;
- Argyle Street EB of Argyle Street / Waterloo Road / Princess Margaret Road junction;
- Argyle Street WB of Argyle Street / Yim Po Fong Street junction;
- Mong Kok Road EB of Sai Yee Street / Mong Kok Road junction;
- Chatham Road North SB of Chatham Road North / Wuhu Street junction;
- Kai Cheung Road WB of Kai Cheung Road / Wang Chiu Road junction;
- Lam Fung Street EB (outside MegaBox) of Sheung Yee Road / Wang Chiu Road junction;
- Wai Yip Street EB of Wai Yip Street / Wai Fat Road junction; and
- Wui Cheung Road EB of Canton Road / Wui Cheung Road junction.

The above road junction capacity assessment indicates that some of the major road junctions are operating with close to or above capacity at the moment. Most of the junctions within the Central Kowloon area are generally more critical during the peak periods with low reserved capacities (R.C.) such as Argyle Street / Sai Yee Street, Argyle Street / Nathan Road, Austin Road / Chatham Road South / Cheong Wan Road.

These regular traffic queues occupy the road spaces of the Corridor and impose unacceptable delay to the through traffic between the eastern and western parts of Central Kowloon area.

3.3 Traffic Forecasts

The opening year of Central Kowloon Route is scheduled at end 2020/early 2021. The updated traffic impact assessment has been carried out by comparing the traffic forecast of

香港九龍紅磡理工大學 QR 棟 6 樓 QR603 室
QR603, 6/F, QR Core, The Hong Kong Polytechnic University, Hunghom, Kowloon, Hong Kong.
電子郵編 E-mail: ptec@inet.polyu.edu.hk 電話 Tel: (852) 3400 2704 / 3400 2714 傳真 Fax: (852) 2356 7583

reference (without CKR) and design (with CKR) scenarios. Based on standard traffic forecasting techniques, THE CONSULTANT has undertaken five sets of traffic forecasts to simulate the peak hour traffic situation at the Central Kowloon areas in future years. These test scenarios are listed below and their results are summarized in Table 1:

1. 2016 Reference Scenario: S2016 – constitute the pre-commissioning and construction stage of CKR scenario (i.e. without CKR and Route 6 components);
2. 2021 Reference Scenario: S2021/A – constitute the without CKR scenario and other components of Route 6;
3. 2021 Design Scenario: S2021/C – constitute the with CKR and TKO-LTT scenario whilst T2 is not in place as a conservative approach to test under this study;
4. 2026 Reference Scenario: S2026/A – constitute the without CKR and other components of Route 6 scenario; and
5. 2026 Design Scenario: S2026/G – constitute the with CKR and other component of Route 6 scenario.

Table 1 : Summary of Modeling Assumptions and Results of the 5 Test Scenarios

	CKR	Other components of Route 6	Road T2	TKO-LTT	Traffic Modeling Results	
					V/C Ratio of Major Road Sections along the Corridor	RC of Major Road Junctions in Central Kowloon
Scenario S2016	×	×	×	×	Many of road links with v/c ratio above 1.0.	Some of the critical junctions have negative RCs.
Scenario S2021/A	×	×	×	×	Most above 1.0. Some as high as 1.30.	18 critical junctions have negative RCs (6 with RC < -15%).
Scenario S2021/C	✔	✔	×	✔	Most of the road sections with v/c ratio below 1.0. Few as high as 1.1.	Many of the critical junctions have positive RCs (3 with RC < -15%).
Scenario S2026/A	×	×	×	×	Many of the road sections with v/c ratio above 1. Some as high as 1.40.	18 critical junctions have negative RCs (RC less than that of S2021A).
Scenario S2026G	✔	✔	✔	✔	Most of the west- bound road sections with v/c ratio below 1. Few above 1.20	Many of the critical junctions have positive RCs (3 with RC < -15%).

Notes: V/C Ratio = Volume over Capacity Ratio for road links; RC = Reserve Capacity for signal junctions

3.4 Summary of Findings

Due to the economic growth in future, it has predicted further increase in traffic demand in the east-west Corridor. As a result, most of the major roads in this Corridor (without CKR

by 2021) will be oversaturated ranging from 10% to 30 % during typical morning and evening peak hours.

For the design year scenarios (with CKR), there is a general improvement in the congestions in the study areas when comparing with the corresponding reference year scenario. The reserved capacities of the critical road junctions are generally increased when comparing with those of do-nothing / reference (without CKR) scenarios in the corresponding years of 2021 and 2026.

Considering the apparent improvement along the major road links and the corresponding locations of the congested road junctions, it is revealed that the junction problems are mainly induced by the population and employment growth of the subject areas, but not induced by CKR.

In the draft updated TIA report, THE CONSULTANT has also proposed some interim/long-term local traffic improvement measures at critical road links/road junctions. It is however considered that these measures are unable to replace the CKR in terms of overall traffic benefits to the road network in the Central Kowloon area.

THE CONSULTANT confirmed that the proposed CKR configuration is required to divert traffic away from the existing east-west Corridor and to provide adequate relief to it.

In addition, the provision of CKR can allow passengers to benefit from a shorter journey which is reflected in travel time savings. Based on the transport model developed by THE CONSULTANT, the average time savings due to the provision of CKR are estimated and shown in **Table 6** of the revised draft report on updated economic assessment (Ref. REP-077-01). It is noted that the annual time saving benefit shares of CKR from 2021 to 2060 are ranged from 23% to 29% for private cars only. Over 70% of these annual time saving benefit shares is mainly distributed to different types of commercial vehicles including: taxi, special purpose bus (e.g. coach), van, goods vehicles and public transport vehicles etc.

Table 6 Annual Time Savings (passenger hours) from 2021 to 2060 with CKR

Item	2021	2030	2040	2050	2060
Car	**(23%) 10470**	33,525	42,155	50,001	**(29%) 57847**
Taxi	4,362	12,652	15,981	19,008	22,035
Special Purpose Bus (SPB)	3,649	11,011	14,480	17,634	20,789
Van	1,100	3,661	4,658	5,565	6,472
Light Good Vehicle (LGV)	887	2,991	3,802	4,539	5,277
Medium Good Vehicle (MGV	715	2,096	2,670	3,191	3,713
Heavy Good Vehicle (HGV)	134	368	466	555	644
Tractor Unit (TU)	326	1,048	1,293	1,516	1,738
Public Transport (PT)	23,846	57,388	65,740	73,333	80,926
Total (100%)	**45,490**	124,740	151,246	175,343	**199,440**

Source: The revised draft report on updated economic assessment (Ref. REP-077-01)

4. Minimum Extent of Temporary Reclamation

4.1 Sites Constraints of CKR

In order to assess whether the minimum extent of temporary reclamation is used for construction of CKR, THE EXPERT has been asked to comment on the length of the preferred alignment being the shortest and complying with relevant highway design standards. It can be seen in the Figure 1 that the proposed S-curve alignment of CKR at the Kai Tak area has significant impacts on the minimum extent of temporary reclamation required. THE EXPERT recognized that there are at least four site constraints of the proposed CKR in relation to the length of the preferred S-curve alignment being the shortest. They are summarized as below:

(1) On the east end, CKR is required to link up with T2 to complete Route 6.

(2) One of the key connection for CKR is an interchange at Kai Tak. It connects to Kai Fuk Road, Kai Cheung Road, and roads to future Kai Tak Development. The CKR mainline has to climb up to ground level in order to make an interchange as shown in Figure 1.

(3) The route has avoid any resumption of existing residential buildings. Under this principle, there is no feasible non-subsea option and the option with the shortest underwater

section is to go under the corridor of the Kowloon City Pier (near the Public Transport Interchange, PTI) and towards the Kai Tak area.

(4) There is a constraint at the bend over the Kai Tak River. A minimum 15m promenade width has to be fulfilled. Therefore the reverse curve (S curve) in minimum desirable radii is required.

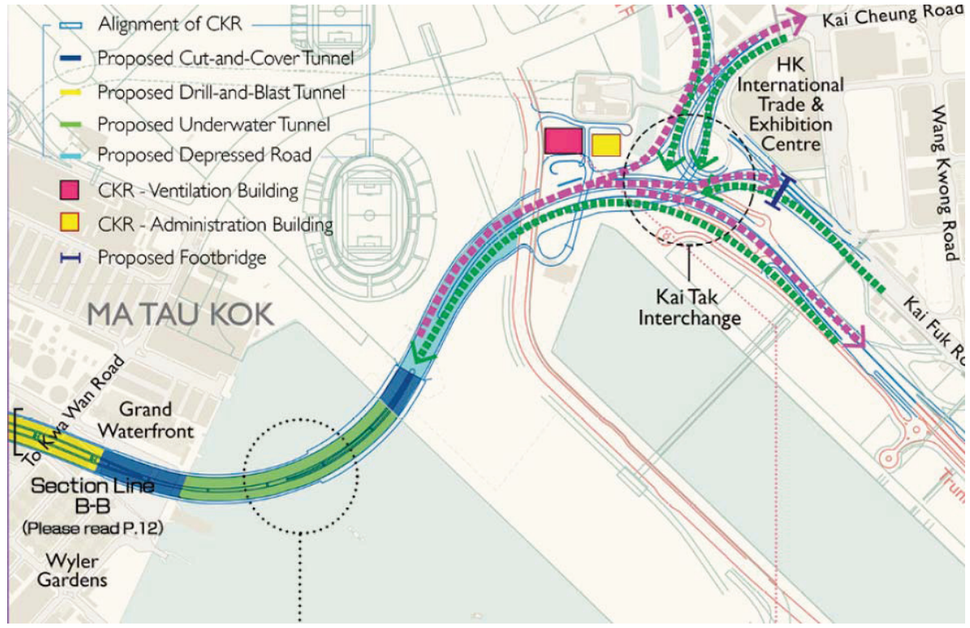

Figure 1 - The Proposed S-Curve Alignment of CKR at Kai Tak area

4.2 Highway Design Standards

In view of the proposed S-curve alignment of CKR at the Kai Tak area, there is a need to assess whether it can comply the relevant highway design standards (particularly on the minimum desirable radius of the S-curve) so as to justify the minimum extent of temporary reclamation used for construction of CKR. Given that the design speed of the CKR mainline is 80km/hr, the minimum radius of the S-curve used at the underwater section of CKR is 330m, and the maximum 4% gradient is about 900m long.

In Hong Kong, the Transport Planning Design Manual (TPDM) has different requirements for determining the design speed of highway.

- The design speed of a road is the speed chosen to correlate the various features of design of the road, such as the minimum radii of horizontal and vertical curves, superelevation, sight distance, gradient, signs and road markings etc. The following table (a) compares the design speeds adopted for rural and urban areas in Hong Kong (HK), United Kingdom (UK) and United States of America (USA).

(a) Design speed

	HK	UK	USA
Rural area	100 km/h	120 km/h	80 - 110 km/h
Urban area	70 km/h (80 km/h for new roads) or above	Less than 120 km/h	80 - 110 km/h

As CKR is located in Kowloon urban area for serving long-haul traffic travelling between east and west of Kowloon, it can be found in the above table (a) that the design speed of 80 km/hr for the CKR mainline is on the lower bound from the international highway design standards.

In order to counter-balance the centrifugal force at the horizontal curve of CKR in Kai Tak, the desirable maximum superelevation of 7% is chosen. As a result,

Desirable Minimum Radius of Horizontal Curve > Rmin = $V^2/2.822$ (7%)
CKR – Design Speed V = 80 km/hr; Rmin = $V^2/2.822$ (7%) = 324 m < 330 m

From the above analysis, it is shown that the minimum radius 330 m of the S-curve used at the underwater section of CKR is close to the desirable minimum radius of horizontal curve required.

On the other hand, it is required to check whether the minimum S-curve radius of 330 m can provide the minimum sight distance (***S***) at the underwater section of CKR for road safety

purpose. The following table (b) displays the minimum sight distances by design speeds adopted in HK, UK and USA.

(b) Sight distance

Design speed (km/h)	Minimum sight distance (m)				
	HK		UK		USA
	Desirable	Absolute	Desirable	Absolute	
120	295	215	295	215	250
110	-	-	-	-	220
100	215	160	215	160	185
90	-	-	-	-	160
85	160	120	160	120	-
80	145	110	-	-	130
70	120	90	120	90	105

As the design speed of CKR mainline is 80 km/hr, it is noted in the above table (b) that the minimum sight distance (***S***) which should not be less than 110 - 145 m is affected by the minimum curve radius (***R***) of 330m as shown below:

$$s = \sqrt{8RT}$$

Within the road tunnel of the underwater section of CKR, the clearance (***T***) from the centre of the nearside lane to the obstruction is equal to (3.65/2) + 3.0 + 1.7 = 6.525m.

By substitution of ***R=330*** and ***T=6.525m*** into the above equation, ***S*** is found to be ***131 m***. Therefore the minimum sight distance (***S***) is falling in the range between 110 m and 145 m.

Given that the design speed of CKR is 80 km/hr. Based on the table (c) below, the maximum desirable gradient of 4% is adopted for the option with the shortest underwater section in order to go under the corridor of the Kowloon City Pier PTI and climb up to the ground level at Kai Tak area.

(c) Gradients

Design speed (km/h)	Maximum gradient				
	HK		UK		USA
	Desirable	Absolute	Desirable	Absolute	
120	4%	8%	3%	4%	-
110					5%
70 - 100					between 5% and 12%

In view of the above analysis, it was demonstrated that the relevant highway design standards adopted for the proposed S-curve alignment of CKR at the Kai Tak area are considered as the desirable minimum so as to minimize the extent of temporary reclamation required for the construction of CKR.

5. Independent Review and Recommendations

5.1 Overriding Public Need

In order to assess the traffic impacts of the CKR project, THE CONSULTANT has conducted comprehensive surveys for calibration and validation of the local traffic model (LTM). It was shown that the model validation results are satisfactory with a maximum error of less than 10% in general. With the use of the calibrated LTM, THE CONSULTANT has made traffic forecasts and economic assessment for scenarios with and without CKR in future design years. It was demonstrated that CKR is essential for alleviation of the traffic congestion problem in the Central Kowloon area. THE EXPERT considers that the assumptions made by THE CONSULTANT to be reasonable and confirm in support of their results for the captioned project.

Previous strategic transport studies (e.g. CTS-3) have predicted further increase in traffic demand along the east-west Corridor, and confirmed the need for a east-west trunk road, the CKR, to avoid more extensive and frequent traffic congestion and even gridlock in the road network due to an incident (e.g. 9 May 2005) at the critical road link or major junction.

PolyU Technology & Consultancy
Company Limited 理大科技及顧問有限公司

The east-west Corridor serving the Central Kowloon areas is already operating beyond its capacity as can be observed on site. Congestion along the Corridor is not limited to the typical morning and evening peak hours of weekdays. It was reported in the 2011 Annual Traffic Census, the vehicular traffic flows travelling between east and west of Kowloon (crossing the screenline A-A) are saturated between 8:00 am and 7:00 pm during weekdays.

Based on the traffic forecasts of THE CONSULTANT for the year of 2021 with and without CKR, THE EXPERT has conducted the level-of-service (LOS) analysis on the screenline of the Corridor (for vehicles travelling between east and west of Kowloon). It was found that LOS D and F will be provided at this screenline in the year of 2021 with and without CKR respectively. The following table shows the criteria for different LOS.

Level of Service	V/C Ratio	Corresponding Traffic Condition
A	Up to 0.3	**Free-flow conditions** Travel speeds at the free-flow speed generally prevail Ability to manoeuvre within traffic stream almost unimpeded Minor disruptions are easily absorbed without change in speed.
B	>0.3 - 0.5	**Easy flow conditions** Travel speeds close to free-flow speed Ability to manoeuvre within traffic stream slightly restricted Minor disruptions are easily absorbed with localised reduction in speed.
C	>0.5 - 0.75	**Generally easy flow conditions.** Travel speeds begin to be restricted by traffic conditions. Ability to manoeuvre within traffic stream is noticeably restricted. Minor disruptions may cause local congestion with short traffic queues.
D	>0.75 – 0.9	**Well used flow conditions.** Travel speeds reduced by increasing traffic volumes. Ability to manoeuvre within traffic stream is severely restricted. Minor disruptions may cause local congestion with traffic queues.
E	>0.9 - 1.1	**Unstable flow conditions.** Travel speeds substantially reduced and are highly variable & unpredictable. Little or no room to manoeuvre within traffic stream. Minor disruptions will cause substantial congestion with long traffic queues.
F	> 1.1	**Forced or breakdown flow conditions.** Crawling travel speed. Highly unstable traffic operations with widespread congestion and extensively long traffic queues.

THE EXPERT regards the LOS F at the Corridor without CKR by the year 2021 to be ineffectual and socially undesirable.

Traffic management measures are already in place to maximize the capacity of the existing road network and suppress the peak hour traffic demand. All these existing measures, however, cannot resolve the traffic congestion problem along the existing east-west

香港九龍紅磡理工大學 QR 棟 6 樓 QR603 室
QR603, 6/F, QR Core, The Hong Kong Polytechnic University, Hunghom, Kowloon, Hong Kong.
電子郵編 E-mail: ptec@inet.polyu.edu.hk 電話 Tel: (852) 3400 2704 / 3400 2714 傳真 Fax: (852) 2356 7583

Corridor. Hence, the CKR is essential, even the Journey Time Indication System (JTIS) and Electronic Road Pricing (ERP) can complement the CKR but cannot replace it. It is because without CKR, there is no reserved capacity at the existing Corridor to cater for the private car and commercial vehicular traffic.

It is also noted in the 2011 Annual Traffic Census, over 60% of vehicular traffic travelling between east and west of Kowloon (crossing the screenline A-A) is commercial vehicles (i.e. taxi, public light buses, goods vehicles, coaches and buses). In order to cater for the commercial traffic demand generated by economic growth in future, there is a need to provide CKR for improving the network connectivity and reliability of the east-west Corridor in Kowloon Peninsula. However, the EXPERT recommends that Government should address the need to regulate land-use developments throughout the Corridor areas in order not to aggravate the congestion problem in the Corridor before the opening of CKR.

In general, THE EXPERT agrees with the findings of the TIA for the dual-3 CKR project. THE EXPERT recognizes the need for the CKR project from traffic ground so as not to bring unacceptable traffic congestion to the Central Kowloon areas.

5.2 Minimum Extent of Temporary Reclamation

In view of the above 4 site constraints of CKR, the reverse curve (S curve) in minimum desirable radii is required for minimum extent of temporary reclamation in relation to the length of the preferred alignment being the shortest and complying with the relevant highway design standards.

In order to minimize the extent of temporary reclamation used for construction of CKR, the design parameters (e.g. design speed of 80 Km/hr, curve radius of 330 m and maximum gradient of 4%) adopted for the proposed S-curve alignment of CKR in Kai Tak area are acceptable but are on the lower bound of the desirable minimum in comparison with the international highway design standards.

The minimum extent of temporary reclamation for the Central Kowloon Route is therefore justified in relation to the relevant site constraints and highway design standards for road safety purpose.

香港九龍紅磡理工大學 QR 棟 6 樓 QR603 室
QR603, 6/F, QR Core, The Hong Kong Polytechnic University, Hunghom, Kowloon, Hong Kong.
電子郵編 E-mail: ptec@inet.polyu.edu.hk 電話 Tel: (852) 3400 2704 / 3400 2714 傳真 Fax: (852) 2356 7583

PolyU Technology & Consultancy
Company Limited 理大科技及顧問有限公司

5.3 Conclusions

(1) It was found that when the V/C ratio (Volume over Capacity Ratio) for road links or reserve capacity of the major intersections is close to 0.9 or less than 10%, there will be unstable flow conditions with stochastic long traffic queues. These unstable conditions will be getting worse and unacceptable in the future years without the opening of CKR.

(2) In conclusion, the dual-3 CKR project is justified for overriding public need from the traffic ground in order to provide reserved capacity at the Corridor for catering the increasing traffic demand due to the economic growth in future. Moreover, THE EXPERT reckons that THE CONSULTANT's traffic forecasts may even be under-estimated as the effects of the recent increase in the economic growth and further development plan in Hong Kong have not been considered in the drafted and supplementary TIA reports.

(3) Finally, THE EXPERT agrees that the S-curve of CKR (at Kai Tak area) in minimum desirable radii is justified for minimum extent of temporary reclamation in relation to the length of the preferred alignment being the shortest and complying with the relevant highway design standards. THE EXPERT recognizes that the minimum extent of temporary reclamation for the Central Kowloon Route is adopted on the basis of the relevant site constraints and highway design standards for the road safety purpose.

********** END **********

香港九龍紅磡理工大學 QR 棟 6 樓 QR603 室
QR603, 6/F, QR Core, The Hong Kong Polytechnic University, Hunghom, Kowloon, Hong Kong.
電子郵編 E-mail: ptec@inet.polyu.edu.hk 電話 Tel: (852) 3400 2704 / 3400 2714 傳真 Fax: (852) 2356 7583

Prepared by

Ir Professor William H.K. Lam
BSc, MSc, PhD, CEng
Chair Professor of Civil & Transportation Engineering
Department of Civil and Environmental Engineering
The Hong Kong Polytechnic University
Yuk Choi Road
Hung Hom, Kowloon
HONG KONG
Tel : (852) 2766-6045
Fax : (852) 2334-6389
E-mail: cehklam@polyu.edu.hk
Web Site: www.cse.polyu.edu.hk/~cehklam

Appendix B

Independent Expert Review of Cogent and Convincing Materials Report for Temporary Reclamation at Kowloon Bay by Professor Charles W.W. NG

Independent Expert Review Report

Review of Construction Method for the Central Kowloon Route (CKR)

Table of Contents

By
Charles W.W. Ng, Ph.D, CEng, FICE, FASCE, FHKIE, FHKEng
Chair Professor of Civil and Environmental Engineering of Hong Kong University of Science and Technology (HKUST)
Director of Geotechnical Centrifuge Facility (HKUST)
Changjiang Scholar (Chair Professorship)
Overseas Fellow of Churchill College, Cambridge University, UK
Fellow of Hong Kong Academy of Engineering

1. Introduction

The Highways Department (HyD) of HKSAR proposes to construct a 4.7 km long dual three-lane trunk road across central Kowloon, linking West Kowloon to the proposed Kai Tak Development (KTD) in the east. The trunk road will start from the Yau Ma Tei Interchange, link to the future Trunk Road T2 at KTD, which will then connect with the future Tseung Kwan O – Lam Tin Tunnel. These trunk roads will form part of a strategic highway link called Route 6, connecting West Kowloon and Tseung Kwan O.

The Highways Department appointed a Joint Venture (JV) consisting of consultants from Mott MacDonald – Meinhardt – Hyder to carry out a preliminary design under the Agreement No. CE58/2006(HY) – Central Kowloon Route (CKR) and Widening of Gascoigne Road Flyer in 2007 and subsequently appointed Arup - Mott MacDonald Joint Venture (AMMJV) to start detailed design at the end of 2010 under the Agreement No. CE43/2010 (HY).

This reviewer has been engaged as an Independent Expert since the preliminary design stage (Ng, 2009). For the proposed CKR, there are two major technical challenges including the selection of appropriate alignment, near Kowloon City and Kowloon Bay in particular, and the corresponding construction method to be adopted. In previous independent expert review report (Ng, 2009), the need of the CKR and the selection of alignments have been discussed and concluded. In this current report, the construction methods proposed by the AMMJV are independently and critically reviewed.

2. Review Principles and Documents

During this independent review, the following four documents have been reviewed carefully:

- Central Kowloon Route – Design and Construction: Draft Geotechnical Risk Management for Tunnel Works (27 July 2012)
- Central Kowloon Route – Design and Construction: Revised Draft Report on Updated Economic Assessment (24 October 2012)
- Central Kowloon Route – Design and Construction: Final Updated Cogent and Convincing Materials for Temporary Reclamation in Kowloon Bay (21st December 2012)
- Central Kowloon Route – Construction of Underwater Tunnel at Kowloon Bay prepared for Professional Forum held on 11 January 2013

In addition, this Reviewer attended a meeting with Harbourfront Commission held on 7 January 2013, a Professional Forum conducted on 11 January and two Public Forum held in Yau Ma Tei and Kowloon City on 12th and 19th January 2013, respectively.

In this report, independent research works, findings and publications by this Reviewer are also used to insist in the assessment described.

3. Local Geology and Ground Conditions at Kowloon Bay

This reviewer carried out an **independent** site investigation in the Kowloon Bay area for a separate research project to investigate the performance of a 40 m long barrette in Kowloon Bay in 1999. Fig 1 shows the location of a pile load test of the 40 m deep barrette conducted by Ng et al. (2000) on the Kowloon peninsula to the east of a runway of the old Kai Tak airport whereas Fig. 2 illustrates observed ground conditions from borehole logs and measured STP-N (standard penetration) numbers. A copy of the paper is enclosed in Appendix. The measured vertical and horizontal ground movements due to the construction of the barrette are reported by Ng et al. (1999). As shown in Fig. 2, the site is on marine reclaimed land and the ground level is at approximately 4.5m above Principal Datum (PD). The ground water level is at about 3m below ground surface. The ground conditions consist of about 6.0m fill material overlying a succession of approximately 9.5m marine clay deposits, 7.5m of sandy clay (probably alluvial), 4.8m alluvial sand of Quaternary age, and about 12m of weathered granitic saprolite which overlie granitic rocks of Upper Jurassic to Lower Cretaceous age. It can be seen from the figure that measured SPT-N values are low and scattered in all soil strata. As the first approximation, the undrained shear strength (in terms of kPa) of soils may be correlated to SPT-N values by a factor of 4 empirically, it is obvious that the shear strength of the first 30-40m depth of the ground is low in the Kowloon Bay area. This is supported by the back-analysed effective shear strength parameters (c' and ϕ') from three-dimensional numerical analyses of the performance of a diaphragm wall panel constructed at Kowloon Bay (see Fig. 11 of Ng et al., 1999). Other details of the ground response are given in the paper, which is enclosed in Appendix. In addition, from borehole information collected at the test site reported by Ng et al (1999), it is evident that the depth to rock head can increase significantly at the Kowloon Bay area. The findings from these previous investigations are consistent with those concluded by the AMMJV consultants.

4. Selection of Construction Methods

Any construction method selected for underground structures such as tunnels must consider ground conditions and soil/rock properties. As for the CKR is concerned, the ground conditions are fairly good for tunnelling at the west of the proposed route since the rock head there is very high. However, the ground conditions deteriorate quite dramatically beyond To Kwa Wan Road to the east. The depth of rock head drops to about 50m below the sea level in the Kowloon Bay area.

Regarding the selection of the best tunnel alignment option for the proposed CKR, there are some governing constraints that were identified in the areas of Kowloon City and Kowloon Bay. These constraints that must be addressed and resolved are listed as follows:

- Congested areas, private lands and buildings – all these mean that any required demolition of buildings and consumption of lands for the proposed CKR will face ownership problems, and possible ground movements/building damages due to construction must be addressed carefully as public risk will be involved.
- Poor ground conditions at the east end of the proposed Route – deep rock head and thick weak soil layers (low shear strength) as discussed in Section 3 above, i.e., shallow bored tunnelling is not suitable with economy and safety.
- Road gradient limit must be observed for safe and proper designs.

Among over 40 alignments studied by previous JV, there are five preferred options (i.e., A-E) as described in the CCM report. Although alignment A (i.e., the In-land option which consists of a number of routes) can avoid the need for temporary reclamation, there is no enough rock cover to protect building foundations above in the affected areas. If the cut and cover method is selected, there is a strong likelihood of demolition of some private buildings along its route. This is almost an impossible task to accomplish it within a reasonable time frame and cost. Moreover, as alignment A requires steep road gradient for the road level of the CKR to match with the road level at Kowloon Bay and T2 trunk road, these requirements essentially rules out the feasibility of this option. Also proposed depressed road section will conflict with the proposed multi-purpose stadium complex at the Kai Tak development.

For alignments C, D and E, they are required to pass through many private lands and buildings. Any demolition of private buildings and consumption of private lands will face ownership difficulties and problems. Other tunnel construction problems associated with these three alignments are discussed later. Therefore, these three alignments should not be considered further.

Given alignment B is the only viable option, three possible construction methods were considered and investigated by the AMMJV consultants. They are listed as follows:

(i) immersed tube tunnel (IMT),
(ii) bored/drill-and-blast tunnel
(iii) the cut-and-cover cofferdam methods (temporary reclamation needed)

They former two methods will not require reclamation but the latter one needs limited amount of temporary reclamation in the Kowloon Bay area. The proposed IMT will involve a large quantity of dredging of marine bed for up to 30m deep and up to 220m wide. The dredging of this large quantity of materials may impose serious environmental problems and the disposal of the dredged materials will not be an easy task. To facilitate the required bulk dredging, Kowloon City Ferry Pier, HKCG Jetty and the Ma Tau Kok Public Pier will have to be demolished and the permanent seawall at Ma Tau Kok needs stabilization work for minimizing excessive ground movements. Comparing with the amount of dredging involved for alignment B, the quantity of dredging required for any alignment C, D and E will be much larger.

For the bored/drill-and-blast tunnel method, favorable ground conditions are required to provide sufficient cover and hence safety. Given the high water table, poor ground conditions and soil properties at Kowloon Bay, closed face tunneling using either slurry or earth pressure balance bored tunnel should be considered (see Fig. 3). A large diameter tunnel boring machine shown in Fig. 4 serves as a reference. Due to the dual 3-lane trunk road configuration and the elevation requirement at the Kai Tak Interchange in the East, these led to an unfavorable but no other alternative design option as given in Fig. 5, in terms of the required super large-diameter (up to 20.5m) bored tunnel at the west and very small cover to diameter (C/D) ratio (i.e., less than 1.5) at the east of Kowloon Bay. It will be extremely difficult and risky to apply a constant pressure inside the tunnel face to balance a triangular distribution of earth and water pressures outside the tunnel face. These unfavorable conditions impose considerable construction risk to construction personnel and the public. For instance, a major blowout failure at the tunnel head occurred on 23rd

February 1998 during the construction of Docklands Light Rail extension in the UK (see Figs 6 and 7). Due to the insufficient overburden above the bored tunnel using a slurry shield (i.e., small C/D ratio), blowout failure (or passive failure) occurred and a 22m diameter and 7m depth crater was created in the playground of a local school at 5am in the morning and windows located at 100m away were damaged due to the failure (ICE, 1998; 2004). It is not difficult to imagine that the failure may have caused substantial injuries or even casualties if it happened when pupils were gathering in the playground during normal schooling hours. It should be note that the diameter of bored tunnel used at Docklands Light Rail extension was only 5.2m which is significantly smaller than the one (up to 20.5m diameter) proposed for the CKR in Kowloon Bay.

Recent **independent** research carried out to investigate passive failure (or blowout) due to the advancement of a 4.46m diameter tunnel at the Geotechnical Centrifuge Facility in the Hong Kong University of Science and Technology (see Fig 8) also reveals that passive failure mechanism is governed by C/D ratio and difficult to be predicted (Wong et al., 2012; Ng & Wong, 2012). The smaller the C/D ratio, the higher the risk will be during construction. Deepening the vertical profile of tunnel in Kowloon Bay for the CKR to achieve adequate rock cover is also not a viable option since a deeper tunnel alignment will make it impossible to link with the road interchange at Kai Tak.

Some engineers may consider grouting and/or ground freezing techniques to be used in Kowloon Bay prior to tunnelling. These techniques are very risky, and most importantly, they may cause environmental problems in the Bay. Worldwide tunnelling experience illustrates that bored tunnel construction in shallow and poor ground conditions is an extremely dangerous and risky method. It should be also noted that this TBM option for the proposed CKR is not a feasible option since the required tunnel diameter will be up to 20.5m. At present, there is no such large diameter tunnelling boring machine available in the world. Therefore, any shallow tunnelling work beyond the To Kwa Wan Road in the Kowloon Bay can be very risky, time consuming and costly for any of alignments B, C, D and E. In addition, there will be floating problems associated with such a large diameter hollow bored tunnel, should it be selected.

It is this Reviewer's opinion that the only reasonable and viable option proposed by the AMMJV consultants is the use of cut and cover tunnel together with vertical stiff diaphragm wall cofferdam. This is a well-known technique locally and internationally. Hong Kong engineers and contractors are familiar and experienced with it and hence it can be a low risk operation. The proposed two-stage construction of the diaphragm wall cofferdam can minimize adverse effects on water circulation in the Bay. Although temporary reclamation (1.8 and 2.0 hectares for Stages 1 and 2, respectively) is required, this method can minimize the amount of dredging by more than 300% as compared with that of the IMT method. The proposed duration for each stage of works (i.e., 26 months each) is reasonable, given the current knowledge of design constraints and parameters, and ground conditions and soil properties.

Regarding the proposed width and extent of reclamation for construction, the proposed underwater cut and cover tunnel is very effective to minimize the reclamation since the tunnel will be cast directly against the vertical diaphragm wall, eliminating the need of formwork and hence minimizing the width of reclamation. This independent Reviewer is satisfied and convinced that there is no other reasonable alternative and the proposed method of using vertical diaphragm wall can minimize impairment and reclamation. It

should also be pointed out that the extent of temporary reclamation is the smallest among all proposed alignments such as C, D and E in the Kowloon Bay.

Concerns were raised about building safety and integrity due to tunnelling underneath Celestial Heights during the Public Forum held for the Kowloon City District on 19 January 2013. Based on **independent** research carried out by this Reviewer recently on tunnelling effects on piles (Ng et al., 2012), one can be assured that boring tunnelling in good quality of rock should not impose any unreasonable threat to building safety and integrity if the design and construction were carried out properly.

5. Conclusions

Based on the cogent and convincing materials provide and reviewed, and also **independent** research work carried out, this Reviewer is convinced that the selection of the alignment B and the proposed use of cut and cover tunnel construction method with temporary reclamation pass the three tests: (i) compelling, overriding and present need, (ii) no reasonable alternative and (iii) minimum impairment and reclamation. There is no other reasonable alternative to the proposed CKR and the proposed reclamation is the minimum.

References

1. ICE (1998). Bulkhead location blamed for DLR blast. New Civil Engineer, Institute of Civil Engineers, February Issue, 3-4.
2. ICE (2004). Docklands tunnel blowout down to "elementary error", says judge. New Civil Engineer, Institute of Civil Engineers, January Issue, 8-9.
3. Ng, C.W.W., Rigby, D., Lei, G. & Ng, S. W.L. (1999). Observed performance of a short diaphragm wall panel. *Géotechnique.* Vol. 49, No.5, 681-694.
4. Ng, C.W.W., Rigby, D., Ng, S. W.L & Lei, G. (2000). Field studies of well-instrumented barrette in Hong Kong. *Journal of Geotechnical and Geo-environmental Engineering, ASCE*. Vol. 126, No. 1, 60-73.
5. Ng, C.W.W. (2009). *Independent Expert Review Report: Review of Construction Method for the Central Kowloon Route*. Highways Department.
6. Ng, C. W. W. & Wong, K.S. (2012). Investigation of passive failure and deformation mechanisms due to tunnelling in clay in centrifuge. *Canadian Geotechnical Journal.* Provisionally Accepted.
7. Ng, C.W.W., Lu, H. & Peng, S.Y. (2012). Three-dimensional centrifuge modelling of twin tunnelling effects on an existing pile. *Tunnelling and Underground Space Technology.* In Press. http://dx.doi.org/10.1016/j.tust.2012.07.008.
8. Wong, K. S., Ng, C. W. W., Chen, Y.M. & Bian, X.C. (2012). Centrifuge and numerical investigation of passive failure of tunnel face in sand. *Tunnelling and Underground Space Technology.* Vol. 28, 297-303.

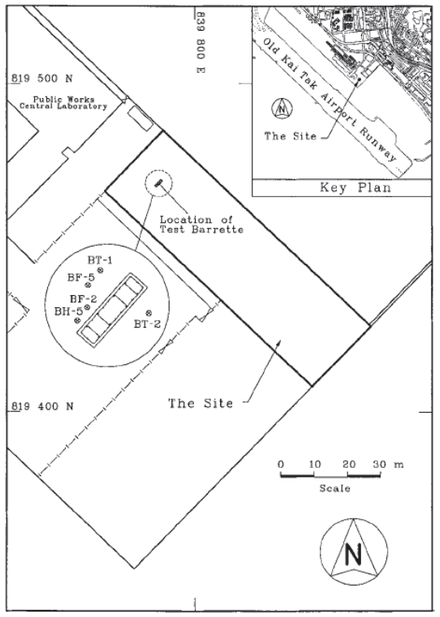

Fig. 1 Independent Study -Ground Conditions at Kowloon Bay (Ng et al, 2000)

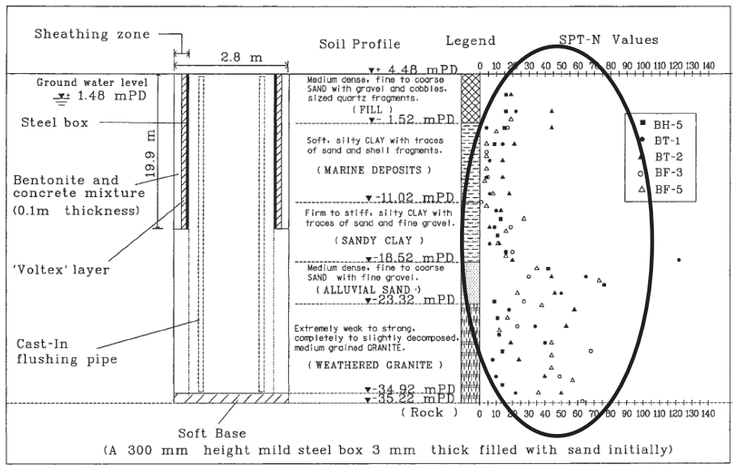

Fig. 2 Poor Ground Conditions at Kowloon Bay (Ng et al, 2000)

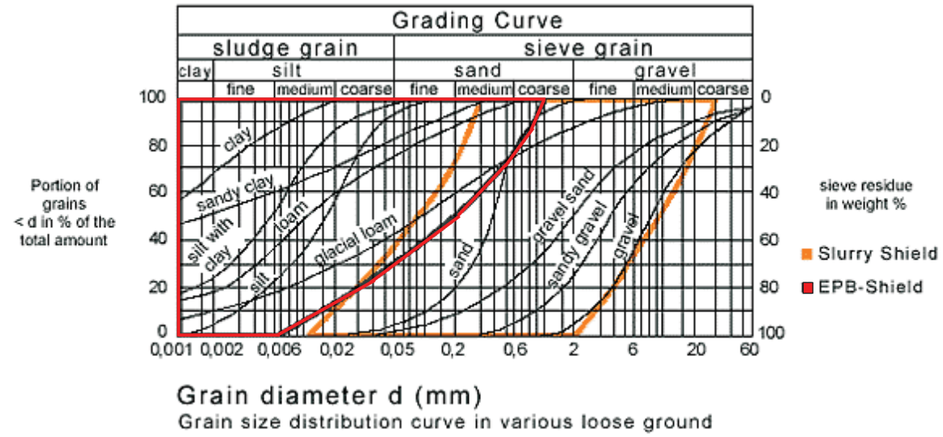

EPB is generally applicable for clay to clayey sand where permeability is relatively low

Fig. 3 Grading Curve Related to the Choice of EPB Shield

Fig. 4 Tunnel Boring Machine (about 14m Diameter)

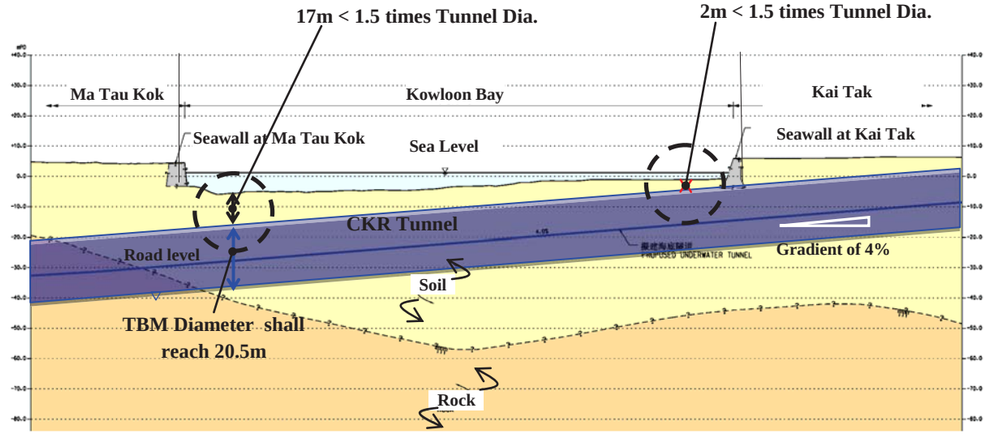

Bored tunnel method is not feasible since tunnel with large diameter (20.5 m) constructed in thick soft soil underlained by rock (very risky)

Fig. 5 Proposed Bored Tunnel Construction Method for CKR

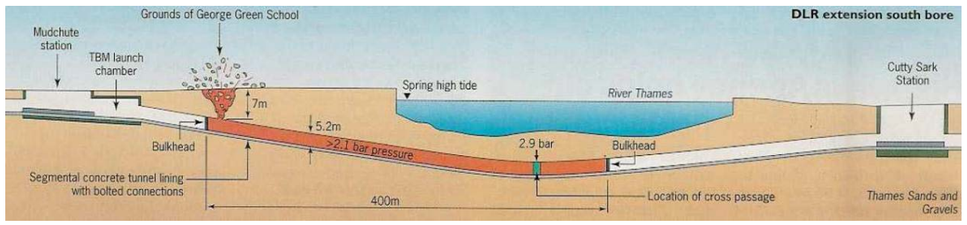

ICE (1998)

- Diameter = 5.2 m
- Slurry shield boring machine using compressed air

Possible causes of failure

- Insufficient overburden above the tunnel
- High compressed air pressure (2.2 bar) within tunnel causing blowout failure

Fig. 6 Blowout Failure of Docklands Light Rail (extension) on 23 Feb. 1998 in UK

The compressed air blast left a huge crater in a Docklands school playing field.

The crater is 22 m wide and 7 m deep in the playground of a school

Massive crater due to compressed air blast

- ICE (1998). Bulkhead location blamed for DLR blast. New Civil Engineer, Institute of Civil Engineers, February Issue, 3-4.
- ICE (2004). Docklands tunnel blowout down to “elementary error”, says judge. New Civil Engineer, Institute of Civil Engineers, January Issue, 8-9.

Fig. 7 Crater Formed in the Playground of George Green School (ICE, 1998 & 2004)

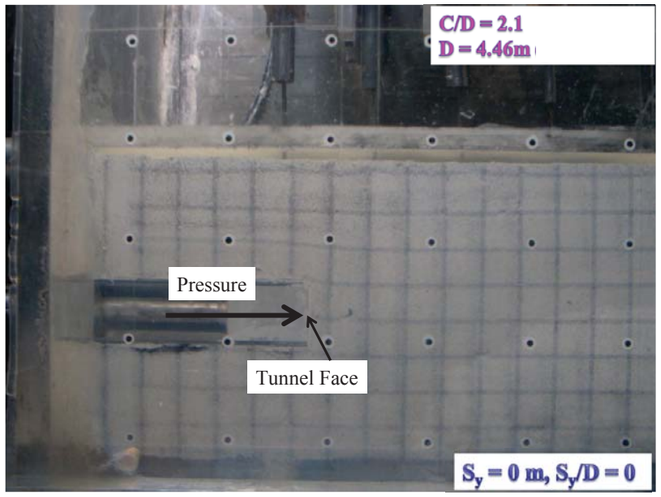

(a)

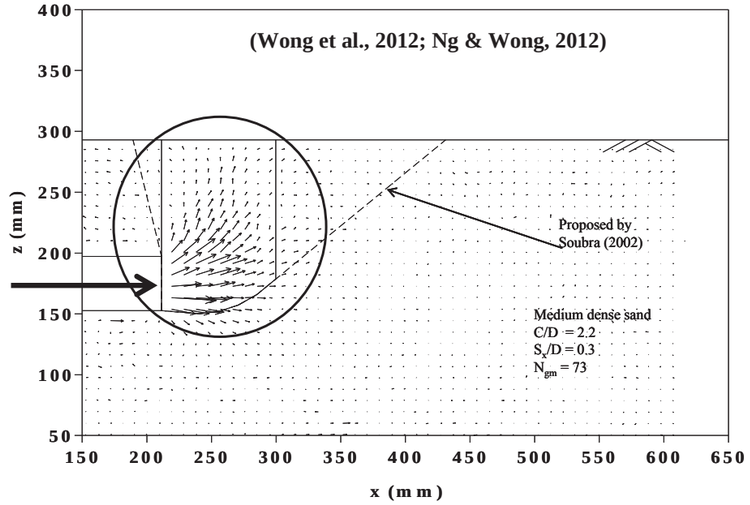

(b)

1. Ng, C. W. W. & Wong, K.S. (2012). Investigation of passive failure and deformation mechanisms due to tunnelling in clay in centrifuge. *Canadian Geotechnical Journal.* Provisionally Accepted.
2. Wong, K. S., Ng, C. W. W., Chen, Y.M. & Bian, X.C. (2012). Centrifuge and numerical investigation of passive failure of tunnel face in sand. *Tunnelling and Underground Space Technology.* Vol. 28, 297-303.

Fig. 8(a) Passive Failure (blowout) of Tunnel Face; (b) Measured displacement vectors leading to blowout

Appendix

a. **Ng, C.W.W**., Rigby, D., Lei, G. & Ng, S. W.L. (1999). Observed performance of a short diaphragm wall panel. *Géotechnique.* Vol. 49, No.5, 681-694.

b. **Ng, C.W.W**., Rigby, D., Ng, S. W.L & Lei, G. (2000). Field studies of well-instrumented barrette in Hong Kong. *Journal of Geotechnical and Geo-environmental Engineering, ASCE*. Vol. 126, No. 1, 60-73.

c. **Ng, C.W.W**., Lu, H. & Peng, S.Y. (2012). Three-dimensional centrifuge modelling of twin tunnelling effects on an existing pile. *Tunnelling and Underground Space Technology.* In Press. http://dx.doi.org/10.1016/j.tust.2012.07.008.

d. Wong, K. S., **Ng, C. W. W**., Chen, Y.M. & Bian, X.C. (2012). Centrifuge and numerical investigation of passive failure of tunnel face in sand. *Tunnelling and Underground Space Technology.* Vol. 28, 297-303.

Ng, C. W. W., Rigby, D. B., Lei, G. H. & Ng, S. W. L. (1999). *Géotechnique* **49**, No. 5, 681–694

Observed performance of a short diaphragm wall panel

C. W. W. NG,* D. B. RIGBY,* G. H. LEI* and S. W. L. NG*

The construction in Hong Kong of a 40 m deep excavated, large, rectangular-section barrette (i.e. a short diaphragm wall panel, 2·8 m long by 0·8 m wide) in sedimentary and weathered soils under bentonite has been heavily instrumented and closely monitored. During excavation, the maximum measured horizontal ground movements were only a few millimetres, with similar subsurface settlements around the panel. On the basis of three-dimensional numerical simulations of the excavation of the trench, an average mobilized shear strain greater than 0·1% around the excavated trench can be deduced. At the soil–wall interface, the initial lateral earth pressures decreased to hydrostatic bentonite pressures during excavation and increased above their initial K_0 pressures after concreting. The measured lateral pressures just after concreting support a theoretical bilinear pressure envelope.

KEYWORDS: deformation; diaphragm and *in situ* walls; earth pressure; numerical modelling; pore pressures.

La construction d'une barrette à grande section rectangulaire excavée à 40 m de profondeur (c'est-à-dire d'un court panneau de mur souterrain de 2,8 m de long par 0,8 m de large) dans des sols sédimentaires et désagrégés sous de la bentonite a fait l'objet de nombreux contrôles aux instruments et a été observée de près à Hong Kong. Pendant l'excavation, les mouvements horizontaux maximum du sol qui ont été mesurés n'ont été que de quelques millimètres, avec des tassements similaires sous la surface autour du panneau. En nous basant sur des simulations numériques en trois dimensions de l'excavation de la tranchée, nous avons pu déduire une déformation de cisaillement mobilisée moyenne supérieure à 0,1% autour de la tranchée excavée. À l'interface sol-mur, les pressions terrestres latérales initiales baissent pour arriver au niveau des pressions de bentonite hydrostatiques pendant l'excavation et elles passent au-dessus de leurs pressions K_0 initiales après le bétonnage. Les pressions latérales mesurées juste après le bétonnage soutiennent la théorie d'une enveloppe de pression bilinéaire.

INTRODUCTION

The use of slurry trenches to construct diaphragm walls for underground structures has become a well-known technique in civil engineering. The construction of the diaphragm walls will inevitably cause initial stress changes and deformations in the ground (Clough & O'Rourke, 1990; Farmer & Attewell, 1973; Ng, 1992; Stroud & Sweeney, 1977; Symons & Carder, 1993). Various techniques, such as numerical modelling (Ng, 1992; Ng *et al*., 1995) and centrifuge modelling (Powrie & Kantartzi, 1996), have been attempted to investigate stress transfer mechanisms and ground deformations due to diaphragm walling. Field monitoring of different panel sizes in different ground conditions is vital to provide essential data for verifying numerical and centrifuge results. In the Far East, well-documented case histories of diaphragm walling are rarely reported in the literature, with one exception. Stroud & Sweeney (1977) carried out a detailed field trial of a diaphragm wall panel, 6·1 m long by 1·2 m wide and about 36 m deep, constructed at Chater Road on Hong Kong Island. Maximum horizontal subsurface movements of 28 mm and 10 mm were recorded at 1 m and 2 m, respectively, away from the face of the trench at about 16 m below ground level. A settlement trough with a maximum value of 6 mm was observed 3 m away from the face of the trench.

Recently the authors have had the opportunity to measure ground deformations and stress changes during the construction of a large, excavated, rectangular-section pile (barrette) for a University-led and industry-supported research project (Shen *et al*., 1998). The excavation and concreting procedures used for the barrette were identical to those used in the construction of a diaphragm wall panel. The barrette was tested for its ultimate vertical load capacity three weeks after construction. However, in this paper, only the performance of the short diaphragm wall panel during construction is documented as a case history. The observed ground deformations during the excavation of the trench of the diaphragm wall panel are compared with a three-dimensional numerical analysis. Moreover, stress and pore water changes at the soil/wall interface during concreting are reported and discussed.

Manuscript received 24 September 1998; revised manuscript accepted 16 February 1999.
Discussion on this paper closes 30 April 2000; for further details see p. ii.
* Hong Kong University of Science and Technology.

SITE LOCATION AND GROUND CONDITIONS

The site is located on the Kowloon peninsula of Hong Kong, to the east of a runway of the old Kai Tak International Airport, adjacent to the Public Works Central Laboratory at Kowloon Bay (Fig. 1). Figs 2 and 3 show a cross-section of the test barrette and the location of some relevant boreholes, together with uncorrected N values from standard penetration tests (SPTs) measured in each soil stratum. The site is on marine reclaimed land and the ground level is at approximately 4·5 m above sea level or Principal Datum (PD). The groundwater level is at about 3 m below the ground surface. The ground conditions consist of, in succession, approximately 6 m of fill material, 10 m of marine deposits, 12 m of alluvium of Quaternary age and 12 m of weathered granitic saprolites overlying granitic rocks of Upper Jurassic to Lower Cretaceous age (Strange, 1990). The ground succession is similar to the site at Chater Road (Stroud & Sweeney, 1977).

It can be seen from Fig. 2 that very scattered SPT N values were obtained in both the alluvium sand and the weathered granite. It should be noted that the idealized geological strata shown in the figure may only be applicable to a local area around the trench. From borehole information, the depth to the rock head has been found to increase quite significantly from the south-east to the north-west direction at the site. The initial horizontal stresses in the ground are not known for certain at Kowloon Bay. However, it is generally believed that the initial K_0 values are less than 0·5 for soils in Hong Kong (Geotechnical Engineering Office, 1993).

DETAILS OF CONSTRUCTION

The test barrette or diaphragm wall trench was excavated using a traditional cable-operated grab. The size of the excavated trench was 2·8 m by 0·8 m in plan and 39·7 m deep (Figs 2 and 3). During construction, the trench was temporarily supported by bentonite slurry with a unit weight (γ_b) of 10·8 kN/m^3. Soil spoil, suspended in the bentonite slurry, was removed after pumping to a desanding unit at the ground surface. After desanding, the bentonite was recharged into the trench. Chiselling of the base took place when the excavated depth reached about 39·6 m below ground level. This caused a small overbreak at the base which was detected by a sonic profiling system. When the excavation reached its final level (39·7 m below ground level), three instrumented reinforcement cages were lowered and spliced together one by one into the trench, which was then concreted at an average rate of 10·32 m/h (or 23·12 m^3/h) using a tremie pipe. The ordinary Portland cement (OPC) concrete used was grade C30/20 (design $f_{cu} = 30$ MPa) with a unit weight (γ_c) of 23·2 kN/m^3. It had a water-to-cement ratio of 0·47 and an average slump of 180 mm. The average uniaxial compressive strength measured from a core taken from the centre of the barrette was 37·5 MPa at 28 days. During concreting, the average temperature measured inside the trench was 27·6°C. The excavation and concreting procedures of the barrette were in fact identical to those of the construction of a typical diaphragm wall panel.

At the upper reinforcement cages, a sheathing zone was formed (see Fig. 2) with the intention of minimizing the skin friction developed between the pile and the upper layers of the surrounding soil during axial load testing.

INSTRUMENTATION

The test barrette at Kowloon Bay was heavily instrumented. The prime objectives of the instrumentation were to study ground deformations due to the construction of the barrette (the diaphragm wall panel) and, more importantly, to investigate the load transfer mechanism and load–settlement characteristics of the barrette during axial load testing. In this paper, only the instrumentation related to the construction of the barrette is reported. Details of other instrumentation and the research strategy are described by Shen *et al*. (1998). Figs 3 and 4 show the locations of various instruments both in and around the trench.

Four Geokon vibrating-wire-total-earth-pressure cells, together with four vibrating-wire piezometers, were installed at the soil–wall interface at four elevations. Two total-earth-pressure cells were installed in both the alluvium and the weathered granite layers to measure total horizontal pressures at the soil–wall interface. The locations of the vibrating-wire piezometers were at about 80 mm above the corresponding pressure cells.

In addition, one pneumatic piezometer was installed inside borehole BF-4 (see Fig. 4) at 35 m below ground level in the weathered granite to monitor pore water pressure changes during the construction and testing of the barrette.

Magnetic extensometers were installed into three boreholes (see Fig. 4). The datum magnets were set into the rock, except in BF-3, owing to some construction difficulties encountered. The extensometers allowed subsurface soil movements to be measured by monitoring the location of each magnetic target with respect to the datum magnet.

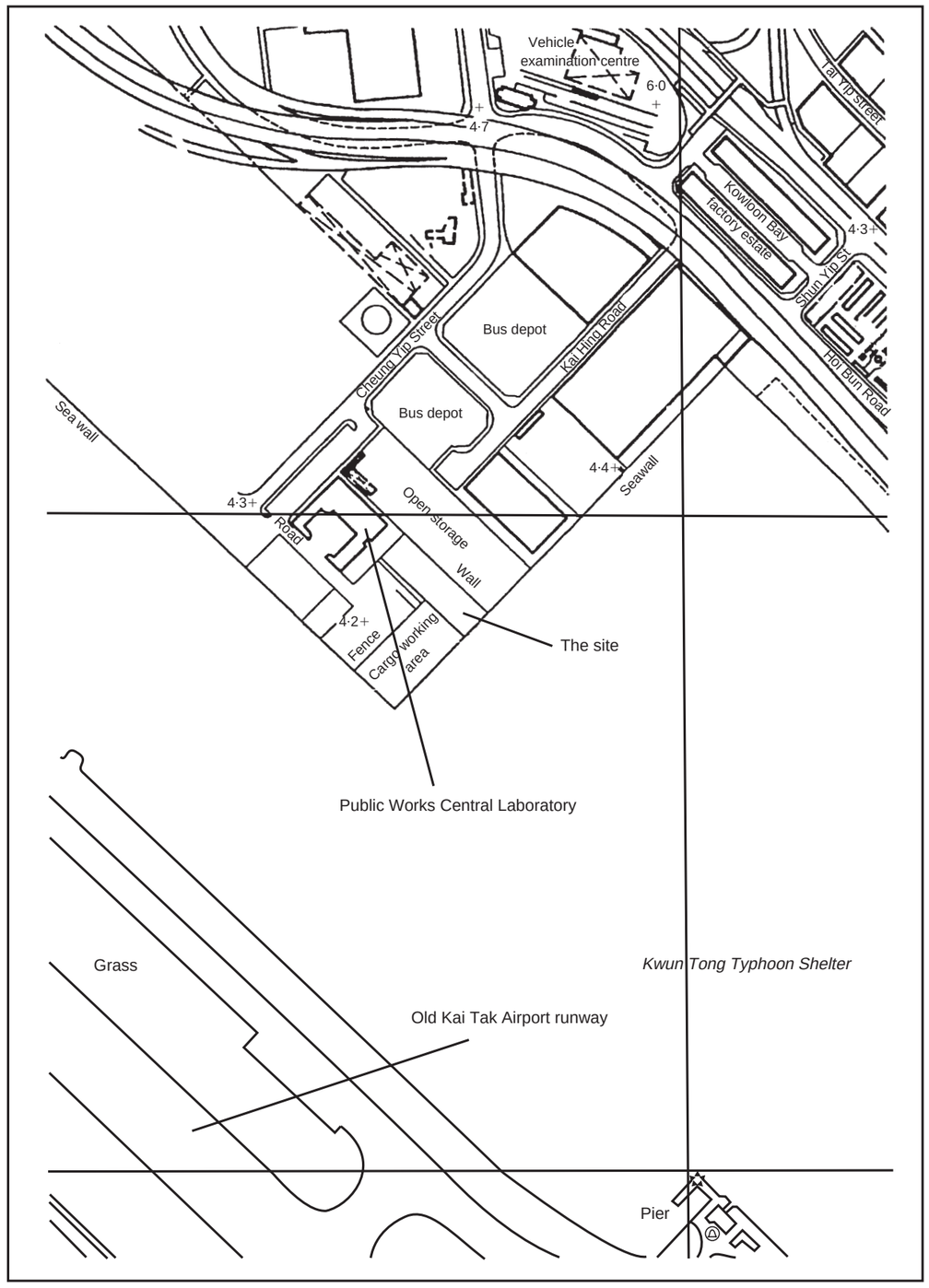

Fig. 1. Location plan of test pile site in Kowloon, Hong Kong

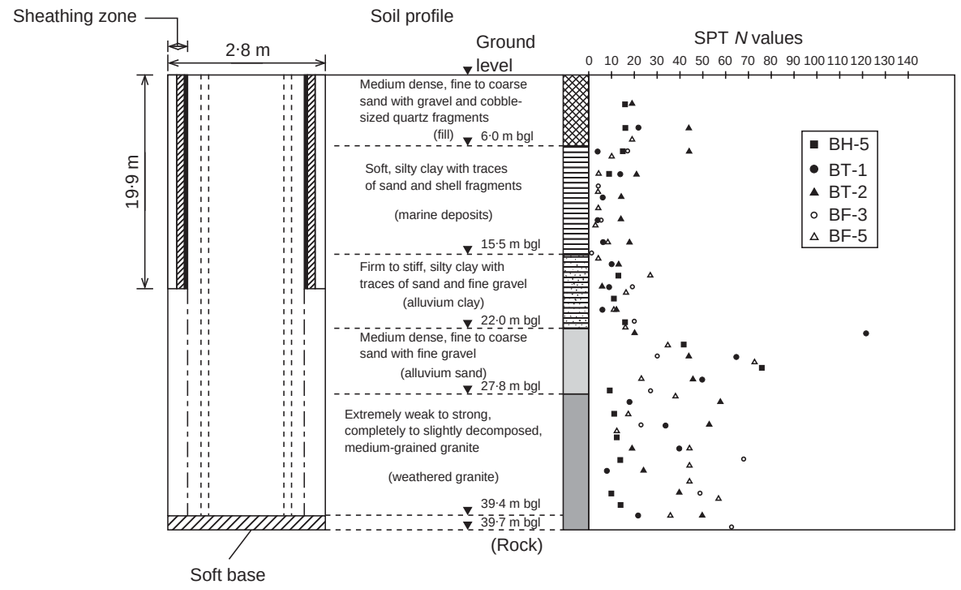

Fig. 2. Borehole logs and SPT *N* values at Kowloon Bay, Hong Kong (bgl, below ground level)

Three conventional inclinometer systems were installed in three boreholes, as shown in Figs 3 and 4. The bottoms of the inclinometers were fixed in rock. The inclinometers were used to measure rotations and hence the lateral movement of the soil around the trial barrette. In addition, settlement markers were installed around the trench, as shown in Fig. 3. The settlement monitoring system consisted of a steel rod. The bottom of the rod was concreted in a hole of 1·5 m depth below ground level. The settlement markers were used to measure surface settlements of the ground due to the construction of the diaphragm wall panel.

GROUND DEFORMATIONS DURING CONSTRUCTION OF THE BARRETTE

The excavation of the trench started on the morning of 5 December 1997 and was completed at midnight 7 December 1997. During excavation, the level of bentonite was kept at about 1·5 m above the ground water table (i.e. at about 3 m PD). The trench was then concreted in the afternoon of 9 December 1997. The horizontal deformation profiles measured are illustrated in Fig. 5. The measurements from the conventional inclinometers are of poor quality. This was probably because the actual movements were too small, only about 2·5 mm maximum horizontal ground movement towards the trench was observed at the ground surface in BF-5 (4 m away from the trench). The resolution of the inclinometers (0·1 mm deviation per metre or a maximum deviation of 4 mm over the 40 m trench) was simply not good enough to differentiate any small movements induced on site.

The measured horizontal displacements generally decrease with depth, except for the localized large displacements appearing at about 32 m below ground level. This localized large ground deformation could be due to overbreak and loss of ground during chiselling at the base of the trench. Generally, small lateral deformations were observed and these may be attributed to limited stress relief during excavation (i.e. the initial horizontal stresses in the ground were not very different from the bentonite pressure) and the significant effect of soil arching (Ng, 1992; Ng *et al*., 1995) around the relatively short panel length. Owing to the limited accuracy of the conventional inclinometers, no clear trend can be identified among the measured values from the three boreholes.

In the measured profiles at Chater Road (Stroud & Sweeney, 1977) and at Kowloon Bay, more significant deep-seated deformation was observed at the former than at the latter site. This was probably due to substantial soil yielding at deeper levels (large deviatoric shear stress) for the longer panel (6·1 m) at Charter Road. Deviatoric shear stress due to the difference between the vertical and horizontal effective stresses would be induced in the soil around trenches during excavation. On the other hand, soil arching around the shorter panel (2·8 m) seems to minimize the ground deformation at Kowloon Bay. Details of soil arching and stress transfer mechanisms due to the construction of a diaphragm wall panel are discussed by Ng *et al*. (1995).

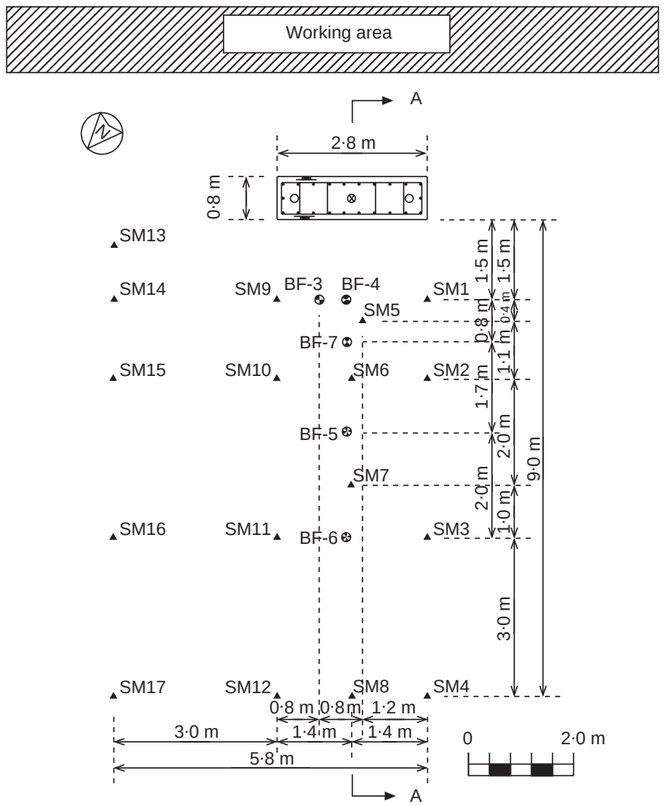

Fig. 3. Plan view of locations for instrumentation

During concreting, the ground surface was pushed, on average, about 1 mm outward laterally away at 4 m and 6 m from the trench by the wet-concrete pressure (see Fig. 5). It should be noted that the theoretical concrete pressure acting on the soil face was higher than the initial horizontal stresses in the ground. At 2·3 m from the trench (BF-7), the observed ground deformation is somewhat unexpected as the measurements indicate that there was a significant lateral movement (about 11 mm) away from the trench at 11 m below ground level (−6·5 m PD). Confirmation of the reliability of this substantial lateral movement can be obtained by considering the subsurface vertical movements measured by the extensometer installed in BF-3 (1·5 m away from the trench).

Figure 6 shows the subsurface vertical movements recorded by the extensometer in BF-3. During the excavation, the measurements showed an increase in settlement at all levels as excavation continued, with a maximum settlement of 2 mm at ME3-5. After concreting, a small recovery of ground settlements was recorded by the uppermost two spider magnets, except at ME3-5, which recorded a substantial upward movement (heave) of 7·5 mm in the soft marine deposit. ME3-5 is 9 m below ground level, just above the spike of ground movement measured by the inclinometer in BF-7. The consistency between the inclinometer and magnetic extensometer readings suggests that these large local deformations in the two orthogonal directions adjacent to the trench might be due to the presence of a weak soil layer or an overbreak and loss of ground during excavation. All other spider magnets in the same borehole show an increase in settlement during concreting and that the settlement ceased after concreting.

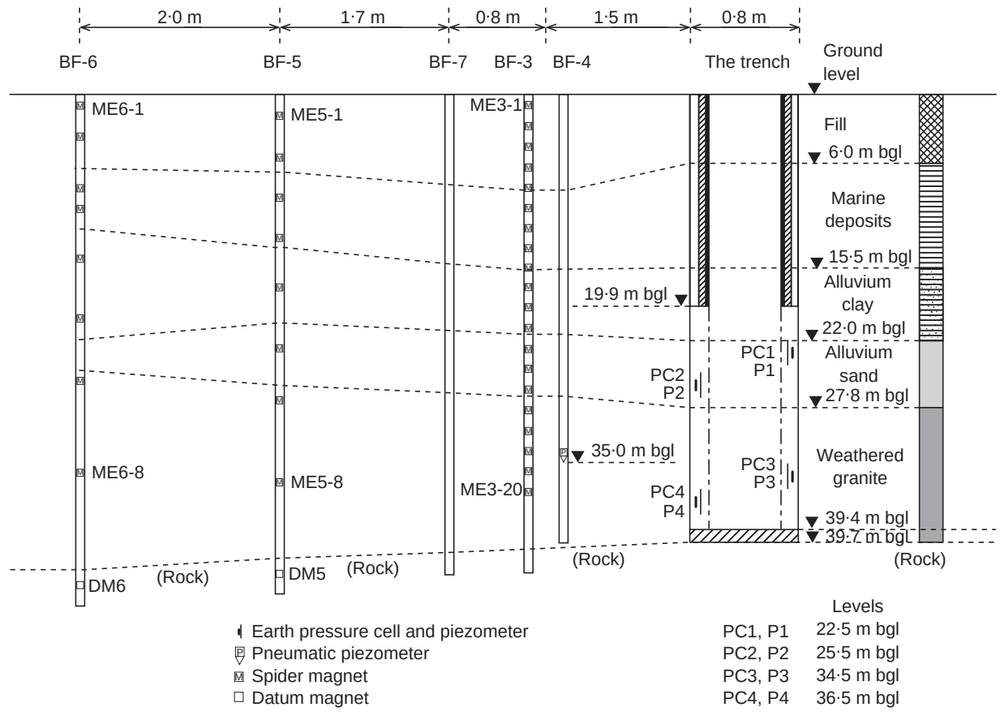

Fig. 4. Typical schematic cross-section A–A showing layout of instrumentation (not to scale)

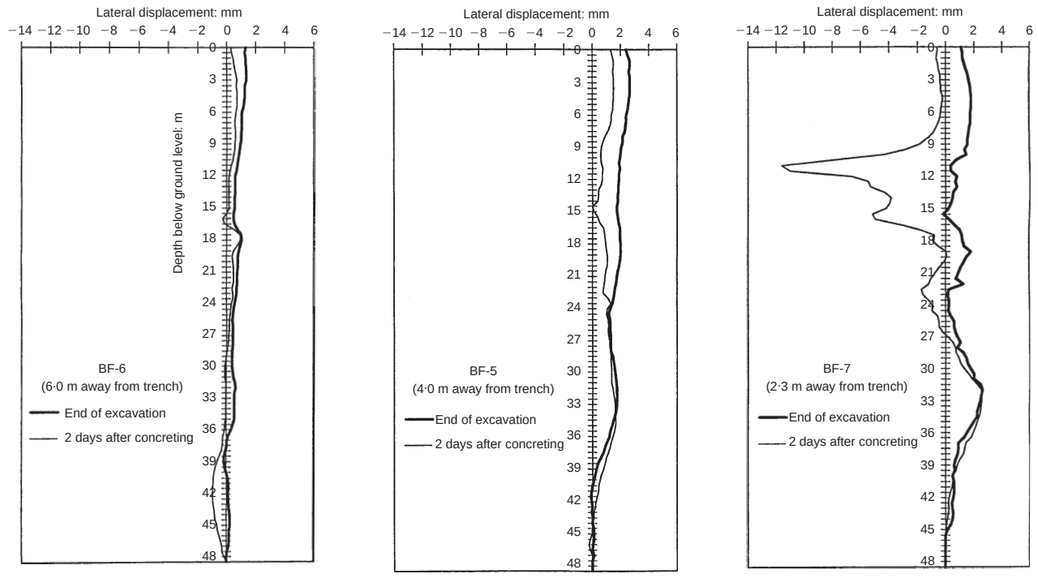

Fig. 5. Ground deformation profiles at different stages of barrette construction (positive lateral displacement: towards the trench; best resolution 0·1 mm deviation/1 m depth)

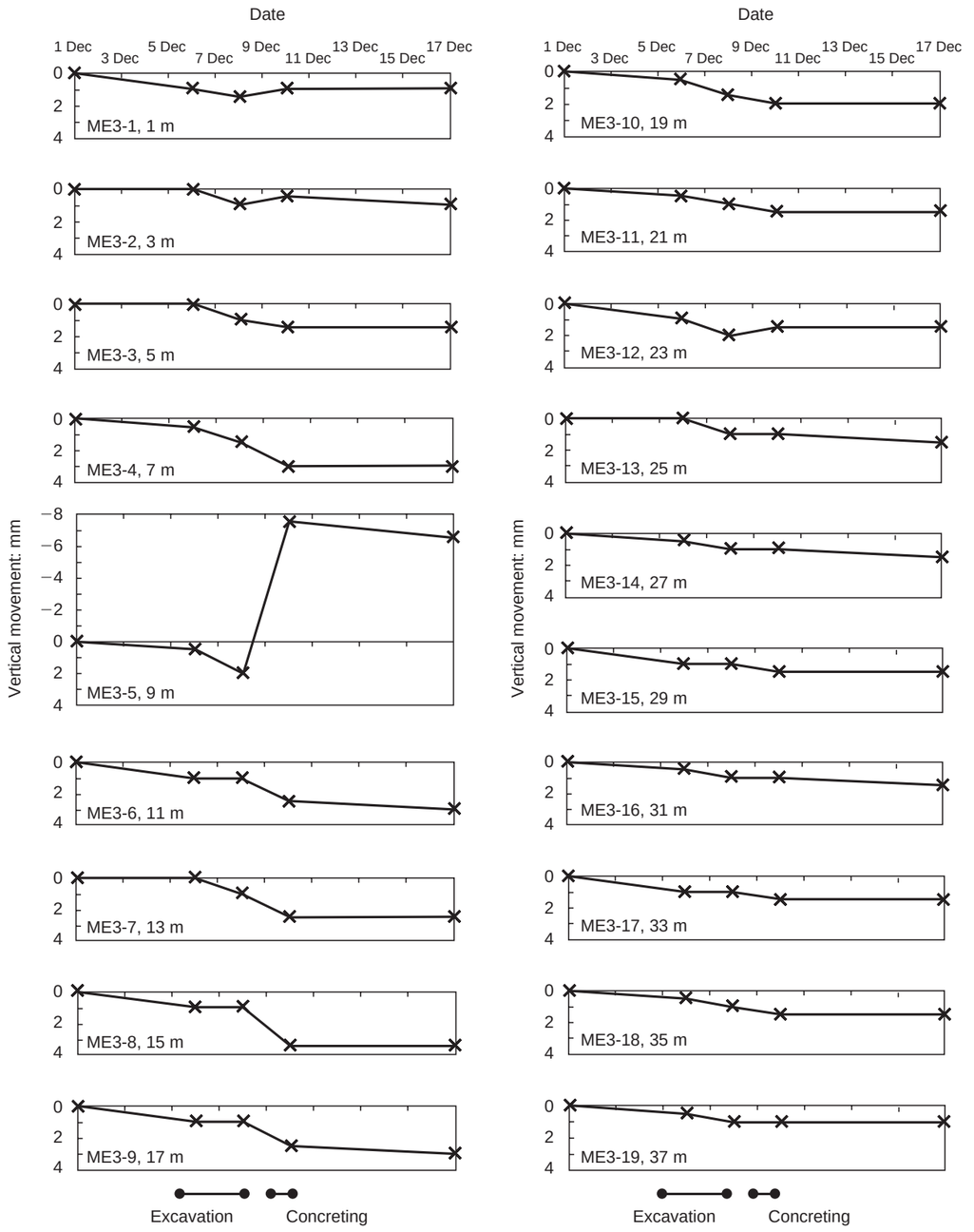

Fig. 6. Variations of subsurface vertical movement with time at BF-3 (1·5 m away from trench) (measured by magnetic extensometer: positive, settlement; negative, heave)

Figure 7 summarizes the subsurface vertical movements measured by the upper magnets installed in both BF-5 and BF-6. The excavation of the trench caused maximum downward movements of 1·5 mm and 2·5 mm, at 2 m depth in BF-5 and at 1 m depth BF-6, respectively. Generally, the deeper the magnet, the smaller the settlement recorded. Recovery of ground loss due to concreting resulted in a substantial reversal of settlement in each borehole. This recovery of ground loss indicates that the lateral stress in the ground could not possibly be larger than the concrete pressure during construction. Low initial lateral stress in the ground can thus be deduced.

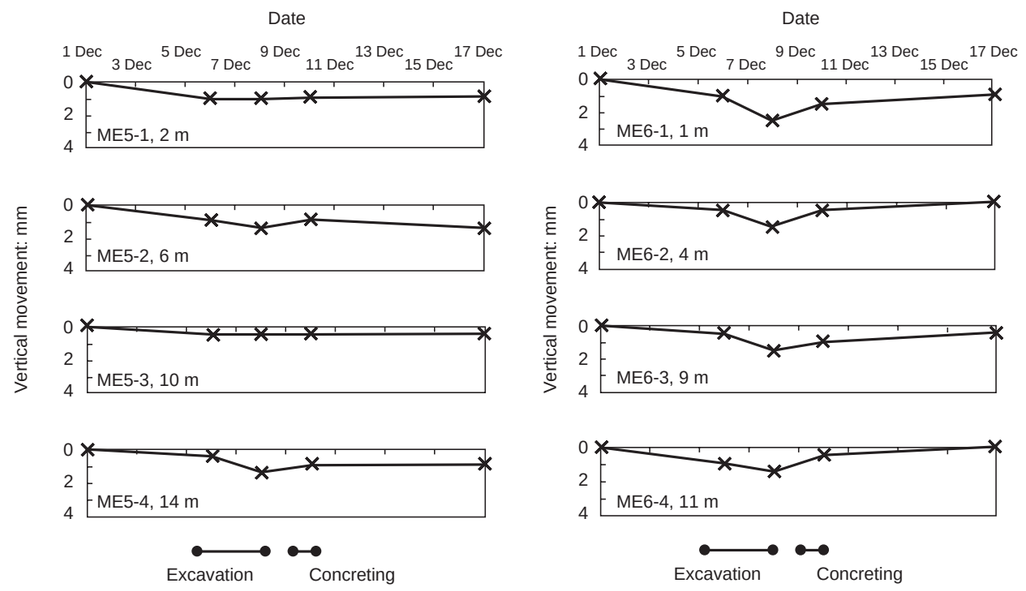

Fig. 7. Variations of subsurface vertical movement with time at BF-5 and BF-6 (measured by magnetic extensometer)

Surface ground settlements were monitored using ordinary levelling techniques. Even allowing for the typical accuracy of ±1·0 mm of the levelling instrument, the observed settlements at various distances from the trench are unexpectedly very small. The maximum settlement measured was 1 mm during the excavation of the trench. During concreting, no recovery of ground loss can be identified.

CONTACT PRESSURES AT THE SOIL–WALL INTERFACE

Four vibrating-wire-total-earth-pressure cells and piezometers were attached to appropriate locations of the reinforcement cage during the construction of the barrette. Once in position, the instruments were jacked horizontally from the ground surface to ensure contact with the surrounding soil. The prime objective of installing the piezometers was to record changes of pore water pressures during the proposed vertical-load test of the barrette a few weeks after construction. In order to prevent the ceramic tips of the piezometers from clogging with bentonite, the ceramic tips were plugged with solid soap. This was expected to take a few days to dissolve before allowing the piezometers to function properly after concreting.

Initial readings of the piezometers and earth pressure cells were taken before the instruments were jacked into position. This allowed a comparison to be made with the calculated bentonite pressures, using a measured unit weight (γ_b) of 10·8 kN/m^3. There was very good agreement between the calculated bentonite pressures and the readings recorded by the vibrating-wire earth pressure cells (Fig. 8). The maximum difference between the calculated and measured pressures was less than 10 kPa. Some minor adjustments were made to the calibration factors.

Some piezometers showed higher pressures than the calculated values (Fig. 9). This was possible because the solid soap used to plug the ceramic tips of the piezometers had little time to dissolve. After taking initial readings, the earth pressure cells and piezometers were bedded in by jacking them out horizontally against the excavated soil surface until cell readings equal to the assumed initial K_0(=0·5) earth pressure were achieved. The jacking pressure was reduced once the concrete level went a few metres above the location of each pressure cell.

Since the initial horizontal stresses in the ground are not known for certain at Kowloon Bay, an initial K_0 value, equal to $(1-\sin\phi')$, was assumed for each soil layer at Kowloon Bay, and the calculated lateral earth pressures are shown in Fig. 8. Low initial K_0 values in fill and decom-

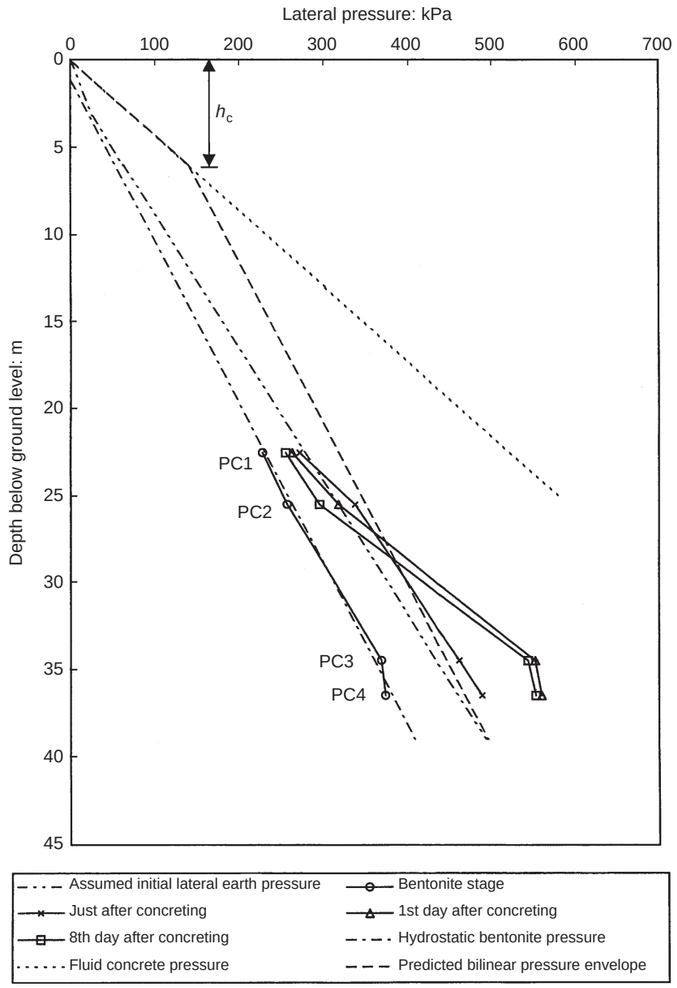

Fig. 8. Variations of lateral pressure distribution with depth

posed granite have recently been verified by back-analysing a deep excavation using the non-linear Simpson's brick model (Malone *et al*., 1997). It was thus expected that there could be a stress reduction during the excavation of the barrette. For equilibrium, the initial total earth pressure had to reduce to the bentonite pressure. The reduction of the total initial stress in the ground due to excavation resulted in mainly horizontal ground movements. Swelling and softening of the soils followed and hence led to a decrease in shear strength and stiffness.

On the basis of field observations and theoretical considerations, Ng (1992) and Lings *et al*. (1994) proposed a theoretical bilinear pressure envelope for predicting lateral pressures developed at the soil–wall interface during concreting in a diaphragm wall panel. The theoretical bilinear equation derived is as follows:

$$\sigma_h = \begin{cases} \gamma_c z & z \leqslant h_c \\ (\gamma_c - \gamma_b)h_c + \gamma_b z & z > h_c \end{cases} \quad (1)$$

where σ_h, z and h_c are the total lateral pressure, the depth below the top of the panel and the critical depth, respectively. According to the guidelines given in CIRIA Report 108 (Clear & Harrison, 1985), the value of the critical depth is mainly governed by the type of cement used, the rate of concreting, the temperature and the size and shape of the trench. The critical depth calculated for the panel at Kowloon Bay is 6·03 m and the predicted bilinear envelope is shown in Fig. 8. The measured values just after concreting agree well with the

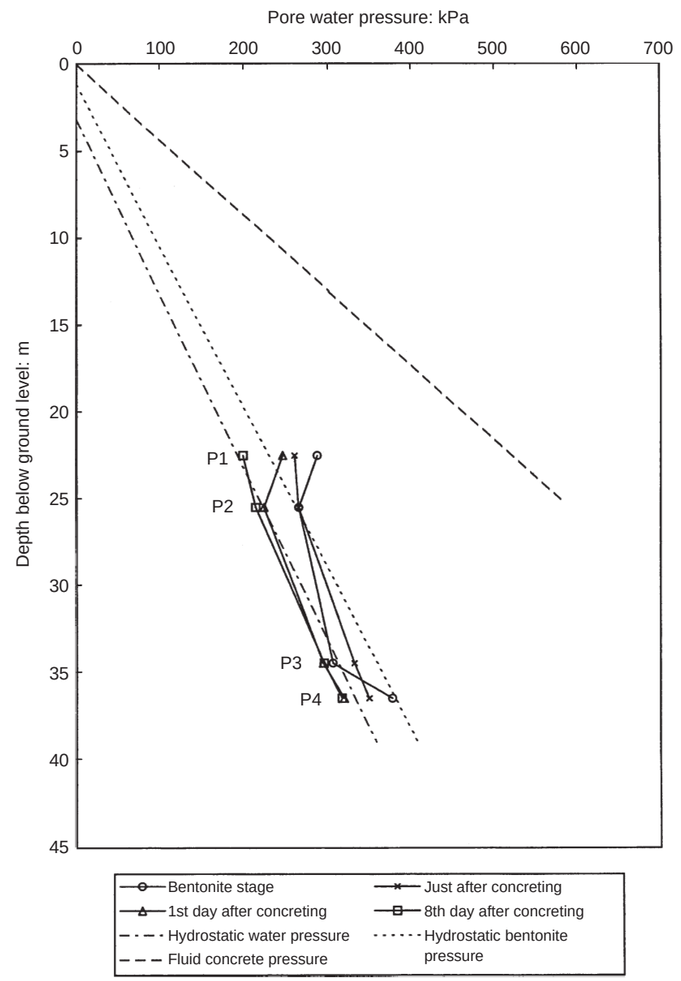

Fig. 9. Variations of pore water pressure distribution with depth

theoretical line predicted by the equation, except at PC1. It is clear that the full fluid concrete pressure did not develop over the full depth of the wall during concreting. The horizontal total pressures increased to some values higher than the assumed initial K_0 pressures, except at PC1, and they pushed the surrounding soil away from the trench, as shown in Fig. 5.

Measurements of lateral earth pressures 1 and 8 days after concreting are also shown in Fig. 8. There were substantial increases in lateral pressure at PC3 and PC4 in the weathered granite, but slight decreases at PC1 and PC2 in the alluvium sand. The increase of pressure in the weathered granite is somewhat unusual and might be due to swelling of the soil and stress redistribution.

Figure 9 shows the observed pore water pressures at the soil–wall interface. As discussed previously, the measured values at the bentonite stage do not fall on the hydrostatic bentonite pressure line, probably because the ceramic tips were plugged with soap initially. Readings taken during and one day after concreting show that excess pore water pressures were generated because of concreting. Dissipation of the excess pore water pressure seemed to be complete 8 days after concreting. The pore water pressures at the soil–wall interface resemble hydrostatic conditions.

Figure 10 shows the measured pore water pressures 1·5 m away from the face of the trench in BF-4 (at 35 m below ground level). The piezometer recorded an increase of 7 kPa above an average pore water pressure of 311 kPa during concreting. The excess pore water pressure largely dissipated

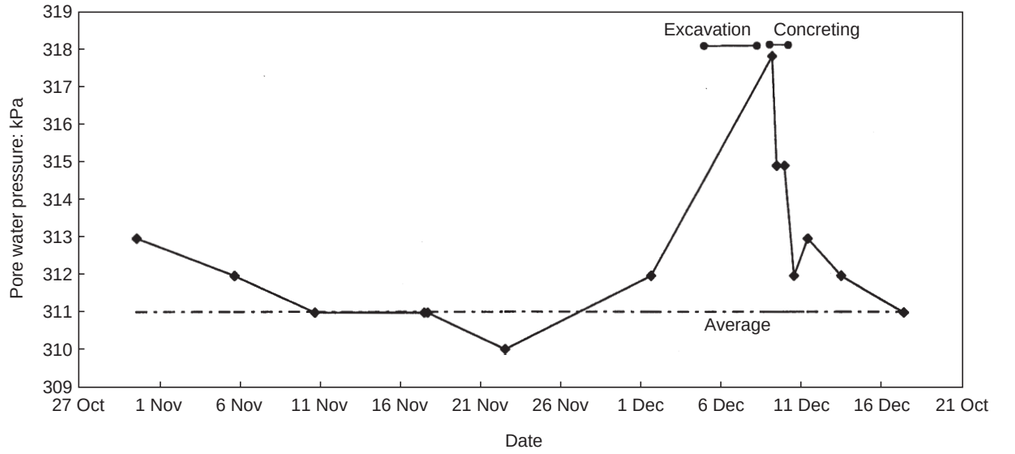

Fig. 10. Variations of pore water pressure with time at BF-4 (1·5 m away from trench) (measured by pneumatic piezometer at −35 mbgl)

within 2 days after concreting, indicating a high permeability of the weathered granite. The rate of pore pressure dissipation is consistent with the case history reported by Stroud & Sweeney (1977).

THREE-DIMENSIONAL MODELLING OF THE TRENCH EXCAVATION

Soil model, parameters and modelling procedures

To model the three-dimensional installation processes of the diaphragm wall panel construction, the finite-difference program FLAC3D (Itasca, 1996) was adopted. Since the three-dimensional soil–structure interaction of diaphragm walling is rather complex, it was decided to choose a relatively simple soil model for ease of interpretation of the computed results. All the soils at Kowloon Bay have been modelled as simple linear elastic and perfectly plastic isotropic materials with a Mohr–Coulomb yield surface. The elastic shear modulus adopted for each soil layer was based on the measured velocity of shear waves (geophysical method) at the same site, from which the maximum shear stiffness at very small strains was determined (Ng *et al*., 1999). The model parameters are summarized in Fig. 11.

To estimate the shear stiffness at moderate shear strains (0·1%) for each soil layer, field-measured shear moduli of the weathered granite obtained from a self-boring pressuremeter (SBPM) were compared with the measured values obtained by the geophysical method. It was found that the elastic moduli of the weathered granite at very small strains obtained by the geophysical method were approximately three times higher than the stiffness at moderate strains measured by the SBPM (Ng *et al*., 1999). An assumption was thus made that the shear moduli at moderate shear strains in other soil strata would also be three times smaller than the elastic moduli obtained using the geophysical method. In this paper, two three-dimensional analyses are described: one uses the small-strain elastic moduli obtained by the geophysical method; the other adopts the deduced shear moduli at moderate strains. The shear strength parameters are taken from published data available in the literature (Cowland & Thorley, 1984).

For comparing the maximum observed ground deformations, only the excavation of the diaphragm wall trench was simulated. This was done by removing model soil elements inside the trench and applying a normal hydrostatic bentonite pressure on the trench faces simultaneously.

Comparisons between measurements and computed results

Figures 12 and 13 compare the measured and computed horizontal deformation profiles and vertical subsurface movements, respectively at various distances from the trench. It can be seen that the accuracy of the magnetic extensometers was generally better than that of the inclinometers. If the elastic moduli obtained from the geophysical method are used, the numerical simulation significantly underpredicts the actual ground deformations, especially for the vertical subsurface movements. This implies that the actual ground response substantially deviated from the elastic behaviour assumed in the three-dimensional analysis. Substantial plastic strains seem to have been induced during the excavation of the trench.

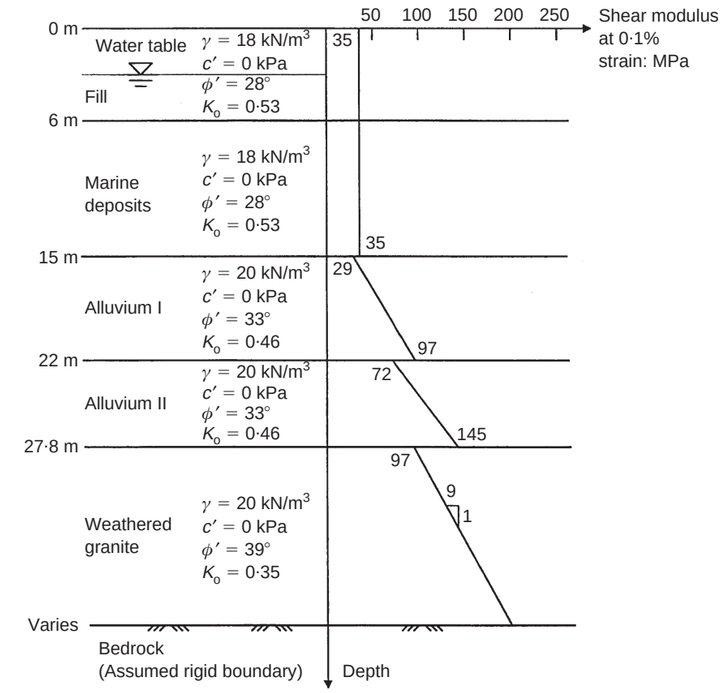

Fig. 11. Summary of soil parameters

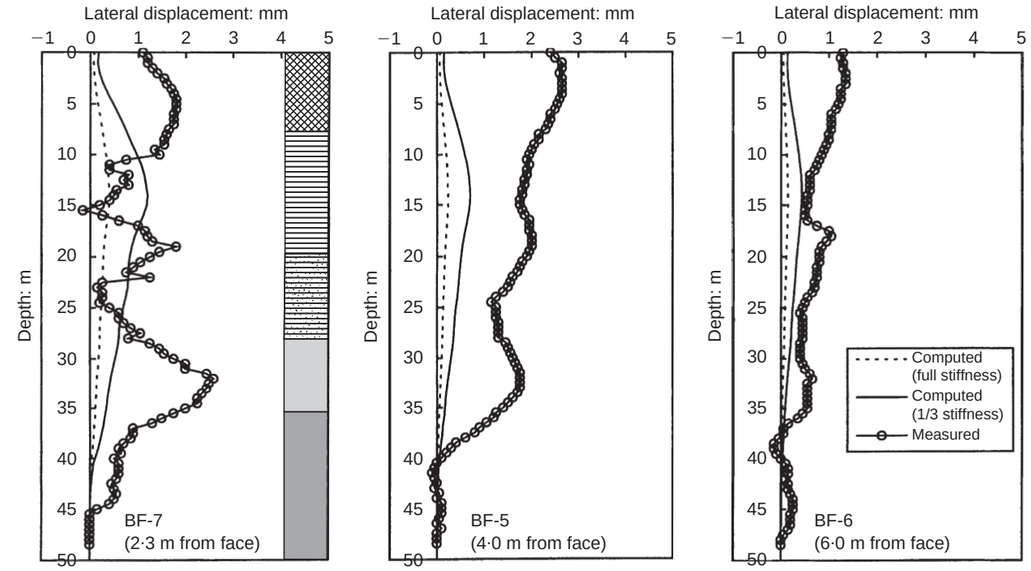

Fig. 12. Comparison between measured and computed horizontal deformation profiles after excavation (positive lateral displacements towards the trench)

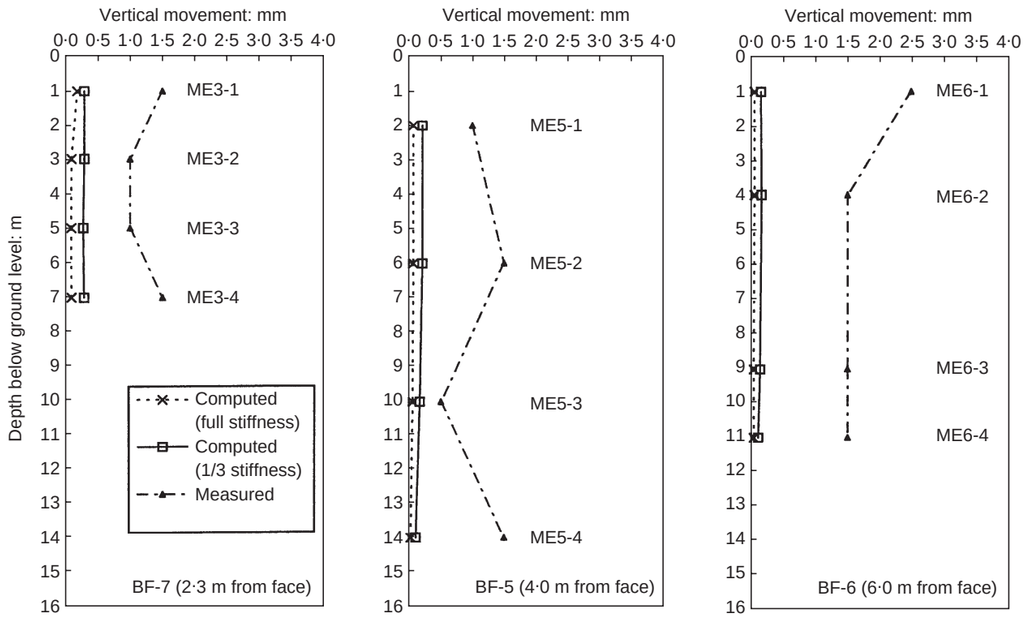

Fig. 13. Comparison between measured upper four magnets and computed subsurface vertical deformations after excavation

On the other hand, if all the soils are assumed to have operated at moderate shear strains (0·1%) during the excavation, the discrepancies between the computed and measured horizontal deformations generally become smaller. However, the discrepancy between the measured and computed vertical movements is still substantial. This discrepancy may be attributed to inappropriate soil parameters or the model used, or both. As an isotropic model was adopted in the analysis, the different responses in the two orthogonal directions seem to suggest that the soils exhibited a certain degree of anisotropy.

The large discrepancies between the measured and computed deformations using the shear moduli at moderate shear strains (0·1%) may be attributed to the presence of the 30 m thick soft, layered strata (i.e. fill, marine deposit, alluvium clay and sand) above the decomposed granite. The stiffness of these soft strata is likely to be considerably less than the assumed moduli adopted in the analysis, possibly owing to the onset of substantial plastic yielding. This would result in a significant reduction of soil stiffness and lead to larger ground movements during excavation. Of course, larger ground deformations would have been computed if a degradation of soil stiffness with increasing strain was allowed in the analysis. According to the comparisons between the measured and computed results, an average shear strain well in excess of 0·1% was mobilized around the trench during the excavation.

No further analyses have been attempted, owing to the limited accuracy of the inclinometers and the unavailability of good-quality soil stiffness parameters (small-strain shear moduli) for any of the soils except the weathered granites.

CONCLUSIONS

The construction in Hong Kong of an excavated large, rectangular-section barrette (i.e. a short diaphragm wall panel) in weathered and sedimentary soils under bentonite has been heavily instrumented and closely monitored. The size of the panel was 2·8 m long by 0·8 m wide by 40 m deep. During excavation, the maximum horizontal ground movements recorded were of the order of a few millimetres, with negligible surface settlements around the panel. A small amount of recovery of the horizontal ground movement was measured during concreting. The observed ground deformations are substantially smaller than the measured values obtained during the construction of a longer panel (6·1 m long by 1·23 m wide in plan) excavated on a site with similar ground conditions.

On the basis of three-dimensional numerical simulations of the excavation of the trench, an average mobilized shear strain greater than 0·1% around the excavated trench can be deduced.

At the soil–wall interface, the initial lateral earth pressures decreased to the hydrostatic bentonite pressures during excavation and then increased above the assumed initial K_0 pressures after concreting. The measured lateral pressures just after concreting show some agreement with a pressure distribution based on a theoretical bilinear pressure envelope.

Excess pore water pressures at the soil–wall interface and around the panel were recorded during construction. Dissipation of the excess pore water pressures seems to have been rapid and to have been completed within a few days.

ACKNOWLEDGEMENTS

This research project is supported by a research grant (HIA96/97.EG03) from the Hong Kong University of Science and Technology and a research grant (CRC96/99.EG04) from the Research Grant Council of Hong Kong. The authors would like to acknowledge the contribution provided by Paul Y. Foundation Ltd, who constructed and tested the heavily instrumented barrette. Other sponsors of this test barrette include the Geotechnical Engineering Office of the Hong Kong Government, Fong On Construction Ltd, Mass Transit Railway Corporation and Geotechnical Instruments Ltd. Technical input and support from Professors C. K. Shen and Wilson Tang of the Hong Kong University of Science and Technology and Messrs Martin Pratt and David Ng of Bachy Soletanche Group are highly appreciated.

REFERENCES

Clear, C. A. & Harrison, T. A. (1985). *Concrete pressure on formwork*. Report 108. London: CIRIA.

Clough, G. W. & O'Rourke, T. D. (1990). Construction induced movements of *in-situ* walls. In *Design and performance of an earth retaining structure*, Geotechnical Special Publication 25, pp. 439–470. New York: American Society of Civil Engineers.

Cowland, J. W. & Thorley, C. B. B. (1984). Ground and building settlement associated with adjacent slurry trench excavation. *Proceedings of the international conference on ground movements and structures*. pp. 723–738.

Farmer, I. W. & Attewell, P. B. (1973). Ground movements caused by a bentonite-supported excavation in London Clay. *Géotechnique* **23**, No. 4, 577–581.

Geotechnical Engineering Office (1993). *Guide to retaining wall design*. 2nd edn. Hong Kong: Geotechnical Engineering Office, Civil Engineering Department.

Itasca (1996). *Fast Lagrangian Analysis of Continua (FLAC-3D)*, version 1.1, user's manuals. Itasca Consulting Group, Inc., Minnesota.

Lings, M. L., Ng, C. W. W. & Nash, D. F. T. (1994). The pressure of wet concrete in diaphragm wall panels cast under bentonite. *Proc. Instn Civ. Engrs, Geotech. Engng*, **107**, 163–172.

Malone, A., Ng, C. W. W. & Pappin, J. (1997). Country report (invited): collapses and displacements of deep excavations in Hong Kong. *30th year Anniversary Symposium of the Southeast Asian Geotechnical Society*, Bangkok, pp, 5-124–5-129.

Ng, C. W. W. (1992). *An evaluation of soil–structure interaction associated with a multi-propped excavation.* PhD thesis, University of Bristol.

Ng, C. W. W., Ling, M. L., Simpson, B. & Nash, D. F. T. (1995). An approximate analysis of the three-dimensional effects of diaphragm wall installation. *Géotechnique*, **45**, No. 3, 497–507.

Ng, C. W. W., Pun, W. K. & Pang, P. L. R. Small strain stiffness of natural granitic saprolites in Hong Kong. *J. Geotech. Geoenv. Engng. ASCE* (in press).

Powrie, W. & Kantartzi, C. (1996). Ground response during diaphragm wall installation in clay: centrifuge model tests. *Géotechnique*, **46**, No. 4, 725–739.

Shen, C. K., Ng, C. W. W., Tang, W. H. & Rigby, D. (1998). Invited discussion paper: testing a friction barrette in decomposed granite in Hong Kong. *Proc. 14th Int. Conf. Soil Mech. Found. Engng, Hamburg*, vol. 4, 2325–2328.

Strange, P. J. (1990). The classification of granitic rocks in Hong Kong and their sequence of emplacement in Sha Tin, Kowloon and Hong Kong Island. *Geo. Soc. Hong Kong Newslett.*, **8**, Part 1, 18–27.

Stroud, M. A. & Sweeney, D. J. (1977). Discussion appendix. In *A review of diaphragm walls*, pp. 142–148. London: Institution of Civil Engineers.

Symons, I. F. & Carder, D. R. (1993). Stress changes in stiff clay caused by the installation of embedded retaining walls. In *Retaining structures*, (ed. C. Clayton), pp. 227–236. London: Thomas Telford.

FIELD STUDIES OF WELL-INSTRUMENTED BARRETTE IN HONG KONG

By Charles W. W. Ng,[1] Member, ASCE, Douglas B. Rigby,[2] Member, ASCE, Sean W. L. Ng,[3] and G. H. Lei[4]

ABSTRACT: A large excavated rectangular pile (barrette) with lateral earth pressure and pore-water pressure cells was successfully constructed and tested in a sequence of marine, alluvial, and weathered granite soils. A ''soft'' base formed beneath the bottom of the barrette permitted over 100 mm of vertical settlement, completely mobilizing the shaft friction at the barrette-soil interface. During the vertical load tests, an unusual and complex response of pore-water pressures and earth pressures at the barrette-soil interface was measured. During each vertical loading cycle (except the last one) and before interface slippage of the barrette occurred, excess positive pore-water pressures were recorded in all soil layers. Upon the initiation of slip at the barrette-soil interface, a sudden drop in the measured pore pressures as well as a substantial drop in lateral earth pressures generally resulted. Subsequent loading or unloading slippage events did not show the same dramatic behavior unless a period of consolidation/recovery was allowed first. This implies that caution must be used in design of barrettes relying heavily on skin friction when shearing induces contractive soil behavior. The current test results indicated that the empirical uncorrected SPT-N value approach and the effective stress β-method were inconsistent.

INTRODUCTION

Limited space and high demand have made land in Hong Kong extremely expensive. Tall buildings are built to optimize the floor area to land area ratio. Many of the tall buildings located along the Victoria Harbor on the Hong Kong Island and the Kowloon peninsula are commonly founded on reclaimed land. Thus deep foundations are required to resist both vertical and horizontal loads due to the weight of the building and wind, respectively. The prevailing deep foundation types for tall buildings on these reclaimed lands are large bored and excavated piles, which are very long, normally in excess of 50 m. These piles can be circular (bored piles/drilled shafts) or rectangular (barrette) in shape and must extend through the fill, underlying soft marine clay, sandy clay, and alluvial sand deposit down into the deep weathered granite soil (saprolite), which is typically less weathered with an increase in depth. The thickness of the weathered granite can be up to 80 m in some places, and its depth can extend to more than 100 m from the ground surface.

Over the last 15 years, barrette foundations have become increasingly popular in parts of Asia such as Hong Kong and Malaysia for many civil engineering structures and tall buildings. The construction method for barrettes is very similar to that adopted for diaphragm walls, where a rectangular trench is excavated under bentonite by heavy grabs or hydrofraise and filled with tremie concrete. In Hong Kong, single barrettes up to a size of 1.5 m wide × 6.6 m long (on plan) have been constructed (Pratt and Sims 1990). Due to their rectangular shape, barrette foundations are particularly suitable to resist large vertical and significant horizontal loads in a chosen direction.

For deep rectangular piles, the current design procedures adopted in Hong Kong are relatively conservative, and they assume a heavy reliance on end-bearing resistance of bedrock in many instances. Without performing at least one full-scale pile load test on site, skin friction in excess of 10 kPa is not permitted normally by the regulations. In some areas, however, bedrock is found at depths of over 100 m. Under such circumstances, excavation of deep foundations to bedrock becomes difficult, time consuming, and expensive. Exceeding the nominal permitted skin friction requires costly and time-consuming full-scale pile tests to verify design values of skin friction. Many Hong Kong engineers would welcome improved design guidelines based on more rational design approaches that would allow for higher default values of skin friction along a pile to be used, or a reduction in the number of verification piles in similar site conditions.

The problem is that estimation of skin friction development along a long barrette (between 40 and 100 m) is a very difficult task. The method of construction, workmanship, rheological properties of the slurry, and concrete placement affect its behavior. Any attempt to increase the design skin friction value must be done with caution. A task force has recently been formed, with participants from the government, some contractors and consultants, and the Hong Kong University of Science and Technology, to carefully study this problem aiming at the development of a more reasonable design guideline for deep pile foundations in Hong Kong. Currently a university-led and industry-supported three-year research project is under way to study skin friction on barrettes founded in weathered granites in Hong Kong by full-scale pile testing, laboratory tests, numerical and centrifuge modeling, and reliability analysis (Shen et al. 1997). Initially, two piling test sites are investigated: one at Kowloon Bay and the other in the Central district. In this paper, the construction of a 2.8 m long by 0.8 m wide and 39.7 m deep barrette at Kowloon Bay, its vertical load-deflection characteristics, and its pore-water pressure and lateral stress changes at the soil/barrette interface are reported and discussed. In addition, the measured skin friction is compared with other test results in Hong Kong.

SITE LOCATION AND GROUND CONDITIONS

The test site is located on the Kowloon peninsula of Hong Kong, to the east of a runway of the old Kai Tak international airport, at the Kowloon Bay area (Fig. 1). Fig. 2 shows the geology and some relevant borehole information obtained at Kowloon Bay. The site is on marine reclaimed land and the ground level is at approximately 4.48 m above Principal Datum (PD). The ground-water level is about 3 m below ground surface. The ground conditions consist of about 6.0 m fill material overlying a succession of approximately 9.5 m marine clay deposits, 7.5 m of sandy clay (probably alluvial), 4.8 m alluvial sand of Quaternary age, and about 12 m of weathered granitic saprolites that overlie granitic rocks of Upper Jurassic to Lower Cretaceous age (Strange 1990). Detailed descriptions and measured N-values by Standard Penetration Tests (SPT) for each type of materials are given in Fig. 2. It can be seen that scattered SPT-N values were obtained in both alluvial sand and weathered granite. The former shows a decreasing N-values with depth, whereas the latter illustrates an opposite trend. Based on results of drained triaxial compression tests on weathered granites, effective cohesion and angle of friction were found to be 0 kPa and 39°, respectively. Typical Atterberg limits for the sandy clay are 40, 20, and 20 for the LL, PL, and PI, respectively (GEO 1996a).

Strictly speaking, the site is not ideal for studying skin friction of excavated piles in weathered granite as the thickness of the granite is relatively thin and the measured SPT-N values are relatively low. However, due to the limited availability of land in Hong Kong for purely research purposes and the time restraints, this existing government test site was chosen. A distinct advantage is that the site investigation records are very comprehensive as this site has been a test site for the Geotechnical Engineering Office of the Hong Kong Special Administrative Region over the years. Various in situ and laboratory tests (Ng et al., unpublished paper, 1999) have been carried out on this site, resulting in ground conditions that are well known.

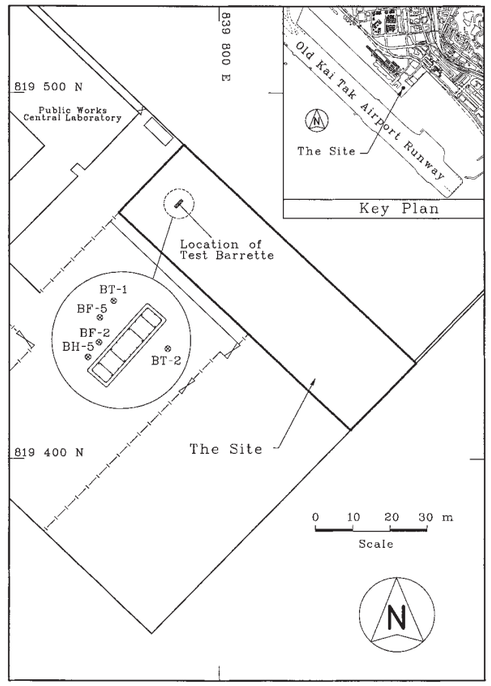

FIG. 1. Location of Test Barrette at Kowloon Bay, Hong Kong

DETAILS OF CONSTRUCTION

The test barrette or the diaphragm wall trench was excavated using a traditional cable-operated grab. The size of the excavated trench was 2.8 by 0.8 m on plane and 39.7 m deep (Figs. 2 and 3). During construction, a concrete guide wall was first placed, and at deeper levels the trench was supported

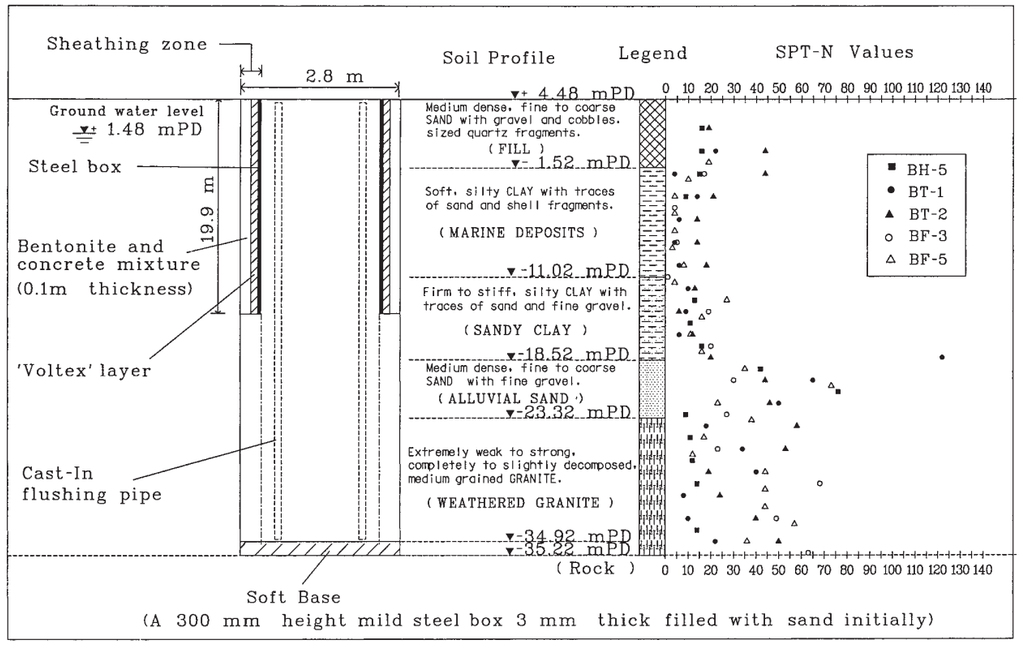

FIG. 2. Borehole Logs and SPT-N Values at Kowloon Bay, Hong Kong

[1]Assoc. Prof., Dept. of Civ. Engrg., Hong Kong Univ. of Sci. and Technol., Clear Water Bay, Kowloon, Hong Kong.
[2]Asst. Prof., Dept. of Civ. Engrg., Hong Kong Univ. of Sci. and Technol., Clear Water Bay, Kowloon, Hong Kong.
[3]Res. Student, Dept. of Civ. Engrg., Hong Kong Univ. of Sci. and Technol., Clear Water Bay, Kowloon, Hong Kong.
[4]Res. Student, Dept. of Civ. Engrg., Hong Kong Univ. of Sci. and Technol., Clear Water Bay, Kowloon, Hong Kong.

Note. Discussion open until June 1, 2000. To extend the closing date one month, a written request must be filed with the ASCE Manager of Journals. The manuscript for this paper was submitted for review and possible publication on April 1, 1999. This paper is part of the ***Journal of Geotechnical and Geoenvironmental Engineering***, Vol. 126, No. 1, January, 2000. ©ASCE, ISSN 1090-0241/00/0001-0060–0073/$8.00 + $.50 per page. Paper No. 20602.

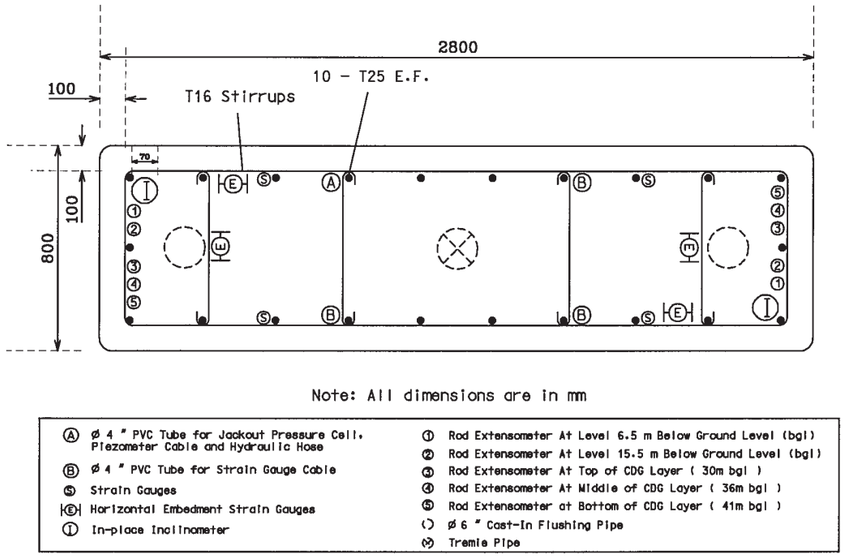

FIG. 3. Layout of Instrumentation (Plan View)

by bentonite with unit weight (γ_b) of about 10.8 kN/m^3. Soil spoil, suspended in the bentonite slurry, was pumped to a desanding unit at the ground surface. After desanding, the bentonite was recharged into the trench. Chiseling of the base was carried out when rock was encountered at a more shallow depth than expected, about 39.6 m below ground. This caused a small overbreak at the base, which was detected by a sonic profiling system. The entire excavation took 62 h to complete and the final excavated depth was 39.7 m below ground. The rate of excavation could have been improved if a 24-h nonstop excavation schedule were followed, as is the normal practice for commercial test barrettes in Hong Kong.

After completion of the excavation, three instrumented reinforcement cages were lowered one-by-one into the trench. Concreting was carried out 43 h after completion of the excavation. The average rate of concreting was 10.32 m/h by using a tremie pipe. The whole barrette trench was filled with concrete in 4.5 h. The Ordinary Portland Cement (OPC) concrete used was grade C30/20 with unit weight (γ_c) of 23.2 kN/m^3. It had a water-to-cement ratio of 0.45 and an average slump of 180 mm. During concreting, the average temperature measured inside the trench was 27.6°C inside the slurry. The excavation and concreting procedures of the barrette, in fact, were identical to the construction of a typical diaphragm wall panel.

The top 20 m of the barrette consisted of a reduced-section sheathing zone (Fig. 2) built with the intention of minimizing the interface skin friction developed between the barrette and the upper soil layers. This sheathing layer consisted of four layers: a 3 mm steel plate welded onto the reinforcement cage, a coating of bitumen, a flexible and weak ''voltex'' layer (geotextile infilled with sodium bentonite), and a thin sheet of plywood. However, the final result was that the plywood was unfortunately attached to the steel plate with a dense matrix of high-strength screws, precluding the possibility of shear between the intermediate ''soft'' layers. As a consequence, the theoretical gap of about 80 mm between the plywood and the surrounding soil was not back-filled with gravel as planned, so that a ''weak'' friction zone would hopefully exist. However, steel rods inserted into this suspected bentonite-filled gap about 2 weeks after concreting were unable to probe beyond a meter or two all round the barrette. Either concrete overflow had partially filled the gap, construction activities failed the soil infilling the gap, or surface materials mixed with solidified bentonite. Thus, in the end, the sheathing zone was not expected to function to effectively reduce skin friction over the top half of the barrette.

At the bottom of the barrette, a ''soft'' base was formed to minimize the effects of end-bearing for mobilizing full skin friction at the soil-wall interface. This was done by placing a 2.8 × 0.8 × 0.3 m in height steel box to the bottom of the trench, before the lowering of the main reinforcement cages. The box was made of 3 mm thick steel plate, and it was initially filled with fine round sand. Seven days after concreting, the sand-filled steel box was drilled through and flushed with pressurized water via two cast-in flushing pipes and one concrete core hole in the middle of the barrette (Fig. 3). Great care was taken to ensure that most of the sand was flushed out to form a ''soft base'' (i.e., void) underneath the barrette.

INSTRUMENTATION

To study the load transfer mechanism and load-settlement characteristics of the barrette constructed at Kowloon Bay, a substantial amount of instrumentation was installed. A summary of the instruments installed inside the barrette is given in Table 1. In addition, four sets of standard dial gauges together with surveying were used to monitor the vertical settlement of the top of the barrette and reference beams during testing.

Strain gauges were placed at 27 levels on the reinforcement cages (Figs. 3 and 4). Four surface mounted and four embedded strain gauges were placed alternatively at different levels

TABLE 1. Summary of Instrumentation at Kowloon Bay

Instrument (1)	Quantity (2)
Strain gauges	132
Rod extensometers	10
In-place inclinometers	2
Vibrating wire piezometers	4
Earth pressure cells	4

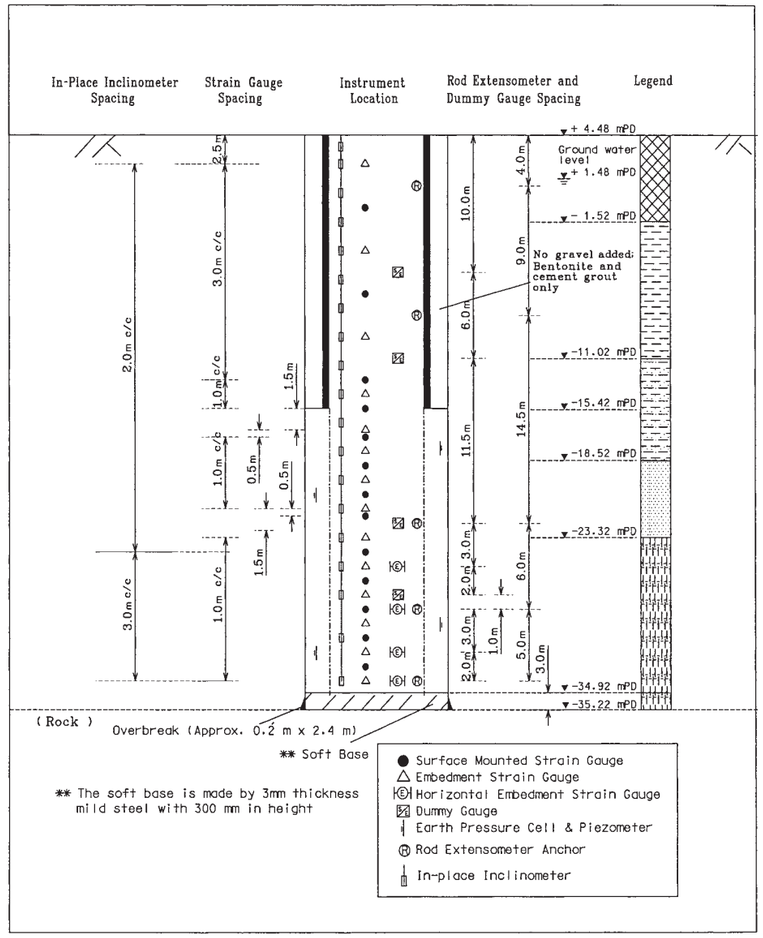

FIG. 4. Layout of Instrumentation (Elevation)

to measure vertical strains induced in the reinforcing bars and in concrete, respectively. Moreover, four levels of horizontally embedded strain gauges, with four gauges in each level, and four levels of dummy gauges (eight in total) were installed in the cage. The horizontally embedded strain gauges were used to determine any Poisson's ratio effects (results are not relevant to this paper). A total of 132 gauges, typically at 3 m and 1 m intervals in the sheathed and unsheathed zones, respectively, were installed to determine the strain distributions along the entire depth. It was found that similar results were recorded by both the surface mounted and embedded strain gauges. Thus, no further distinctions between the two types of gauges are made in this paper.

Ten aluminum rod extensometers were sleeved individually in PVC tubes and installed to five depths at two different locations inside the barrette to monitor displacements between each depth and reference steel plate at the top of the barrette (Figs. 3 and 4). After the pile test it was found that although the extensometers reflected a reasonable pattern of elastic pile shortening and rebound during loading and unloading cycles, some of the relative magnitudes measured were clearly unreliable. This was likely caused by friction developed between the metal rods and the PVC tubes having a 12.5 mm outer diameter and 12.6 mm inner diameter, respectively. Recently, extensometers consisting of 15 mm steel rods placed in 50 mm steel tubes filled with oil have given reliable results in Hong Kong.

A total of 38 biaxial servoaccelerometer sensors were installed at 19 levels (most of them at 2 m interval) in two cast-in pipes inside the barrette. The locations of the in-place inclinometers and the levels of sensors were indicated in Figs. 3 and 4, respectively. The bottoms of the inclinometers were socketed in rock. These two in-place inclinometers were designed to measure rotations and hence horizontal movements of the barrette during loading. From the measurements, it was concluded that no significant bending deflection of the barrette was induced during the vertical load tests.

A total of four vibrating wire total earth pressure cells, together with four vibrating wire piezometers, were installed at the barrette-soil interface at four levels within the layers of sandy clay, alluvial sand, and weathered granite. The depths of the earth pressure cells and piezometers are shown in Fig. 4. These total earth pressure cells and piezometers were attached to appropriate locations of the reinforcement cage during the construction of the barrette. Once in position, the instruments were jacked out horizontally to ensure contact at

reasonable pressures with the surrounding soil. Each vibrating wire piezometer was located about 80 mm above the corresponding pressure cell.

LOAD AND DISPLACEMENT BEHAVIOR OF PILE

The loading system for the test barrette consisted of two 1,000 ton hydraulic jacks pushing against kentledge formed from steel billets. The kentledge rested on two parallel sets of concrete blocks spaced 6 m apart, center to center. A pile cap at the top of the barrette and a steel spreader beam above the jacks were used to transfer the manually applied loads. The pile head displacement was measured by using four dial gauges symmetrically resting on two reference beams. Settlement of these reference beams was monitored by the conventional surveying technique.

The test program originally comprised four loading and unloading cycles (Fig. 5). However, after the applied load reached 7,455 kN at the second cycle, substantial settlement was recorded and the applied load could not be held constant within the prescribed maximum settlement tolerance of 0.05 mm/10 min. It was therefore decided to unload the barrette to 4,555 kN and to hold it for 80 h (about 3 days). After the holding period, the testing program resumed and two more loading cycles were performed. The barrette-soil interface appeared to gain strength as a result of consolidation, which is discussed later. Due to the presence of the ''soft base'' (i.e., void) underneath the barrette, the barrette ultimately settled about 100 mm, enabling the skin friction to be fully mobilized along the shaft.

Prior to calculating the distribution of axial load and shear stress along the length of the barrette, it is necessary to adopt appropriate values of Young's modulus for the barrette. Since the conditions of concrete curing inside the trench are very different from those in a standard curing tank in the laboratory, continuous concrete cores were taken from at the center along the depth of the barrette to determine the Young's modulus of the in situ concrete. The measured secant Young's modulus varying with depth (at about 1 m spacing) is shown in Fig. 6. Although there is a general increase of Young's modulus with depth due to the natural compaction process of the concrete under its own weight, the measured data are fairly scattered. For accurately converting the measured strains in the barrette to stresses, the actual measured modulus at each tested depth and corrected for steel present was adopted in the calculations.

Fig. 7 shows the deduced axial load versus depth for the last loading cycle. An axial stress was calculated from the average measured strains at each level and the corresponding measured Young's moduli (Fig. 6) from concrete cores taken from the center of the barrette. From the calculated axial stress, the axial load with depth was then determined considering the local barrette cross-sectional area. It can be seen that the deduced axial load at the top of the barrette is consistent with the applied load recorded by the hydraulic jacks (shown as dotted lines). The load distribution along the depth shows features common to a typical friction barrette. Due to the presence of the ''soft base,'' minimal base resistance was mobilized, except at the maximum load of 8,905 kN, where the base resistance increased substantially from 560 to 1,600 kN. This substantial increase was likely caused by the mobilization of some end bearing resistance due to the crushing of the 300 mm steel box underneath the barrette (possibly not all of the sand was flushed out from the box).

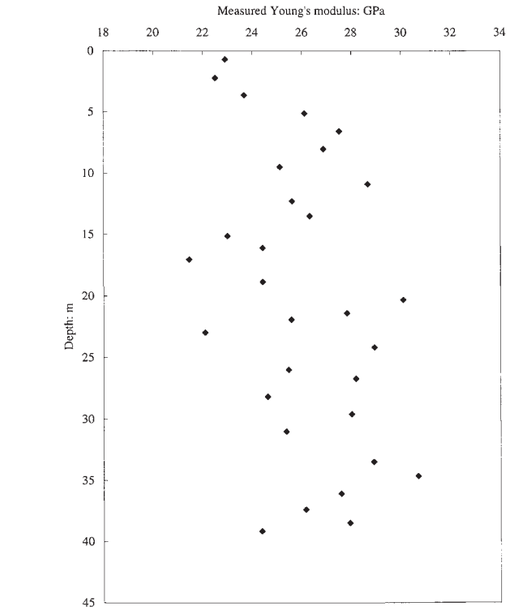

FIG. 6. Variation of Measured Young's Modulus of Concrete with Depth

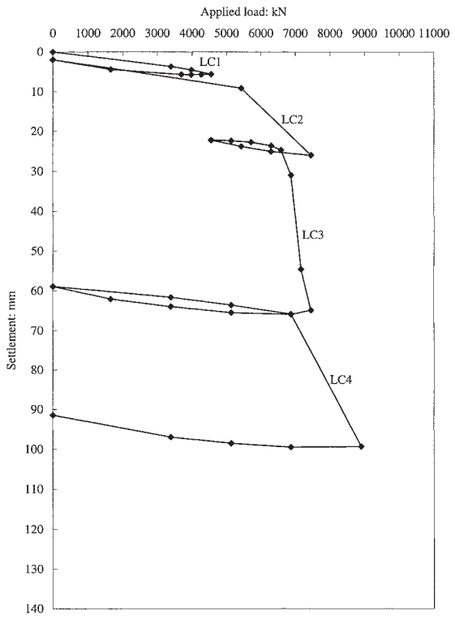

FIG. 5. Load-Settlement Response of Test Barrette

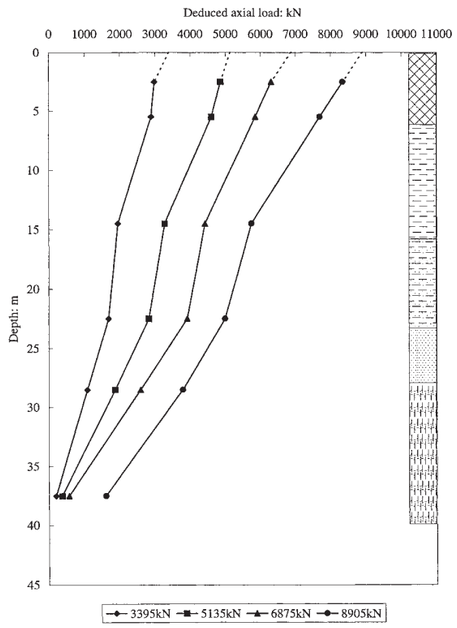

FIG. 7. Deduced Axial Load Distribution at Load Test Cycle 4

BARRETTE SKIN FRICTION

From the gradient of the barrette normal stresses with depth, mobilized skin friction (interface shear stress, τ) is calculated and plotted against deduced local displacement of the barrette in each soil stratum as shown in Fig. 8. Shear stress was fully mobilized in all soil strata when the displacement reached approximately 40 mm (or at 2.4% of the 1.7 m equivalent diameter of the barrette), after which the magnitude of shear stress remained essentially constant. Some peak strength behavior with softening at the interface was observed in the fill, sandy clay, and alluvial sand. The large skin friction mobilized in the fill material may possibly be attributed to the surcharge effects resulting from the dead weight of the concrete blocks supporting the kentledge load. On the other hand, no peak strength behavior could be identified at the barrette-weathered granite interface. Fig. 9 shows the distribution of mobilized skin friction with depth. Within the sheathed zone, a constant and substantial amount of shear stress was mobilized, apparently indicating that no ''weak'' zone existed around the sheathed barrette (except at depth below 15 m; see Fig. 7). The mobilized shear stress in the sandy clay was smallest, whereas the mobilized shear stresses in the fill, marine deposits, and weathered granite are in the same order of magnitude at the maximum applied load. Below the sheathed zone, the distribution of maximum mobilized shear stress follows the trend of the measured SPT-N values (Fig. 2). At the maximum applied load (8,905 kN), the mobilized skin friction of about 30 kPa was found for the fill, marine clay, alluvial sand, and weathered granite, and about 15 kPa for the sandy clay.

For comparing shear stress mobilized in similar soils at different construction sites, it is a common practice to normalize the measured shear stress with an average uncorrected SPT-N value, i.e., τ/N, (before construction) in Hong Kong. Fig. 10 shows the comparison between the normalized maximum shear stress measured at the current test site and at the International Trademart, which is about 1.4 km away in Kowloon Bay (Ho 1994). At the latter site, a 2.2 m by 0.8 m by 56.8 m deep barrette was also excavated by cable-operated grabs and founded in about 20 m thick layer of weathered granite, which has an average higher value of SPT-N value (typically ranging from 15 to 110) than the former site. For SPT-N values smaller than 35, the magnitude of measured skin friction is consistent between two sites. No comparison can be made between the measurements from the two sites for higher SPT-N values. However, the ranges of the values τ/N obtained from the former and the latter sites are 0.9 to 2.9 and 1.3 to 2.3, respectively.

PORE PRESSURE RESPONSE AT SOIL/BARRETTE INTERFACE

After installation of the piezometers, readings were taken continuously to compare them with the initial hydrostatic pore-water pressures in the ground (the initial ground-water table was located at about 1.3 mPD). It was found that the measured pore-water pressure at gauge P1 at the sandy clay layer (Fig. 11) was slightly higher than the corresponding hydrostatic value (1.3 mPD) before the loading test. Piezometric level (head) is defined as the sum of the pore-water pressure head and the elevation head at each location. The measured piezometric heads recorded at P3 and P4 were a little lower than the hydrostatic conditions in the weathered granite before the commencement of the load test. Labels LC1–LC4 denote the commencement of the first to the fourth load cycles, respectively. Similarly, labels UC1–UC4 represent the start of the first to the fourth unloading cycles.

When the first loading cycle (LC1) was carried out, all piezometers responded positively to each increment of applied load [Fig. 11(b)], recording an ultimate increase of head of almost 3 m in the sandy clay (P1) and about 1 m in both the alluvial sand (P2) and weathered granite (P3 and P4). During the first unloading cycle (UC1), the pore pressure in the sandy clay and alluvial sand remained steady while a slight and gradual reduction of pore pressure was recorded at P3 and P4 in the weathered granite. Each loading and unloading increment is clearly confirmed by the pile shortening and rebound measurements from the rod extensometer data.

During loading cycle 2 (LC2), again increments of applied load resulted in increments of positive pore pressure until failure occurred. A further increase of approximately 6 m head of water was measured in the sandy clay, 2 m in the alluvial sand

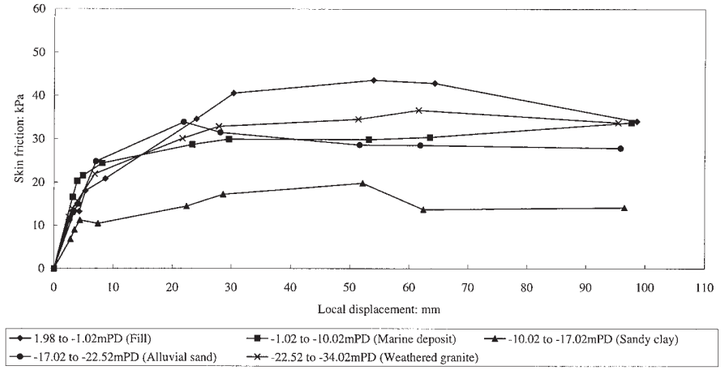

FIG. 8. Mobilization of Skin Friction with Local Displacement

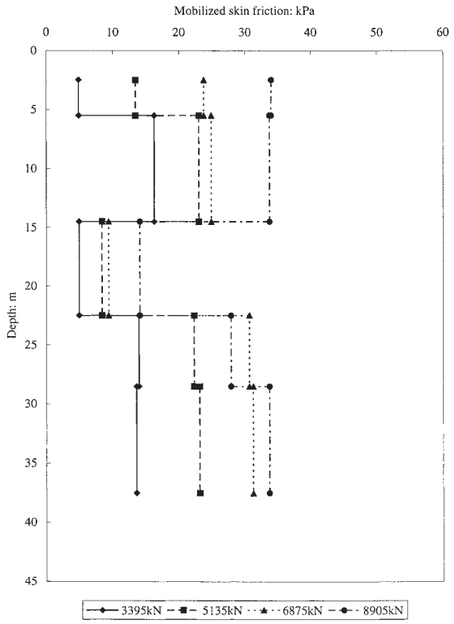

FIG. 9. Distribution of Mobilized Skin Friction (LC4)

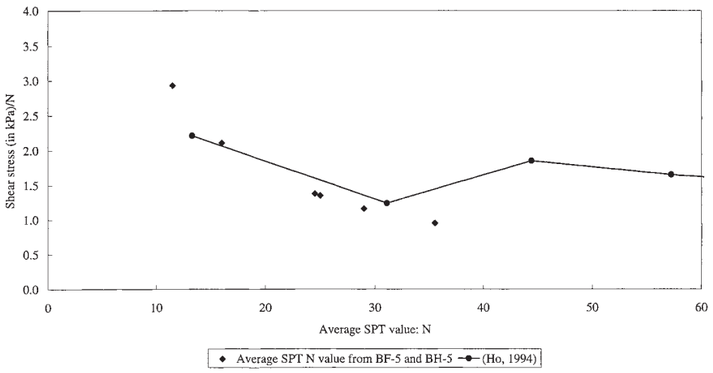

FIG. 10. Relationship between Normalized Maximum Shear Stress in Weathered Granite and Average SPT Value, N

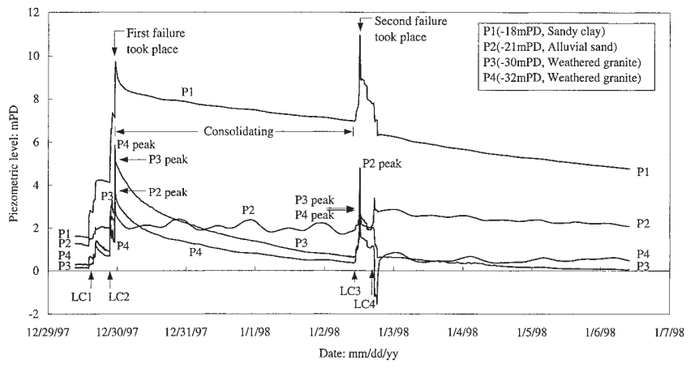

FIG. 11(a). Variations of Piezometric Level During Load Testing

and 4–5 m in the weathered granite, respectively. The minor drops in water pressure occur together with reduction in applied loading due to continued settlement of the pile. At failure the settlement rate of the barrette increased significantly and the settlement increased to about 25 mm (Fig. 5) and the pore pressures began to suddenly drop at the same time in all soil layers [after the loading slip shown in Fig. 11(b)]. Slip at the barrette-soil interface is inferred at failure since all rod extensometer data held constant, indicating that the entire barrette was moving downward as a rigid body (about 20 mm). After about 5 min of slippage, the load was reduced and then subsequently maintained for a holding period of 80 h. During this time the excess pore pressures dissipated almost completely in the weathered granite but only slightly in the sandy clay and, surprisingly, in the alluvial sand [Fig. 11(a)]. Also visible in this figure at P2 in the alluvial sand are measurements of tidal action. The shifted frequency and the attenuated relative magnitudes of the high and low tides correspond to actual tidal values from 12/30/97 to 1/2/98 (''Quarry'' 1997, 1998) almost perfectly, indicating proper functioning of the P2 pore-water pressure gauge.

Pore pressure behavior during the third loading cycle (LC3) was very similar to cycle 2. Loading increments resulted in corresponding increases in all four piezometers; overall, the increase of excess pore water pressure amounted to about 4 m head in the sandy clay, 3 m in the alluvial sand, and 2.5 m head in the weathered granite [Fig. 11(c)]. Failure and slippage of about 40 mm occurred at approximately the same load (7,455 kN) as cycle 2, again accompanied by significant and sudden drops of pore pressure at all the piezometers (due to

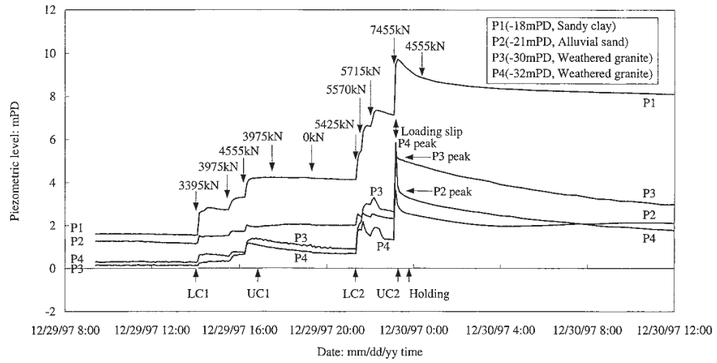

FIG. 11(b). Variations of Piezometric Level during First Two Load Test Cycles

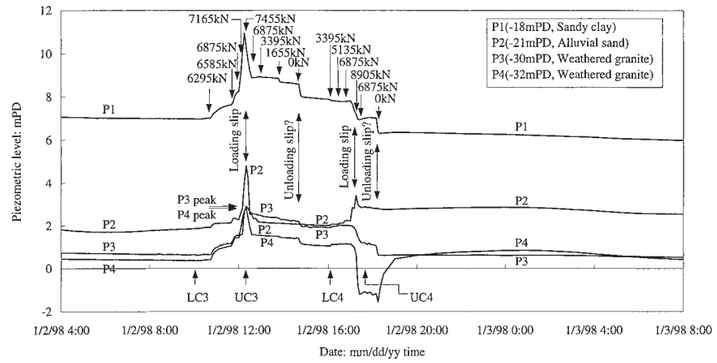

FIG. 11(c). Variations of Piezometric Level during Last Two Load Test Cycles

loading slip). During unloading (UC3) the measured pore pressures continued to drop slightly until another sudden drop of pore pressures was observed at the last unloading stage to 0 kN (except P2) which was most significant in the sandy clay.

Loading cycle 4 (LC4) varied from previous loading cycles since it occurred shortly after a barrette-soil interface failure. Increments of applied load in LC4 caused only slight increases of pore-water pressure in the alluvial sand and weathered granite while pore pressures remained essentially steady in the sandy clay [Fig. 11(c)]. As the load reached its maximum value of 8,905 kN (Fig. 5), failure occurred (about 30 mm of downward slippage), again resulting in substantial drops of pore-water pressures in all soil layers but the alluvial sand where an increase of water pressure followed by a drop was measured [Fig. 11(c)]. One piezometer in the weathered granite recorded a significant drop in pore pressure to a ''negative'' value, lower than the original in situ water pressure. Like UC3, water pressure values were steady until the last unloading step, when sudden changes in pore-water pressure resulted in all layers except the alluvial sand. Two of the piezometers recorded the standard drop in pore pressure, while the third ''negative'' reading piezometer showed a sharp increase back to a more reasonable value.

After the load test, dissipation of excess pore-water pressures continued [Fig. 11(a)]. As expected, the rate of dissipation was much slower in the sandy clay soil (P1) than in the weathered granite (P3 and P4). Dissipation at the alluvial sand interface was slow during loading, but generally the excess pore pressures generated returned near their equilibrium value (around 2 m of head) fairly quickly after slip. Nearly all the excess pore-water pressure was dissipated in the weathered granite by January 6, 1998, i.e., 80 h after the load test. On the other hand, about 3 m and 1 m excess pore-water head still remained in the sandy clay and alluvial sand layers, respectively, at this same time. What appeared to be tidal behavior was picked up at P2 and P4, but it is difficult to see since actual peak tide magnitudes dropped by 50% and the scan frequency of instruments was reduced substantially after the pile test.

CHANGES OF LATERAL STRESS AT SOIL/BARRETTE INTERFACE

After the vibrating wire earth pressure cells had been lowered into the excavated trench filled with bentonite, initial readings were taken before the instruments were jacked into position. This allowed an in situ calibration of the pressure cells to be made between the measured values and the theoretical bentonite pressures, using a measured unit weight of bentonite (γ_b) = 10.8 kN/m^3. It was found that there was good agreement between the calculated bentonite pressures and the readings recorded by the earth pressure cells; the maximum difference between the calculated and measured pressure was less than 10 kPa. At this point the cells were jacked out laterally to engage the soil.

Just after concreting, the lateral earth pressures increased to values close to the assumed in situ earth pressures before excavation. The measured total earth pressures at the soil/concrete interface also corresponded well with the theoretical bilinear concrete pressure envelope proposed by Ng (1993) and Lings et al. (1994) for concrete case under bentonite during diaphragm wall construction. Over the next two days lateral

pressures remained essentially unchanged in the sandy clay and alluvial sand soils, but increased about 100 kPa in the weathered granite. Further details of the earth pressure measurements and interpretations during the construction of the barrette are reported by Ng et al. (1999).

During the subsequent three-week curing period before the vertical load test, a gradual continuous decrease of lateral earth pressure was measured at all lateral earth pressure cells (about 30 kPa in the sandy clay and alluvial sand and about 60 kPa in the weathered granite). The observed reduction in the contact earth pressure may in large part be due to soil consolidation as indicated by the dissipation of excess positive porewater pressures generated during the construction of the barrette. In addition, the reduction in earth pressure might be caused by small shrinkage of the pressure cell units as a result of a fall in temperature after hydration of cement in the concrete. Lings et al. (1994) also reported reductions in earth pressure at the soil/diaphragm wall interface of a heavily overconsolidated stiff clay.

After the three-week curing period, the final result was an overall decrease of about 20–30 kPa below the assumed initial lateral earth pressures in the sandy clay and alluvial sand, and an increase of about 60 kPa above the original pressures in the weathered granite. This observed net increase in lateral earth pressure could be attributed to the swelling of weathered granite as result of stress relief during the excavation of the trench for constructing the barrette. Davies and Henkel (1981) have reported swelling behavior in weathered granite during the construction of diaphragm wall panels.

The measured earth pressures during the four cycles of load testing are shown in Fig. 12. The earth pressure cells all remained virtually constant during the first load and unload cycles (LC1 and UC1) when the barrette displacement was small [Fig. 5; Figs. 12(a and b)]. With the beginning of load cycle 2, some small drops of lateral earth pressure were seen in the weathered granite soil layer until the onset of pile failure (interface slip). Upon application of the maximum vertical load of 7,455 kN, a sudden and large reduction of about 100 kPa was measured at cells PC3 and PC4 in the weathered granite. At the same time there were noticeable falls in the other earth pressure cells also (about 20 kPa at PC1 in sandy clay and 45 kPa at PC2 in the alluvial sand). During the partial unloading and early holding period, there was a small recovery in earth pressure at all cells. Over the rest of the holding period, a slow but steady 25 kPa increase of pressure was measured in the weathered granite, while pressures in the sandy clay and alluvial sand remained almost constant [Figs. 12(a and b)]. Twice-a-day uniform fluctuations in lateral pressure were visible at all cells due to tidal pressures.

After the period of maintained load, further loading (LC3) did not cause a significant variation in earth pressures until a vertical load of 7,455 kN was applied and slip at the barrette-soil interface occurred. At this time a significant reduction in earth pressures (75 to 100 kPa) was again recorded by PC3 and PC4 [Fig. 12(c)] in the weathered granite. Small drops in the other earth pressure cells were also recorded at this time. During unloading of cycle 3 (UC3), pressure at PC1 and PC2 basically held constant while a slight recovery was again observed for the cells in the weathered granite.

Application of loading and unloading cycle 4 resulted in an

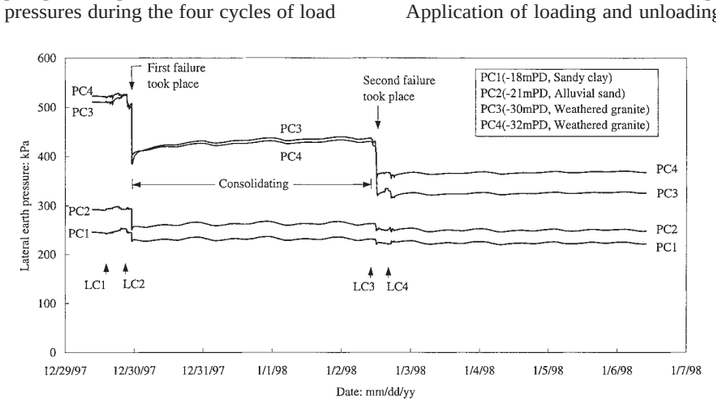

FIG. 12(a). Variations of Lateral Earth Pressure during Load Testing

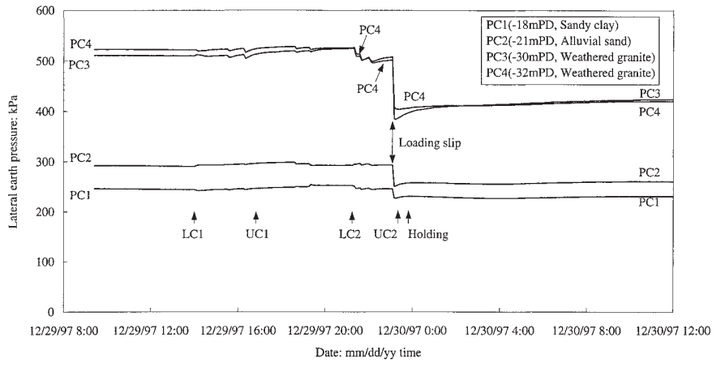

FIG. 12(b). Variations of Lateral Earth Pressure during First Two Load Test Cycles

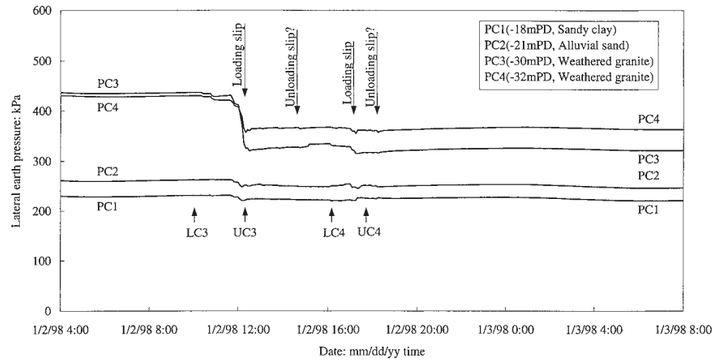

FIG. 12(c). Variations of Lateral Earth Pressure during Last Two Load Test Cycles

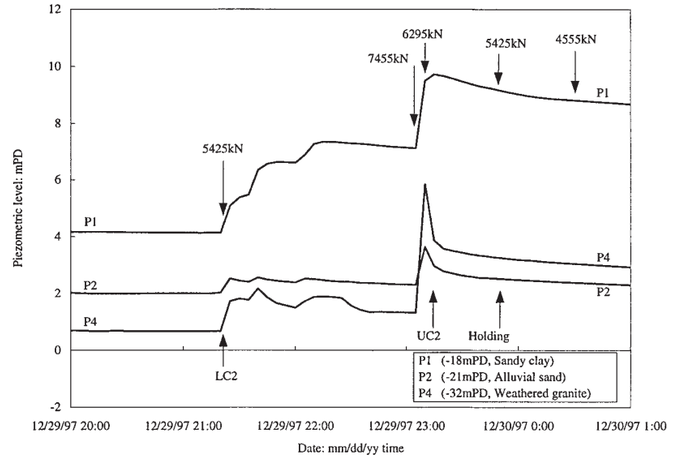

(a)

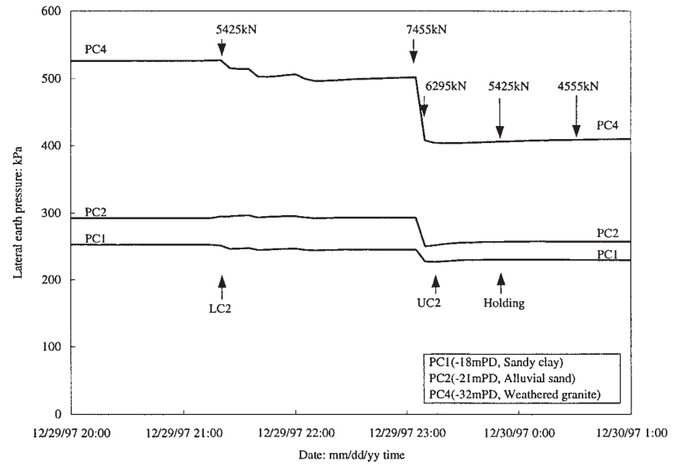

(b)

FIG. 13. Details of Pressure Changes at Interface during Load Cycle 2

overall constant lateral stress readings at all cells except for minor drops in pressure in three of the four cells at the onset of slip at about 7,000 kN. The lateral earth pressure over the next week remained constant in all soil layers.

SUMMARY AND POSSIBLE EXPLANATION OF BARRETTE-SOIL INTERFACE BEHAVIOR

The barrette-soil interface behavior consisting of shear strains, relative movements, pore pressure changes, and lateral earth pressure changes are clearly related. To more easily examine the relationships involved, pore pressure and lateral earth pressure measurements are combined on the same figure for two load cycles. Fig. 13 presents cycle 2 data illustrating virgin loading, slip, and partial unloading behavior (see also cycle 1 and 3 data). Fig. 14 gives details of cycle 4, which shows nonvirgin loading, slip, and unloading behavior soon after pile failure (cycle 3). In general, the behavior can be summarized as follows:

- Vertical pile loading produces shear strains in the soil near the barrette, inducing increased pore-water pressure and no significant changes in lateral earth pressures (highest in the sandy clay, lowest in the alluvial sand).
- Vertical pile unloading leaves pore pressures and lateral earth pressures essentially unchanged.
- At relatively large loading increments near pile failure, virgin slippage (shear failure) along the barrette-soil interface results in a reduction of pore pressures (usually highest in the sandy clay) and significant drops in lateral earth pressures (highest in the weathered granite).
- Finally, subsequent reloading of the pile soon after a failure does not result in pore pressure increases (except in alluvial sand), but when slip initiates, pore pressures again drop while lateral earth pressures maintain their values.

The mainly elastic simple shear of the interface soils apparently produces a ''loose'' or contractive volumetric response at the soil layers. Since the sandy clay and weathered granite soils have significant clay content, their shearing occurs under undrained conditions, producing increases in the pore-water pressure. Induced excess pore pressures may be higher in the normally consolidated sandy clay layer because of the higher clay content and since more simple shear occurs higher up the barrette (due to increased shortening of the pile). The increases in pore pressure in the alluvial sand layer are somewhat difficult to understand, but the excavation under bentonite would produce a normally consolidated bentonite cake layer at the barrette-sand boundary.

With its high clay content, the sandy clay may act in an undrained manner with no reductions in lateral earth pressure, while the small drops of earth pressure in the weathered granite are likely the result of higher permeability, allowing some consolidation to occur. The very slow dissipation of pore pressures in the sandy clay and relatively rapid dissipation in the weathered granite soil provide further confirmation [Figs. 11(a and b)].

Barrette-soil interface slip triggers consequential new behavior with the general sudden drop in both pore pressure and lateral earth pressure. The mechanisms involved in this basically consistent and repeated behavior are complex. It is possible that the soil behaves or tends to behave in a contractive manner when it is subjected to shearing. The pore pressure may drop because slip occurs during stress reversal, and this allows relaxation of the shear strains leading to a reduction of previous undrained pore-water pressure buildup. On the contrary, this slip also apparently permits some localized drainage and hence contraction of the soil to occur (possibly due to the sudden stress/strain reversal or reorganization of stresses in the local soil matrix). This would cause a release of the large confining stresses induced during previous shearing because the concrete wall of the barrette is rigid and does not act as a constant pressure interface. Any contraction of the soil away from the wall will lead to a reduction in total contact pressure. This might explain the sudden and large reductions of lateral earth pressure compared to the much smaller reductions in pore-water pressure. It should be noted that the concrete wall has a much higher stiffness relative to that of the adjacent soils. The observed complex pattern of interface pore pressure behavior described in the present barrette field test has been observed both in the field (Earth 1986; Matlock 1992) and the laboratory where pile/normally consolidated clay interface tests have been carried out measuring excess pore pressures during two-way cyclic loading as reported by Rigby and Desai (1996) and Rigby (1997). One observation of these authors is that the two-way cyclic shear of a pile-clay interface results in a continuous increase in excess pore pressure unless interface slip failure occurs, causing a sudden drop in excess pore-water pressure.

After cycle 2, at the Kowloon Bay test, when the soil was allowed to consolidate and strengthen, subsequent shearing of the soil during load cycle three resulted in the type of virgin loading behavior described previously for cycle 2 [Figs. 11(b and c)]. In contrast, load cycle 4 immediately followed cycle 3 so the behavior was more consistent with continued slip behavior since the interface was still weak.

A further interesting point is the occurrence of the same ''slip'' pattern of behavior at a small scale [Figs. 11(c) and 12(c)], during the last pile unloading step for cycles 3 and 4. In cycle 1 failure had not occurred yet, and in cycle 2 the barrette was not fully unloaded, so the sudden drops of pore pressure observed in both cycles 3 and 4 seem to be indicative of possible additional slip occurring.

STANDARD PRACTICE FOR DESIGN OF BARRETTES IN HONG KONG

Barrette design in weathered granite in Hong Kong has been essentially based on empirical approaches (Pratt and Sims 1990). An empirical relationship between an uncorrected SPT-N value before construction and allowable skin friction of 0.5N kPa with a limit of 100 kPa and an allowable end bearing pressure of 5N with a limit of 1,200 kPa are commonly used in Hong Kong. With this allowable load approach, the overall factor of safety (FOS) is not explicitly defined. However, a FOS greater than 2 is anticipated according to experience gained in Hong Kong.

To compare the current measured skin friction at Kowloon Bay with other tested barrettes in weathered granite in Hong Kong, the two most common approaches are adopted. Figs. 15 and 16 show the interpreted field test results from seven relatively well-documented case histories for barrette construction in weathered granite. Details of B1–B5 tests and test B6 are given by GEO (1996b) and Lo (1997), respectively. The test at the International Trademart in Kowloon Bay (Ho 1994) is identified as B5, and the current test is marked as B7 in the figures. The shaft friction coefficient β (GEO 1996b) is defined as the ratio between the ultimate skin friction and the mean vertical effective stress, assuming that the effective cohesion is zero. It can be seen that there is a large scatter in the deduced skin frictions; β varies from 0.1 to 0.46 whereas τ/N falls between 0.77 and 2.3. The variability may be a result of different methods of construction, quality of workmanship, quality and consistency of SPT testing, natural variations of ground conditions, and methods of interpretation.

By plotting the current test result (B7) in Fig. 15, the mobilized shear stress over SPT-N ratio is close to 1.5. This suggests an implicit FOS greater than 2. On the other hand, the deduced β value based on the effective stress principle is only 0.1 (Fig. 16), which is only half of the value obtained from a

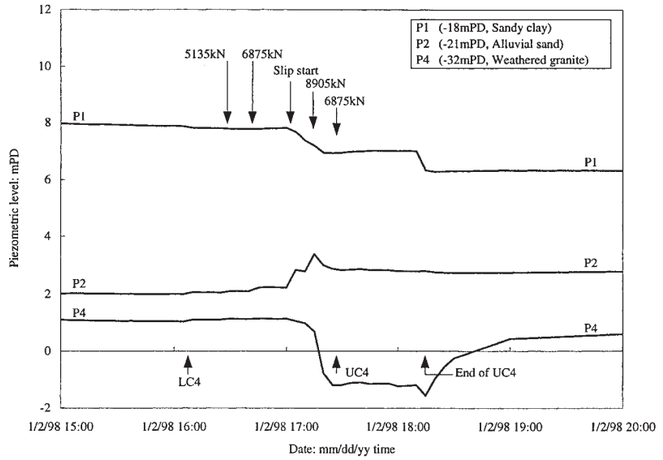

FIG. 14. Details of Pressure Changes at Interface during Load Cycle 4

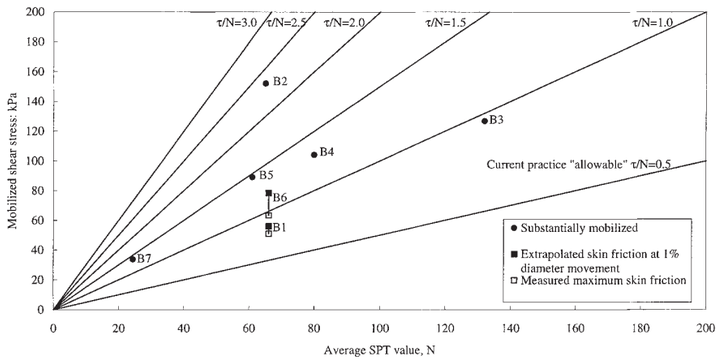

FIG. 15. Relationship between Skin Friction and Mean SPT Value, N for Barrettes

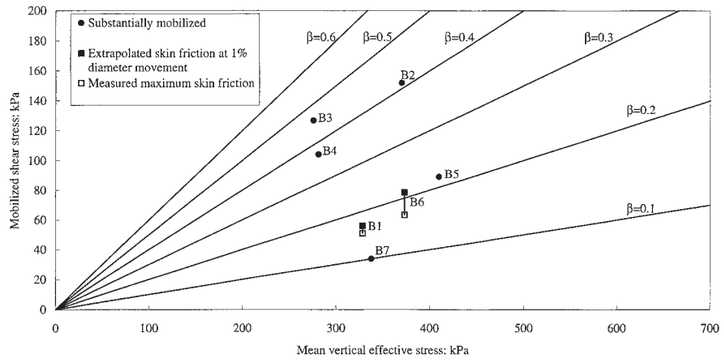

FIG. 16. Relationship between Skin Friction and Mean Vertical Effective Stress for Barrettes

similar site (i.e., B5). This low β value may be attributed to the unintended long delay in concreting after completion of the excavation (43 h). A thicker bentonite cake may have formed at the granite/barrette interface leading to a lower skin friction mobilized at the granite/barrette interface. The test results shown in Figs. 15 and 16 clearly indicated that the current empirical uncorrected SPT-N value approach and the effective stress β-method were inconsistent.

CONCLUSIONS

1. A well-instrumented 2.8 m by 0.8 m by 39.7 m deep excavated concrete pile (barrette) was successfully constructed and tested purely for research purposes in Hong Kong. This test pile was a joint effort and collaboration between the university, government agencies, and the industry. Due to the formation of a ''soft'' base at the bottom of the barrette, vertical displacement of more than 100 mm (6% of equivalent diameter) was permitted. This large vertical displacement of the barrette enabled skin friction at the barrette/soil interface to be fully mobilized.
2. The shear stress in all soil layers was fully mobilized at about 2.4% of the equivalent pile diameter with no or little softening behavior observed. At the maximum applied load (8,905 kN), the mobilized skin friction of about 30 kPa was found for the fill, marine clay, alluvial sand, and weathered granite, and about 15 kPa for the sandy clay. Normalized shear stress (τ/N) of the weathered granite ranged from 0.9 to 2.9 were obtained.
3. During the vertical load tests, specially installed instrumentation allowed the measurement of an unusual and complex response of pore-water pressures and earth pressures at several points along the barrette/soil interface. During each load cycle (except LC4), a buildup of excess positive pore-water pressure was recorded in the sandy clay and weathered granite as the vertical applied load on the barrette increased. The increase in pore-water pressure was likely caused by the undrained contractive behavior of the soils. There was no significant change in lateral earth pressure during each load and unload cycle, except at the occurrence of a large vertical displacement of the barrette. When loading caused significant slippage of the barrette within the soil, a consistent and substantial reduction in lateral total earth pressures resulted together with a drop of excess pore-water pressures. The earth pressure drop was most significant in the weathered granite soils, the changes in pore-water pressure more significant in the sandy clay.
4. The increases of pore-water pressure during pile loading and the sudden significant drop of lateral earth pressure at the onset of pile failure for some soil layers illustrate that the complex barrette-soil interaction will likely be best understood using a soil mechanics perspective. A possible mechanism to explain the behavior is that slip occurring during stress reversal permits some localized drainage and contraction of the soils. Since the concrete wall of the barrette is rigid and does not act as a constant pressure interface, any contraction of the soils away from the wall will lead to a reduction in total contact pressure.
5. The current test results indicated that the empirical SPT-N value approach and the β-method were inconsistent.

ACKNOWLEDGMENTS

The writers are grateful for the contribution provided by Paul Y. Foundation Ltd., who constructed the heavily instrumented research pile. Other sponsors of this test barrette include the Geotechnical Engineering Office of the Hong Kong Government, Fong On Construction Ltd., MTRC, Geotechnical Instruments Ltd., and the Hong Kong Institution of Engineers. In addition, the writers would like to acknowledge the financial support from the two research grants, HIA and CRC, awarded by the Hong Kong University of Science and Technology and the Research Grant Council of Hong Kong, respectively. Technical input and support from Professors C. K. Shen and Wilson Tang of the Hong Kong University of Science and Technology, and Martin Pratt and David Ng of Bachy Soletanche Group, are highly appreciated.

APPENDIX. REFERENCES

Davies, R. V., and Henkel, D. J. (1981). ''Geotechnical problems associated with the construction of Chater Station, Hong Kong.'' *Geotech. Seminar, Session No. 5*, HKIE.

Earth Technology Corporation. (1986). ''Pile segment tests—Sabine Pass: Some aspects of the fundamental behavior of axially loaded piles in clay soils.'' *ETC Rep. No. 85-007*, Houston/Long Beach.

Geotechnical Engineering Office (GEO). (1996a). ''R&D project PIL10a research on large-section excavated piles—trial piles, TNK959, Kowloon Bay.'' *Soil Testing Rep. No. 631*, Department of Civil Engineering of the Hong Kong Government of the Special Administrative Region, China.

GEO. (1996b). ''Pile design and construction.'' *GEO Publ. No. 1/96*, Department of Civil Engineering of the Hong Kong Government of the Special Administrative Region, China.

Ho, K. K. S. (1994). ''Behaviour of the instrumented trial barrette for the Trademart Development at N.K.I.L. 6032, Kowloon Bay.'' *Spec. Proj. Rep. SPR8/94*, Geotechnical Engineering Office, Department of Civil Engineering of the Hong Kong Government of the Special Administrative Region, China.

Lings, M. L., Ng, C. W. W., and Nash, D. F. T. (1994). ''The pressure of wet concrete in diaphragm wall panels cast under bentonite.'' *Geotech. Engrg. Proc. Instn. of Civ. Engrs., U.K.*, London, 107(July), 163–172.

Lo, D. O. K. (1997). ''Behavior of the instrumented test barrette for the west Kowloon corridor stage IV project.'' *Spec. Proj. Rep. SPR 2/97*, Geotechnical Engineering Office, Civil Engineering Department of the Hong Kong Special Administrative Region, China.

Matlock, H. (1992). ''Field and laboratory testing.'' *Proc., U.S.-Canada NSF Workshop on Recent Accomplishments and Future Trends in Geomech. in the 21st Century*, M. Zaman, C. S. Desai, and A. P. S. Selvadurai, eds., 58–64.

Ng, C. W. W. (1993). ''Lateral stress development in diaphragm walls during concreting.'' *Proc. Int. Conf. on Retaining Struct.*, Thomas Telford, London, 77–80.

Ng, C. W. W., Rigby, D., Lei, G. H., and Ng, S. W. L. (1999). ''Observed performance of a short diaphragm wall panel.'' *Géotechnique*, London, 49(5), 681–694.

Pratt, M. and Sims, M. J. (1990). ''The application of new techniques to solve deep basement and foundation problems.'' *Proc. Int. Conf. on Deep Foundation Practice*, 189–195.

''Quarry bay times and heights of high and low waters 1997.'' (1997). *Tide Tables for Hong Kong 1997*, Royal Observatory, Hong Kong, 25.

''Quarry bay times and heights of high and low waters 1998.'' (1998). *Tide Tables for Hong Kong 1998*, Royal Observatory, Hong Kong, 20.

Rigby, D. B. (1997). ''Pore pressure behavior of clay-steel interfaces.'' *Proc., 2nd Int. Symp. on Struct. and Found. in Civ. Engrg.*, HKUST, Hong Kong, 251–256.

Rigby, D. B., and Desai, C. S. (1996). ''Testing and constitutive modeling of saturated interfaces in dynamic soil-structure interaction.'' *Rep. to Nat. Sci. Found.*, Dept. of Civ. Engrg. and Engrg. Mech., University of Arizona, Tucson, Ariz.

Shen, C. K., Ng, C. W. W., Tang, W. H., and Rigby, D. (1997). ''Testing a friction barrette in decomposed granite in Hong Kong.'' *Proc., 14th Int. Conf. Soil Mech. and Found. Engrg.*, Vol. 4, 2423–2426.

Strange, P. J. (1990). ''The classification of granite rocks in Hong Kong and their sequence of emplacement in Sha Tin, Kowloon and Hong Kong Island.'' *Geotech. Soc. of Hong Kong Newsletter*, Hong Kong, 8(1), 18–27.

Tunnelling and Underground Space Technology xxx (2012) xxx–xxx

Contents lists available at SciVerse ScienceDirect

Tunnelling and Underground Space Technology

journal homepage: www.elsevier.com/locate/tust

Three-dimensional centrifuge modelling of the effects of twin tunnelling on an existing pile

C.W.W. Ng, H. Lu *, S.Y. Peng

Department of Civil and Environmental Engineering, Hong Kong University of Science and Technology, Clear Water Bay, Kowloon, Hong Kong

ARTICLE INFO

Article history:
Received 6 March 2012
Received in revised form 11 July 2012
Accepted 23 July 2012
Available online xxxx

Keywords:
Twin tunnelling
Piles
Three-dimensional
Soil–structure interaction
Centrifuge modelling
Dry sand

ABSTRACT

Tunnelling activity inevitably induces soil stress changes and ground deformation, which may affect nearby existing pile foundations. Although a number of studies have been carried out to investigate the effects of tunnelling on existing piles, the excavation of only one tunnel is often considered. The fundamental interaction between twin tunnel construction and an existing pile foundation has not been thoroughly studied. In this study, a series of three-dimensional centrifuge model tests investigating the effects of twin tunnel construction on an existing single pile in dry sand were conducted. The influence of the depth of each tunnel relative to the pile was investigated by constructing the twin tunnels either close to the mid-depth of the pile shaft or near the pile toe. The pile settlement induced by the excavation of the twin tunnels is found to be closely related to the depth of each tunnel relative to the pile. The measured cumulative pile settlement due to tunnelling near the toe is about 2.2 times of that due to tunnelling near the mid-depth of the pile shaft. Apparent losses of pile capacity of 36% and 20% are identified due to the construction of twin tunnels near the pile toe and at the mid-depth of the pile, respectively. Although there is an increase in the axial force induced in the pile when a tunnel is constructed at the mid-depth of the pile, significant increases in bending moment is not observed in any of the tests.

1. Introduction

Tunnel construction inevitably causes soil stress changes in the ground and hence induces ground movements. Uncontrolled ground movements induced by tunnelling may cause cracking in buildings and gas mains, or induce additional loads on piles of nearby structures. In urban cities, it is not uncommon to encounter existing piles during tunnel constructions. Estimation of the effects of tunnelling on existing pile foundations of buildings poses a major challenge to designers. It is particularly vital to estimate the tunnelling effects when two new tunnels are to be built near an existing pile.

Bezuijen and Schrier (1994) studied the influence of bored tunnels on pile foundations. They pointed out that the pile settlement can be quite significant if the distance between pile and tunnel is less than the tunnel diameter. Loganathan et al. (2000) assessed tunnelling-induced ground deformations and their adverse effects on pile foundations in clay. Tunnelling-induced bending moment and axial force in the piles of a pile group were investigated by modelling volume loss of a tunnel in a single stage. They concluded that the tunnelling-induced bending moment may be critical when the centerline of the tunnel is located near the pile toe. Jacobsz et al. (2004) investigated the adverse effects of tunnelling beneath a pile in dry sand. An influence zone was identified above and around the tunnel in which the pile could suffer significant settlement, depending on the volume loss induced by the tunnelling. Lee and Chiang (2007) studied the tunnelling-induced bending moment and axial force in a single pile in saturated sand. Tunnels were embedded at various cover-to-diameter ratios. The authors concluded that the depth of the tunnel relative to the pile has a significant influence on the distribution of the bending moment along the pile. As far as the authors are aware, the three-dimensional centrifuge modelling of the effects of twin tunnelling on a single pile has not been reported.

Mroueh and Shahrour (2002) carried out three-dimensional elastoplastic finite element analyses to study the influence of a tunnel construction on a single pile as well as on pile groups. The numerical results showed that there is a significant reduction in the tunnelling-induced axial force and bending moment in the piles furthest away from the tunnel due to the group effect. Lee and Ng (2005) carried out a three-dimensional, elasto-plastic, coupled-consolidation numerical analysis to investigate the effects of an open face tunnel excavation on an existing loaded pile. It is shown that the factor of safety (FOS) of a pile can be reduced from 3.0 to 1.5 due to the additional settlement of a pile induced by tunnelling when a settlement-based failure criterion (Ng et al., 2001a) is used.

* Corresponding author. Tel.: +852 5104 8252; fax: +852 2243 0040.
E-mail addresses: cecwwng@ust.hk (C.W.W. Ng), luhu@ust.hk (H. Lu), muffinpp@ust.hk (S.Y. Peng).

0886-7798/$ - see front matter © 2012 Elsevier Ltd. All rights reserved.
http://dx.doi.org/10.1016/j.tust.2012.07.008

ARTICLE IN PRESS

The effects of tunnel construction on the nearby pile foundations are obviously three dimensional. A fundamental understanding of the three-dimensional tunnel-soil-pile interaction is needed. In addition, few researchers have investigated the effects of twin tunnelling on piles, except Pang (2007), who reported the field monitoring and numerical study of the effects of twin tunnelling on an adjacent pile foundation in Singapore. A northbound tunnel and a southbound tunnel were constructed near piles one after the other. The smallest clear distance between the tunnels and piles was 1.6 m. Results of the field study showed that the piles were subjected to a large dragload due to an induced soil settlement in residual soil. However, strain gauges are only instrumented along pile portion near tunnels. The pile settlement due to tunnelling is not reported.

In this study, a series of three-dimensional centrifuge model tests were performed to investigate the behavior of a single pile due to the construction of twin tunnels one after the other. The effects of the three-dimensional tunnel excavation process were simulated in-flight by controlling the volume loss at 1.0% in each stage of the three-dimensional excavation of each tunnel. The twin tunnels in each test are located at either mid-depth of the pile or the pile toe. In addition to measurements of ground surface settlement and pile settlement, the bending moment and axial force induced in the pile by the tunnelling in different stages of construction were captured. The objective of this study is to investigate the response of an existing pile when a new tunnel excavation is to be carried out nearby. It is intended that results from this study can assist engineers and designers to choose and design the location (i.e., the depth) of the new tunnel.

2. Centrifuge modelling

2.1. Experimental program and setup

The fundamental principle of centrifuge modelling is to recreate the stress conditions, which would exist in a full-scale problem, in a model of a greatly reduced scale. This is done by subjecting model components to an enhanced body force, which is provided by centripetal acceleration ($r\omega^2$) when a centrifuge rotates at a constant angular velocity (ω) about the center of the centrifuge arm with radius, r. For instance, an 100 m prototype stress conditions can be replicated in a centrifuge by an 1 m height model when the Earth's gravity (g) is enhanced by 100 times (i.e., $r\omega^2 = Ng = 100g$). Thus, centrifuge is suitable for simulating stress-dependent materials such as soils. More details, scaling laws and centrifuge applications are given by Schofield (1980), Taylor (1995) and Ng et al. (2006). Table 1 summarizes all the relevant scale laws in this study.

In total, four centrifuge model tests were carried out at the Geotechnical Centrifuge Facility of the Hong Kong University of Science and Technology (Ng et al., 2001b, 2002). The 400g ton centrifuge has an arm radius of 4.2 m and is equipped with a two-dimensional hydraulic shaking table and a four-axis robotic manipulator. All of the centrifuge tests were carried out at an acceleration of 40g.

Table 1
Centrifuge scaling factor.

Physical quantity	Scaling factor (model/prototype)
Gravitational acceleration	n
Length	$1/n$
Area	$1/n^2$
Volume	$1/n^3$
Settlement	n
Stress	1
Strain	1
Force	$1/n^2$
Density	1
Mass	$1/n^3$
Flexural stiffness	$1/n^4$
Bending moment	$1/n^3$

Fig. 1a shows the schematic elevation view of Test T. A single pile is located at the center of each model container. Test T is designed to investigate the behavior of a pile due to a single tunnel constructed near pile toe in dry sand. The model pile had a diameter of 20 mm (0.8 m in prototype) and was 600 mm long (24.0 m in prototype). The pile cap was elevated by 110 mm and therefore the embedded depth of each pile was 490 mm (19.6 m in prototype). The tunnel diameter (D) was 152 mm (6.08 m in prototype). The C/D ratio (cover-to-diameter ratio) of the tunnel is 2.7. The horizontal distance from the centerline of the tunnel to the pile was $0.75D$. In addition, a separate test (Test L) is carried out to obtain the load settlement curve of the single pile without tunnelling effects. This test has the same configuration of Test T but only without the model tunnel.

As shown in Fig. 1b, Test TT was designed to study the effects on the pile induced by the construction of twin tunnels, one after the other, near the pile toe. The C/D ratio of each tunnel is 2.7, same as that in Test T. Fig. 1c shows the schematic elevation view of Test SS. This test was designed to investigate pile responses induced by the construction of twin tunnels near the mid-depth of pile shaft. The C/D ratio of each tunnel is 1.5. A summary of the test program is given in Table 2.

Fig. 2a and b shows the plan views for Test T and Tests TT and SS, respectively. In Test T, the model tunnel had a length of 228 mm, which was equal to $1.5D$. The three-dimensional tunnel construction was simulated in three stages, with the tunnel face advancing by a distance of $0.5D$ in each stage. In Tests TT and SS, the longitudinal length of each tunnel was 380 mm, which was equivalent to $2.5D$. The tunnel excavation was simulated in five stages, again with the tunnel face advancing by a distance of $0.5D$ in each stage. A photograph of the model package is shown in Fig. 3a.

2.2. Simulation of tunnel construction

In simulating of tunnel advancement, it is common to model overall volume loss resulting from tunnelling effects in practice (Taylor, 1995; Mair, 2008), rather than trying to simulate different construction steps in centrifuge. Obviously, this implies that some construction details like erection and deformation of tunnel liners, stiffness of liners and workmanship are not simulated separately. Only the overall result like volume loss due to actual tunnelling is simulated. Obviously, this type of modelling is not ideal. However, it does capture the essential effects (i.e., volume loss) of tunnelling and can meet the comparative objective of different simulated cases in this paper.

In the single tunnel test, the model tunnel consisted of three cylindrical rubber bags. In the twin tunnel tests, each model tunnel consisted of five cylindrical rubber bags (see Fig. 3b). Between two rubber bags was a rigid aluminum divider to control and separate the volumes of water inside so that volume change in each rubber (i.e., the tunnel volume loss) can be controlled independently. Each rubber bag was filled with de-aired water. Three-dimensional tunnel construction was simulated in-flight by draining away a controlled amount of water from each rubber bag one by one. The amount of water drained away was controlled as 1.0% of the total volume of the cylindrical rubber bag. This is to simulate an equivalent volume loss of 1.0% of excavated cross section area of the tunnel face during each stage of tunnel construction. Since the effects of tunnel excavation were modelled by inducing an equivalent volume loss resulting from various construction factors and tunnel

Please cite this article in press as: Ng, C.W.W., et al. Three-dimensional centrifuge modelling of the effects of twin tunnelling on an existing pile. Tunnel. Underg. Space Technol. (2012), http://dx.doi.org/10.1016/j.tust.2012.07.008

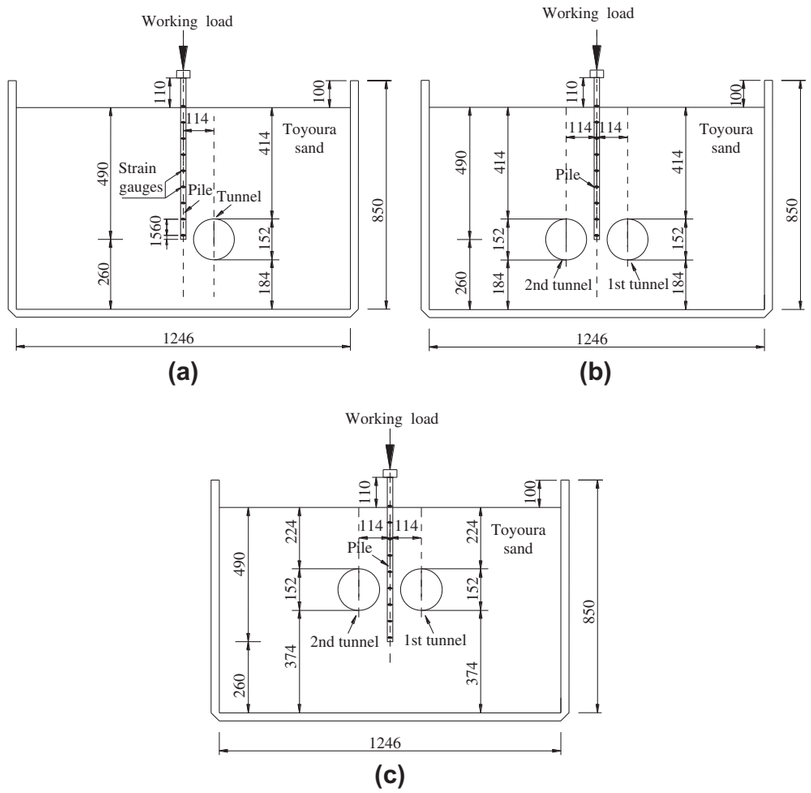

Fig. 1. Elevation view of centrifuge model: (a) Test T; (b) Test TT; (c) Test SS. All dimensions are in mm in model scale.

Table 2
Test program.

Test ID	C/D	Remark	Relative density of sand (%)
L	N/A	Pile load test	60
T	2.7	Single tunnelling near pile toe	60
TT	2.7	Twin tunnelling near pile toe	65
SS	1.5	Twin tunnelling near pile shaft	62

N/A denotes not applicable.

liner in the field, model tunnel liner is not needed to be simulated in the centrifuge tests.

2.3. Model piles and instrumentation

The instrumented model pile was fabricated from an aluminum tube (see Fig. 1a). Nine levels of full Wheatstone bridge of strain gauges were installed to record bending moment and axial force along the entire pile length. The strain gauges were protected by a thin layer of epoxy. Prior to a centrifuge test, calibration was carried out to obtain a relationship between an applied bending moment to the pile and the corresponding reading of each full Wheatstone bridge. For structural elements, the bending stiffness (EI) of pile was chosen as the vital governing property to be satisfied. It can be derived that the scaling requirement for a model pile $(EI)_m$ is equal to $N^{-4}(EI)_p$ (refer to Table 1), where N is the number of times of gravity enhanced in a centrifuge test, E is Young's modulus, I is the second moment of area for a cross-section, and subscripts m and p refer to the model and prototype scale, respectively. The model pile had an axial rigidity (E_mA_m) of 7473 kN and a bending rigidity (E_mI_m) of 273 N m^2, which are corresponding to prototype E_pA_p of 11,957 MN and E_pI_p of 701 MN m^2 of a real concrete pile, respectively. The pile is "wished-in-place" in the sand bed. Thus, pile installation effects are not simulated.

In each test, the pile was loaded in-flight (i.e., while the centrifuge is spinning) using a hydraulic jack. A load cell was installed at the piston of the jack to control applied load. Settlement of the pile was measured by a linear variable differential transformer (LVDT) located at the pile head.

2.4. Model preparation

Dry Toyoura sand ($G_s = 2.65$, $e_{max} = 0.977$, $e_{min} = 0.597$, $\varphi'_{cv} = 31°$) (Ishihara, 1993) was used in each test. Each centrifuge model was prepared by the pluvial deposition method. Sand was "rained" from a hopper, which was kept 500 mm above the surface. The measured average relative density of each test is also given in Table 1. Since the scaling factor for soil density is one (see Table 1), soil with a relative density of 60–65% (refer to Table 2) in prototype was modelled in each centrifuge test. It is well understood that the stiffness of a soil (i.e., shear modulus, G or Young's modulus, E_s) is dependent on its density and stress level. The stress level is simulated correctly and prototype soil density is prepared in a centrifuge. Therefore, the stiffness of the ground should be comparable to that of full scale in prototype.

Please cite this article in press as: Ng, C.W.W., et al. Three-dimensional centrifuge modelling of the effects of twin tunnelling on an existing pile. Tunnel. Underg. Space Technol. (2012), http://dx.doi.org/10.1016/j.tust.2012.07.008

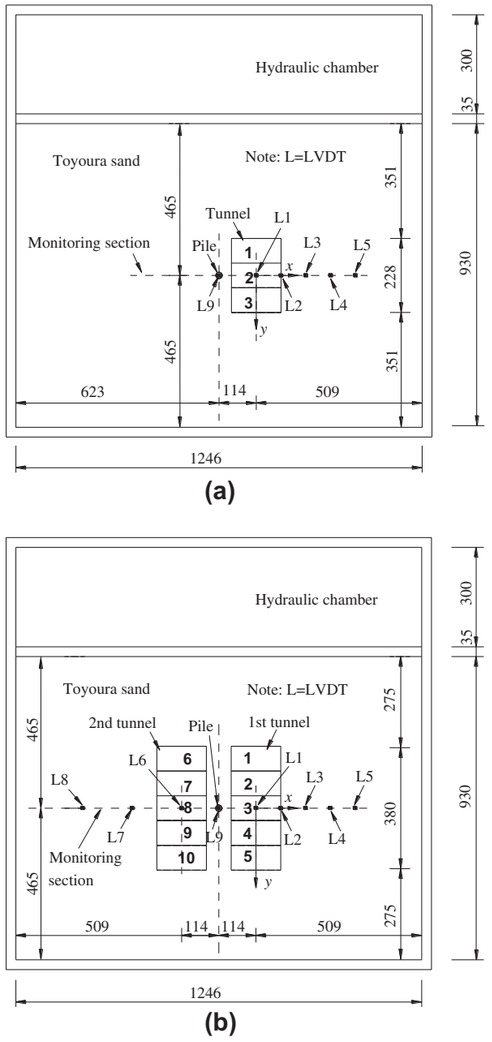

Fig. 2. Plan view of centrifuge model: (a) Test T; (b) Test TT and Test SS. All dimensions are in mm in model scale.

2.5. Test procedure

After model preparation, the acceleration of the centrifuge was increased to 40g. The model pile was loaded in-flight at 40g in a number of steps. In each step, an incremental vertical load of 100 N (160 kN in prototype) was applied. Each load increment was maintained for 3 min. Once the load had reached the working load (1200 N), tunnel construction with the designed volume loss of 1.0% was carried out. Three construction stages were simulated in-flight by draining away water from each of the rubber bags one after the other in Test T, as shown in Fig. 2a. A similar procedure was adopted in Tests TT and SS, except five tunnel construction stages were simulated. Throughout each test, ground surface settlement, settlement of the pile, induced bending moment and axial force along the pile were recorded.

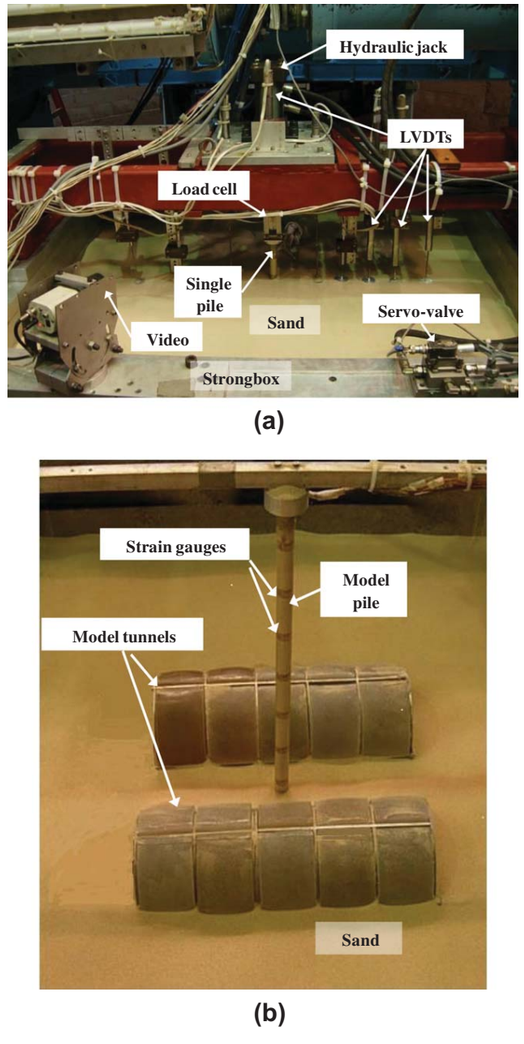

Fig. 3. (a) A typical model setup; (b) model tunnels and model pile.

3. Test results

All test results presented in this paper are in prototype scale, unless stated otherwise.

3.1. Determination of the axial load carrying capacity of the pile

Prior to tunnelling, it is necessary to obtain the capacity of the pile so that the working load can be deduced. A pile load test

Please cite this article in press as: Ng, C.W.W., et al. Three-dimensional centrifuge modelling of the effects of twin tunnelling on an existing pile. Tunnel. Underg. Space Technol. (2012), http://dx.doi.org/10.1016/j.tust.2012.07.008

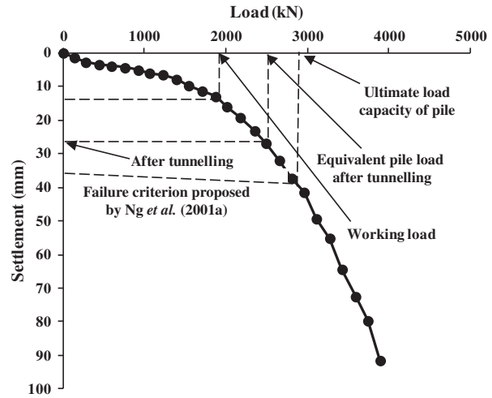

Fig. 4. Load settlement relationship obtained from load test without tunnelling (Test L).

(i.e., Test L) was carried out. Fig. 4 shows the measured load settlement relationship. The load applied to the pile cap was gradually increased to 4 MN at increments of 100 kN in each step. The ultimate axial load capacity was determined based on a displacement-based failure criterion proposed by Ng et al. (2001a). This failure criterion is expressed as follows:

$$\delta_{ph,max} \cong 0.045 d_p + \frac{1}{2}\frac{P_h L_p}{A_p E_p} \quad (1)$$

where $\delta_{ph,max}$ is the maximum pile head movement which defines the ultimate load, P_h is the pile head load, L_p is the pile length, E_p is the elastic modulus of pile shaft, A_p is the cross-sectional area of the pile, and d_p is the pile diameter. The failure criterion proposed by Ng et al. (2001a) is a semi-empirical method for estimating an approximate interpreted failure load for pile. The method is based on a moderately conservative estimation of the movement required to mobilize toe resistance and incorporates observations of shaft shortening from actual pile loading tests. Both the 5%*D* criterion proposed by O'Neill and Reese (1999) and 10%*D* criterion proposed by Weltman (1980) do not include shortening of pile shaft and thus they may not be appropriate for long piles. Both criteria are displacement-based failure criteria. The 5%*D* and 10%*D* criterion defines the failure load of pile as the load causing a settlement of 5% and 10% of the pile diameter, respectively.

As shown in the figure, the ultimate load capacity of the pile was 2.88 MN. A working load of 1.92 MN was adopted with a factor of safety of 1.5. A pile settlement of 1.6%d_p was observed due to the applied working load.

3.2. Ground surface settlement

Fig. 5a shows the extents of ground surface settlement (S) measured by LVDTs 1–8 (as shown in Fig. 2) in Tests T and TT. Both the measured surface settlement and the transverse distance from the centerline of the first tunnel in Test TT and the only tunnel in Test T (x) were normalized by the diameter of tunnel (D).

In Test T, only half of the ground surface settlement trough was measured. At the end of the three stages of tunnel excavation, the measured maximum settlement was 0.27%*D* above the centerline of the tunnel. At a distance of 2*D* from the centerline of the tunnel, a surface settlement of 0.03%*D* was also measured. In Test TT, a maximum settlement of 0.24%*D* occurred at the centerline of the first tunnel after its completion. The consistency between the

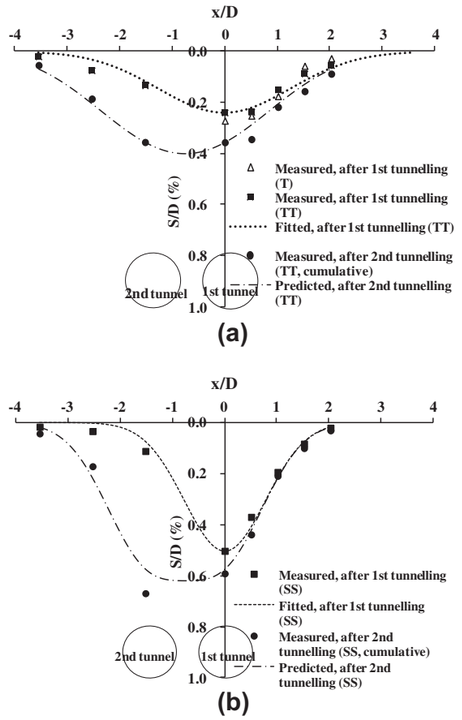

Fig. 5. Ground surface settlement induced by tunnel excavation: (a) Test T and Test TT; (b) Test SS.

two measured maximum settlement values illustrates the repeatability of the tests. After the excavation of the second tunnel in Test TT, the measured maximum surface settlement above the second tunnel was almost the same as that due to the construction of the first tunnel. The measured maximum accumulated settlement was 0.35%*D* after the excavation of the twin tunnels. Since no LVDT was installed between the centerlines of the two tunnels, the location where the maximum settlement occurred could not be identified. However, the maximum settlement was unlikely to have occurred above the centerline of the second tunnel.

The ground surface settlement profile due to tunnel construction may be represented by a Gaussian distribution (Peck, 1969). Ground surface settlement S is defined as

$$S = S_{max}\exp(-x^2/2i^2) \quad (2)$$

$$S_{max} = \frac{V_s}{\sqrt{2\pi}i} \quad (3)$$

where S_{max} is the maximum settlement at the tunnel centerline, i and x are the lateral distances from the tunnel centerline to the point of inflection and any other points on the settlement trough, respectively. V_s is the volume of settlement trough.

Eq. (2) was adopted to fit the measured values of ground surface settlement induced by excavation of the first tunnel in Test TT. As expected, the measured S_{max} was located above the centerline of the first tunnel. The best-fitted curve using an i of 7.5 m is shown in Fig. 5a. As proposed by O'reilly and New (1982), i can be represented by KZ, where Z is the vertical distance from ground surface to the center of tunnel. Following the above equation, the deduced

Please cite this article in press as: Ng, C.W.W., et al. Three-dimensional centrifuge modelling of the effects of twin tunnelling on an existing pile. Tunnel. Underg. Space Technol. (2012), http://dx.doi.org/10.1016/j.tust.2012.07.008

K value for the best-fitted curve is 0.39, which lies between the values 0.25 and 0.45 suggested by Mair and Taylor (1997) for tunnelling in sand.

Based on the design chart proposed by Peck (1969), the maximum settlement calculated using Eq. (3) is 38 mm (0.63%*D*), which is more than twice the measured data. This is consistent with the findings by Attewell and Farmer (1974), who also observed that the method proposed by Peck (1969) overestimates the maximum settlement for tunnelling in sand.

To predict the surface settlement above twin tunnels, Attewell et al. (1986) suggested summing the Gaussian curves induced by two tunnels. In this study, the best-fitted Gaussian curve is deduced from excavation of the first tunnel, as shown in Fig. 5a. Incremental settlement due to the second tunnelling is assumed the same as that during the first tunnel excavation. Superimposed curve based on the two Gaussian curves are also shown in the figure. It can be seen that the combined settlement curve fits quite well with the measured values at the end of the second excavation, except that settlement above the shoulder of the first tunnel.

Fig. 5b shows the measured surface settlement profiles in Test SS. After excavation of the first tunnel, a maximum settlement of 0.50%*D* occurred above the centerline of the first tunnel. After excavation of the second tunnel, the location of maximum surface settlement shifted to above the centerline of the second tunnel and the measured maximum value was 0.67%*D*. By fitting a Gaussian curve to the measured surface settlement profile after the construction of the first tunnel in Test SS, the fitted *K* value was found to be 0.39, consistent with that in Test TT. Similarly, by summing the two best-fitted Gaussian curves, the resulting settlement distribution is also included for comparison in Fig. 5b. The maximum settlement obtained from the summation of the two fitted curves was located above the centerline of the twin tunnels. Moreover, the measured settlement was 16% larger than the combined maximum value. It is evident that the incremental maximum settlement induced by the excavation of the second tunnel was larger than that induced by the first tunnel. Addenbrooke (1996) and Chapman et al. (2007) also found that the incremental surface settlement induced by the second tunnel is larger than that induced by the first tunnel when C/D of twin tunnels is larger than 3.0, which is higher than Test TT in this study. However, it should be noted that volume loss in each individual tunnel was not controlled in their studies. On the contrary, this study simulates tunnelling by controlling the volume loss to be 1% in all tests. This might be the reason why the magnitudes of incremental settlements induced by the twin tunnelling are close in Test TT.

Comparing the measured surface settlements in Tests TT and SS, it can be observed that the maximum surface settlement in Test TT (i.e., 0.35%*D*) was substantially smaller than that in Test SS (i.e., 0.67%*D*). This was because C/D (=1.5) the twin tunnels in Test SS was smaller than that in Test TT (C/D = 2.7). Mair et al. (1993) reported that the maximum surface settlement above one tunnel is inversely proportion to the depth of the tunnel for a given volume loss, tunnel diameter and constant value of *K*. Based on this study, it is evident that the surface settlement induced by twin tunnelling also decreases with increasing C/D ratio.

3.3. Pile settlement and apparent loss of pile capacity due to tunnelling

Fig. 6 shows the development of the normalized pile settlement (S_p) during each tunnel construction stage. Location of the tunnel at any stage is indicated by the distance between tunnel face to the centerline of the pile (y). Both the measured S_p and the distance from the tunnel face to the centerline of the pile (y) were normalized by the tunnel diameter (D).

In Test T, as the tunnel face advanced at a depth of C/D = 2.7 from y/D = −0.75 to −0.25, a pile settlement of 0.04%*D* was

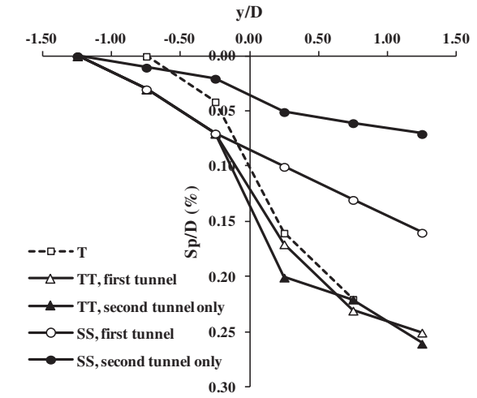

Fig. 6. Pile settlement induced by excavations of twin tunnels.

induced. A significant increase in pile settlement (0.12%*D*) occurred when the tunnel face advanced from y/D = −0.25 to 0.25. When the tunnel face reached y/D = 0.75, the pile settlement increased to 0.22%*D* (1.7% of the pile diameter). About 55% of the pile settlement was induced when the tunnel face was between y/D = −0.25 and 0.25.

In Test TT, it can be seen that the development of the pile settlement during each tunnel construction stage was very similar, in terms of the pile settlement profile and magnitude, to that observed in Test T. Significant increases in pile settlement also occurred when the tunnel face was between y/D = −0.25 and 0.25. When the face of either tunnel advanced from y/D = 0.75–1.25, the pile settlement only increased from 0.22%*D* to 0.25%*D* (1.9% of the pile diameter). About 90% of the pile settlement induced by each tunnel occurred when the face of each tunnel was between y/D = −0.75 and 0.75. Thus, the tunnelling influence zone of pile settlement was identified to be between y/D = −0.75 and 0.75. At C/D = 2.7, surprisingly the excavation of the first tunnel had almost the same effects on the pile settlement as the excavation of the second tunnel. It may suggest that each individual tunnel construction induced limited plastic strains around the pile toe. This implies that soil around the pile toe remains almost "elastic". Hence, the influence of the second tunnelling on pile settlement is almost the same as that resulted from the first tunnel.

In Test SS, the induced settlement increased almost linearly as the excavation of the first tunnel progressed at C/D = 1.5. After the excavation of the first tunnel, a pile settlement of 0.15%*D* (1.1% of the pile diameter) was measured. The induced pile settlement due to the first tunnel in this test was 40% less than that due to the first tunnel in Test TT. Based on their centrifuge tests, Lee and Chiang (2007) also reported that pile settlement induced by tunnelling near the mid-depth of pile shaft is smaller than that induced by tunnelling near the pile toe. This is because the load transfer mechanisms of the two cases are different (to be discussed in detail later). The pile settlement due to the excavation of the second tunnel in this study was 0.07%*D* (0.5% of the pile diameter), which was only about 47% of that due to the first tunnel. This may be because a significant amount of the vertical load applied to the pile was transferred downwards to the pile toe after the excavation of the first tunnel. Therefore, the effects of the construction of the second tunnel on pile settlement were smaller than those of the construction of the first tunnel. By comparing the measured results between Tests TT and SS, it is evident that the pile settlement induced by twin tunnelling is closely related to the relative location of a tunnel to the pile.

Please cite this article in press as: Ng, C.W.W., et al. Three-dimensional centrifuge modelling of the effects of twin tunnelling on an existing pile. Tunnel. Underg. Space Technol. (2012), http://dx.doi.org/10.1016/j.tust.2012.07.008

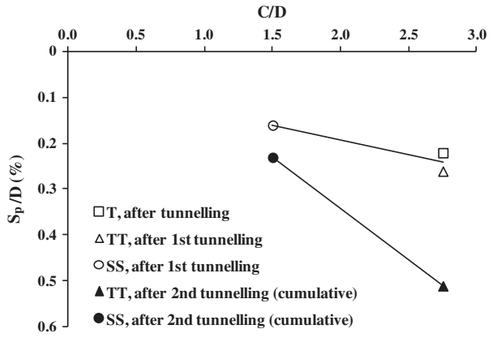

Fig. 7. Pile settlement induced by tunnelling at different C/D ratios.

Fig. 7 shows the normalized pile settlement induced by tunnelling at different C/D ratios. Open symbols denote pile settlements induced by the first tunnel, whereas solid symbols are cumulative pile settlements induced by both tunnels. After excavating the first tunnel, the pile settlement was about 0.15%D for C/D = 1.5 in Test SS, whereas the pile settlements were about 0.23%D for C/D = 2.7 in Test T and Test TT. It is clear that tunnelling near the pile toe induced 1.5 times of the pile settlement than tunnelling at the mid-depth of the pile shaft. After the excavation of the twin tunnels in Tests TT and SS, the cumulative pile settlement increased to 0.23%D for C/D = 1.5 in Test SS and to 0.50%D for C/D = 2.7 in Test TT. It is evident that twin tunnelling near the pile toe induced about 2.2 times of pile settlement than tunnelling at the mid-depth of pile shaft.

Since pile capacity is often interpreted using settlement criteria, the induced pile settlement due to tunnelling can be considered as an apparent loss of pile capacity (ALPC). Before tunnel excavation, pile settles 12 mm due to the initial applied working load (1.92 MN). An additional pile head settlement of 15 mm (0.24%D) is induced due to tunnelling in Test T (see Fig. 6). By using the load-settlement relationship shown in Fig. 4, a total pile settlement of 27 mm may be regarded as an equivalent load of 2.49 MN applied to the pile. Thus, the increase in equivalent pile load can be calculated to be 0.57 MN (i.e., 2.49–1.92 MN) due to the tunnel excavation. Since the ultimate load capacity of the pile was 2.88 MN as obtained from the load settlement curve using the displacement-based failure criterion proposed by Ng et al. (2001a), it can be considered that an ALPC of 20% occurred due to the tunnel excavation. The ALPC was about 21% after excavating the first tunnel in Test TT, but it increased to about 36% after the second tunnel was constructed. In Test SS, the ALPCs were about 14% and 20% after the first and second tunnels were constructed, respectively. The ALPCs suggest that the serviceability limit state of the pile after tunnelling should be considered.

3.4. Axial forces along the pile

Fig. 8a shows the measured axial force along the pile in Test T. The depth (z) was normalized by the tunnel diameter. Before the tunnel face reached the pile (i.e., $y/D = -0.25$), no significant change in axial force was recorded. As the tunnel face reached the pile toe (i.e., $y/D = 0.25$), the axial force along the pile decreased. This may imply that the shaft resistance of the pile was further mobilized when the pile settled more than the surrounding soil. This is consistent with the significant pile settlement in Fig. 6. The maximum reduction in axial force occurred at z/D = 2.0 and the magnitude of maximum reduction was 119.8 kN (i.e., 6.2% of the working load). Although the end bearing resistance was not measured at the pile toe directly in this study, the measured axial force at z/D = 3.1 (0.6 m above the toe of the 19.6 m pile, as shown in Fig. 1) may be used to deduce the variation of end bearing resistance due to tunnelling. The measured axial force at z/D = 3.1 decreased as the tunnel face reached the pile toe. This revealed that there was a reduction in toe resistance due to stress relief which resulted from the 1% volume loss during tunnelling.

As the tunnel face passed the pile (i.e., y/D = 0.75), the axial force along the pile increased. It can be observed that the maximum reduction in axial force occurred when tunnel face finally reached the piles. The magnitude of maximum reduction in axial force cannot be captured in plane strain model tests. This illustrates the importance of carrying out three-dimensional model tests.

Fig. 8b shows the measured axial forces along the pile in Test TT. The development of axial force due to the first tunnelling was consistent with that in Test T. As expected, the maximum reduction in axial force also occurred when the first tunnel finally reached the pile (i.e., y/D = 0.25). As the excavation of the first tunnel continued to a distance of y/D = 1.25 away from the pile, the axial force almost reduced to the value before tunnel excavation.

When the second tunnel was being excavated, the maximum reduction in axial force was 353.1 kN at z/D = 1.9. The reduction was more than 197% larger than that caused by the excavation of the first tunnel (118.6 kN). After the excavation of the second tunnel, the final reduction in axial force decreased to 75% of its maximum value. This illustrates the complex load transfer among the soil, the pile and the tunnels during tunnelling which could only be captured in three-dimensional simulations.

Fig. 8c shows the axial forces along the pile in Test SS. In contrast to the reduction in axial forces measured in Tests T and TT, the axial force in the pile increased during the first tunnelling at the mid-depth of the pile (i.e., z/D = 2.0). The maximum increase in axial force recorded occurred at z/D = 1.55 above the first tunnel when its face reached y/D = 1.25. When the second tunnel was being constructed, the measured axial force continued to increase but at a reduced rate until the end of tunnel construction. The final maximum recorded increase in axial force was 423.2 kN (22% of the working load), which was 32% larger than that measured at the end of the first tunnel (320.0 kN or 16.7% of the working load).

By inspecting the distributions of axial force closely, it can be seen that the axial force increased at depths above the tunnels. This suggests that there was a decrease in shaft resistance caused by downward soil movement and also by the reduction in confining stress due to the 1% volume loss from each tunnel excavation. In contrast to the induced axial force above z/D = 1.5, the induced axial force below z/D = 1.5 decreased with depth. This implies that there was an increase in shaft resistance below z/D = 1.5 when the pile settled during tunnel construction as shown in Fig. 6. The measured axial force at z/D = 3.1 (near the toe) increased by 125.7 kN (i.e., 6.5% of the working load) at the end of the construction of the first tunnel.

3.5. Shaft resistance and load transfer mechanisms

Fig. 9a shows the average shaft resistance along the pile in Test T and Test TT. Each pile shaft is divided into two parts: the upper portion of pile shaft above the depth of tunnel crown and the lower portion below tunnel crown. Based on the axial force measured using strain gauges, the average unit skin friction (f) may be calculated as follows:

$$f = \frac{\Delta Q}{pl} \tag{4}$$

where ΔQ is the difference between measured axial loads from any two consecutive strain gauges, l is the length of each portion, and p is the perimeter of the pile. In this way, load transfer mechanism of the pile can be clearly illustrated. In Test T, as the tunnel face advanced from $y/D = -0.75$ to -0.25, no significant change in shaft resistance was observed. However, as the tunnel face further advanced from $y/D = -0.25$ to 0.25, the average shaft resistance of the pile below the tunnel crown (i.e., $z/D > 2.7$) decreased significantly and that above the tunnel crown (i.e., $z/D < 2.7$) increased significantly. Due to reduction in confining stress induced by tunnel

Please cite this article in press as: Ng, C.W.W., et al. Three-dimensional centrifuge modelling of the effects of twin tunnelling on an existing pile. Tunnel. Underg. Space Technol. (2012), http://dx.doi.org/10.1016/j.tust.2012.07.008

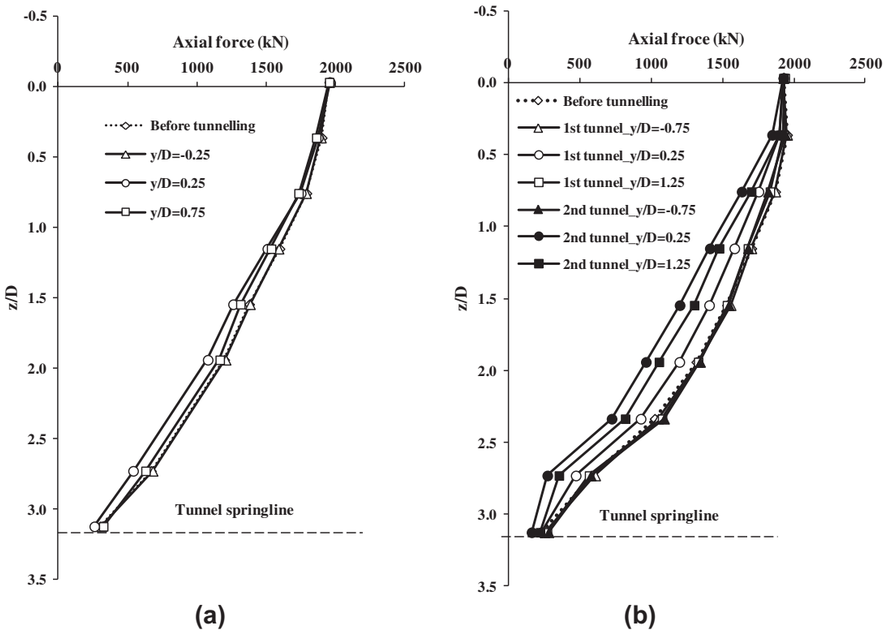

Fig. 8. Axial forces of pile at various tunnelling stages: (a) Test T; (b) Test TT; (c) Test SS.

Please cite this article in press as: Ng, C.W.W., et al. Three-dimensional centrifuge modelling of the effects of twin tunnelling on an existing pile. Tunnel. Underg. Space Technol. (2012), http://dx.doi.org/10.1016/j.tust.2012.07.008

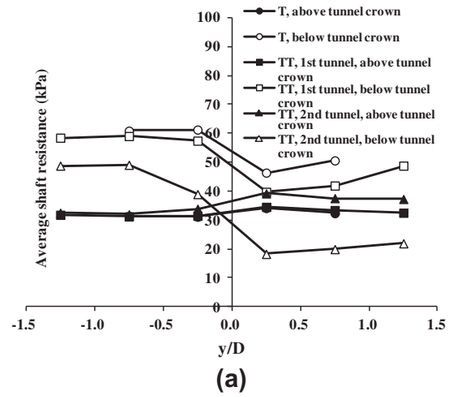

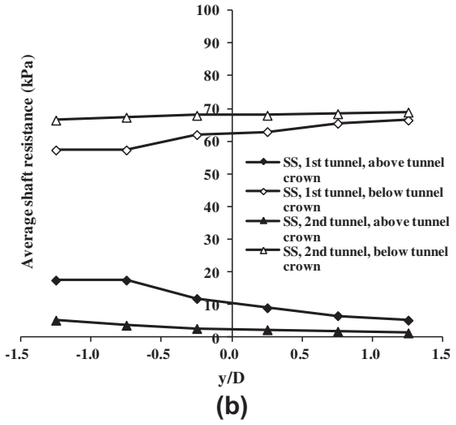

Fig. 9. Average shaft resistance along pile: (a) Test T and Test TT; (b) Test SS.

excavation, the end bearing resistance and shaft resistance of the pile at depths below the tunnel crown (i.e., $z/D > 2.7$) was reduced. In order to maintain vertical equilibrium, the pile had to settle more than the surrounding soil to mobilize shaft resistance at the upper portion of the pile shaft. This caused an increase in load taken by the upper portion and is called upward load transfer.

As the tunnel face passed the pile (i.e., as it advanced from $y/D = 0.25$–0.75), the shaft resistance of the pile above the tunnel crown (i.e., $z/D < 2.7$) decreased whereas that below the tunnel crown (i.e., $z/D > 2.7$) increased. Due to the downward soil movement and the decrease in normal stress acting on the pile induced by tunnel excavation, the shaft resistance decreased along the pile above the tunnel crown (i.e., $z/D < 2.7$). To maintain the vertical equilibrium, the shaft resistance along the pile below the tunnel crown (i.e., $z/D > 2.7$) and the end bearing resistance increased as shown in Fig. 8c. The decrease of pile load from the upward portion resulted in an increase of load in the lower portion of the pile for maintaining the vertical equilibrium. This is called downward load transfer. This is in contrast to the load transfer mechanism when tunnel face was close to the pile ($y/D = -0.25$ and 0.25). As a result, the axial force increased when the tunnel face passed the pile and advanced from $y/D = 0.25$–0.75. Therefore, the maximum reduction in axial force occurred when the tunnel face reached the pile as shown in Fig. 8. This is due to the two distinct load transfer mechanisms.

In Test TT, during the excavation of the first tunnel, the development of average shaft resistance above and below the tunnel crown was consistent with that in Test T. Two types of load transfer can again be observed. When the second tunnel was being excavated, the reduction in average resistance below the tunnel crown was larger than that in the excavation of the first tunnel. This is because part of the applied working load had been transferred to the lower part of the pile after the excavation of the first tunnel, as illustrated in Fig. 8b.

Fig. 9b shows the average shaft resistance along the pile in Test SS. Unlike in Test TT, only downward load transfer was observed in Test SS. During the excavation of the first tunnel, the average shaft resistance decreased significantly above the tunnel crown (i.e., $z/D < 1.5$) and increased below the tunnel crown (i.e., $z/D < 1.5$). Because vertical equilibrium of pile can be achieved by transferring the load taken by the upper part of the pile to the lower part of the pile, settlement of pile was relatively small compared with that when the tunnel face was near the pile toe as illustrated in Fig. 6. This is consistent with the centrifuge results reported by Lee and Chiang (2007).

When the second tunnel was being excavated, the average shaft resistance decreased above the tunnel crown (i.e., $z/D < 1.5$) and increased below the tunnel crown (i.e., $z/D < 1.5$), similar to that when the first tunnel was being excavated. At the end of the construction of the two tunnels, the mobilized shaft resistance of the pile was significantly reduced to almost zero above the crown of each tunnel. The change in average shaft resistance due to the excavation of the second tunnel was much smaller than that due to the excavation of the first tunnel. This is consistent with the measured pile settlement results shown in Fig. 6. The ALPC induced by the excavation of the second tunnel (6%) was only 43% of that induced by the first tunnelling (14%). After the excavation of the first tunnel, a significant amount of applied working load was transferred to the pile shaft below the tunnel crown and the pile toe. Thus, the effect of the second tunnel at the same depth was smaller. Clearly, the three-dimensional load transfer mechanism for twin tunnelling near the pile shaft is different from that for twin tunnelling near the pile toe. A pile suffers significant settlement when an upward load transfer is observed, but it experiences smaller settlement when the load transfer is downward. In this study, the ALPC for twin tunnelling near the pile toe (36%) was 1.8 times of that for tunnelling near the mid-depth of pile shaft (20%), as illustrated in Fig. 6.

3.6. Induced bending moments in the pile

Fig. 10a shows the measured tunnelling induced bending moment along the pile in Test T and Test TT. Bending moments were taken to be positive if tensile stress was induced at the side facing the first tunnel. In Test T, the maximum tunnelling-induced bending moment occurred near the tunnel crown (i.e., $z/D = 2.7$) with a magnitude of 61.5 kN m, which was 7.7% of the bending moment capacity of the pile ($M_{yield} = 800$ kN m). In Test TT, the maximum bending moment occurred near the crown of the first tunnel (i.e., $z/D = 2.7$) after its excavation. The maximum induced bending moment was 84.3 kN m (10.5% of M_{yield}). After the excavation of the second tunnel, the maximum bending moment decreased to 70.8 kN m (8.9% of M_{yield}). Centrifuge test results reported by Loganathan et al. (2000) are also included in the same figure for comparison. The maximum bending moment also occurred near the tunnel crown based on their test results. The bending moment at $z/D < 2.0$ in this study is different from that reported by Loganathan et al. This may be because the pile head in this study was constrained by the hydraulic jack. The general profiles of bending moment are similar though.

Please cite this article in press as: Ng, C.W.W., et al. Three-dimensional centrifuge modelling of the effects of twin tunnelling on an existing pile. Tunnel. Underg. Space Technol. (2012), http://dx.doi.org/10.1016/j.tust.2012.07.008

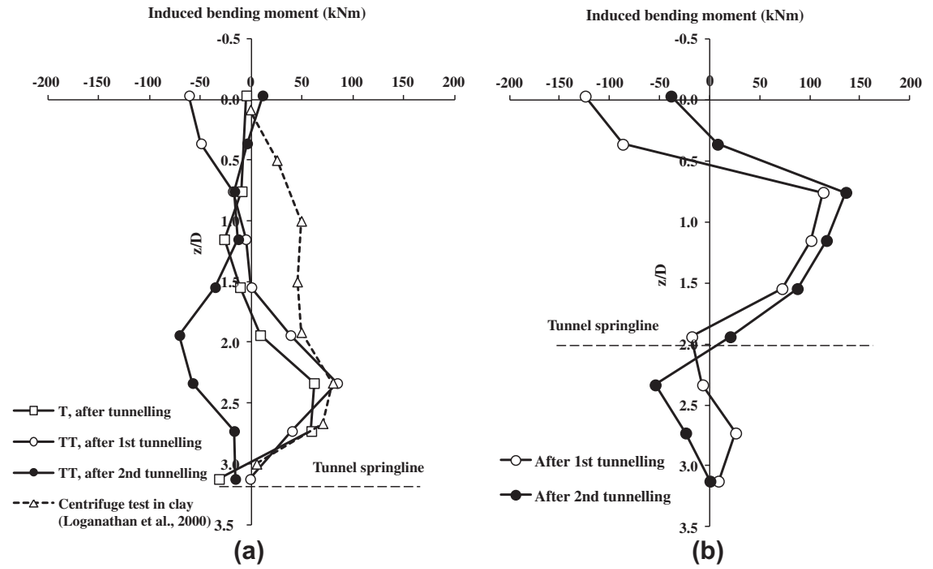

Fig. 10. Tunnelling-induced bending moment on pile: (a) Test T and Test TT; (b) Test SS.

Fig. 10b shows measured tunnelling induced bending moment along the pile in Test SS. After the first tunnel was excavated, the maximum bending moment occurred above the tunnel crown (i.e., $z/D = 0.8$). The magnitude is 113.3 kN m (14.2% of M_{yield}). A bending moment of 38.7 kN m occurred near the ground surface. This may be also due to constrain of the hydraulic jack. After the second tunnelling, the maximum bending moment was 136.0 kN m (17.0% of M_{yield}). It is the maximum value in all the three tests. Therefore, it can be concluded that the induced bending moment to the pile by twin tunnelling is relatively insignificant.

4. Summary and conclusions

A series of centrifuge model tests were carried out to investigate the effects of twin tunnel construction on an existing single pile in dry sand. In each centrifuge model test, two tunnels were simulated three-dimensionally one after the other in-flight. Based on the test results, the following conclusions may be drawn:

(a) The settlement of a pile induced by twin tunnelling is closely related to the depth of each tunnel relative to the pile. Near the pile toe (i.e., Test TT), the excavation of the first tunnel results in a pile settlement of about 1.9% of the pile diameter. The magnitude of incremental pile settlement due to the construction of the second tunnel only is about the same. Based on the displacement-failure load criterion proposed by Ng et al. (2001a), the apparent loss of pile capacity (ALPC) is about 21% after the construction of the first tunnel construction, and increases to about 36% (cumulative) after the construction of the second tunnel.

(b) For twin tunnelling near the mid-depth of the pile shaft (i.e., Test SS), the pile settlement induced by excavating the first tunnel is 1.1% of the pile diameter, which is only about 60% of that induced by the first tunnel constructed near the toe in Test TT. Due to the load transfer from the upper to lower part of the pile after the construction of the first tunnel, the construction of the second tunnel (also near the pile shaft) induces a much smaller pile settlement of only 0.5% of the pile diameter. The ALPCs are about 14% and 20% after the excavation of the first and second tunnels, respectively.

(c) The pile settlement induced by twin tunnelling is closely related to C/D ratios (cover-to-diameter ratio) of tunnels and the relative location of a tunnel to the pile. The cumulative pile settlement due to tunnelling near the toe is about 2.2 times of that due to tunnelling near the mid-depth of the pile shaft.

(d) For construction of each tunnel near the pile toe, two distinct load transfer mechanisms, i.e., an upward first and then a downward load transfer can be identified in Tests T and TT. An upward load transfer is identified when a tunnel face approaches to within $0.25D$ of the pile. Due to the reduction in confining stress as a result of the approaching tunnel near the toe, both the shaft resistance near the toe and the end bearing resistance of the pile decrease. As a result, a larger shaft resistance is mobilized in the upper half of the pile (or upper load transfer) while the pile settles to maintain the vertical equilibrium under the applied pile load. On the contrary, a downward load transfer is observed after the tunnel face has passed the pile by a distance of $0.25D$. The shaft resistance along the upper portion of the pile decreases due to downward soil movement and stress relief induced by tunnelling, resulting in an increase in the shaft resistance along the lower portion of the pile and in the end bearing resistance so that the vertical equilibrium of the pile can be maintained. Due to the two distinct types of load transfer, the maximum reduction in axial force occurs when a tunnel face reaches the pile (in Test TT).

(e) When each tunnel is excavated near the mid-depth of the pile shaft (in Test SS), only a downward load transfer can be identified. The shaft resistance along the upper half of the pile decreases whereas the shaft resistance along the lower half of the pile increases as tunnel advances. However, there is an increase of 320 kN and 423 kN (i.e., equivalent to

Please cite this article in press as: Ng, C.W.W., et al. Three-dimensional centrifuge modelling of the effects of twin tunnelling on an existing pile. Tunnel. Underg. Space Technol. (2012), http://dx.doi.org/10.1016/j.tust.2012.07.008

17% and 22% of the working load) in the pile axial force above the crown after the construction of the first and second tunnels, respectively. At the end of the construction of the two tunnels, shaft resistance of the pile is significantly reduced to almost zero above the crowns of the tunnels.

(f) The induced bending moment due to twin tunnelling is insignificant. The maximum bending moment induced in the pile by excavation of single or twin tunnels is only about 17% of the ultimate bending moment capacity.

(g) When C/D is 1.5, the surface settlement induced by the excavation of the second tunnel is larger than that induced by the excavation of the first tunnel. Simply predicting ground surface settlement by summing the two Gaussian curves can underestimate the actual value by up to 16%.

(h) In this study only volume loss induced due to tunnelling is modelled. The effect of removal of soil inside of tunnel is not simulated. Since all the tests were carried out using the same method (by simulating volume loss), measured results obtained from different cases investigated are comparable and conclusions drawn from this study should not be affected.

Acknowledgements

The authors would like to acknowledge the financial support provided by the Research Grants Council of the HKSAR (General Research Fund Project No. 617608).

References

Addenbrooke, T.I., 1996. Numerical Modeling in Stiff Clay. Ph.D. Thesis, Imperial College, London.
Attewell, P.B., Farmer, I.W., 1974. Ground deformations resulting from shield tunnelling in London clay. Can. Geotech. J. 11, 380–395.
Attewell, P.B., Yeates, J., Selby, A.R., 1986. Soil Movements Induced by Tunnelling and Their Effects on Pipelines and Structures. Chapman and Hall, New York.
Bezuijen, A., Schrier, J.S., 1994. The influence of a bored tunnel on pile foundations. Centrifuge 94, Singapore, pp. 681–686.
Chapman, D.N., Ahn, S.K., Hunt, D.V.L., 2007. Investigating ground movements caused by the construction of multiple tunnels in soft ground using laboratory model test. Can. Geotech. J. 44 (10), 631–643.
Ishihara, K., 1993. Liquefaction and flow failure during earthquakes. Géotechnique 43 (3), 351–415.
Jacobsz, S.W., Standing, J.R., Mair, R.J., Hahiwara, T., Suiyama, T., 2004. Centrifuge modeling of tunnelling near driven piles. Soil Found 44 (1), 49–56.
Lee, C.J., Chiang, K.H., 2007. Responses of single piles to tunnelling-induced soil movements in sandy ground. Can. Geotech. J. 44 (10), 1224–1241.
Lee, T.K., Ng, C.W.W., 2005. Effects of advancing open face tunnelling on an existing loaded pile. J. Geotech. Geoenviron. Eng., ASCE 131 (2), 193–201.
Loganathan, N., Poulos, H.G., Stewart, D.P., 2000. Centrifuge model testing of tunnelling-induced ground and pile deformations. Géotechnique 50 (3), 283–294.
Mair, R.J., Taylor, R.N., Bracegirdle, A., 1993. Subsurface settlement profiles above tunnels in clay. Géotechnique 43 (3), 315–320.
Mair, R.J., Taylor, R.N., 1997. Bored tunnelling in the urban environment. State-of-the-art report and theme lecture. In: Proceedings of 14th International Conference on Soil Mechanics and Foundation Engineering, vol. 4, Hamburg, Balkema, pp. 2353–2385.
Mair, R.J., 2008. Tunnelling and geotechnics: new horizons. Geotechnique 58 (9), 695–736.
Mroueh, H., Shahrour, I., 2002. Three-dimensional finite element analysis of the interaction between tunnelling and pile foundations. Int. J. Numer. Anal. Methods Geomech. 26, 217–230.
Ng, C.W.W., Yau, T.L.Y., Li, J.H.M., Tang, W.H., 2001a. New failure load criterion for large diameter bored piles in weathered geomaterials. J. Geotech. Geoenviron. Eng., ASCE 127 (6), 488–498.
Ng, C.W.W., Van Laak, P.A., Tang, W.H., Li, X.S., Zhang, L.M., 2001b. The Hong Kong geotechnical centrifuge. In: Proc. 3rd Int. Conf. Soft Soil Engineering, pp. 225–230.
Ng, C.W.W., Van Laak, P.A., Zhang, L.M., Tang, W.H., Zong, G.H., Wang, Z.L., Xu, G.M., Liu, S.H., 2002. Development of a four-axis robotic manipulator for centrifuge modeling at HKUST. In: Proc. Int. Conf. Physical Modeling in Geotechnics, St. John's Newfoundland, Canada, pp. 71–76.
Ng, C.W.W., Zhang, L.M., Wang, Y.H., 2006. In: Proceedings of 6th Int. Conf. on Physical Modelling in Geotechnics (TC2), vols. 1 and 2. Taylor & Francis.
O'Reilly, M.P., New, B.M., 1982. Settlements above tunnels in the United Kingdom-their magnitude and prediction. In: Proceedings of the Conference Tunnelling '82, IMM London, pp. 173–181.
O'Neill, M.W., Reese, R.C., 1999. Drilled Shaft: Construction Procedures and Design Methods. Federal Highway Administration, Washington, DC.
Pang, C.H., 2007. The Effect of Tunnel Construction on Nearby Pile Foundation. Ph.D. Thesis, National University of Singapore.
Peck, R.B., 1969. Deep excavation and tunnelling in soft ground. In: Proc. 7th Int. Conf. Soil Mech. Found. Engng., pp. 225–290.
Schofield, A.N., 1980. Cambridge geotechnical centrifuge operations. Géotechnique 30 (3), 227–268.
Taylor, R.N., 1995. Geotechnical Centrifuge Technology. Blackie Academic and Professional, London.
Weltman, A.J., 1980. Pile Load Testing Procedures. DOE and CIRIA Piling Devel. Group Rep. PG7. Construction Industry Research and Information Association, London.

Please cite this article in press as: Ng, C.W.W., et al. Three-dimensional centrifuge modelling of the effects of twin tunnelling on an existing pile. Tunnel. Underg. Space Technol. (2012), http://dx.doi.org/10.1016/j.tust.2012.07.008

Tunnelling and Underground Space Technology 28 (2012) 297–303

Contents lists available at SciVerse ScienceDirect

Tunnelling and Underground Space Technology

journal homepage: www.elsevier.com/locate/tust

Centrifuge and numerical investigation of passive failure of tunnel face in sand

K.S. Wong [a,*], C.W.W. Ng [a], Y.M. Chen [b], X.C. Bian [b]

[a] Department of Civil and Environmental Engineering, Hong Kong University of Science and Technology, Clear Water Bay, Kowloon, Hong Kong
[b] Department of Civil Engineering, Zhejiang University, 388 Yuhangtang Road, Hangzhou 310058, China

ARTICLE INFO

Article history:
Received 19 July 2011
Received in revised form 20 October 2011
Accepted 13 December 2011
Available online 9 January 2012

Keywords:
Tunnel face
Failure mechanism
Passive failure pressure
Surface displacement
Sand

ABSTRACT

Tunnelling is one of the major construction methods to sustain the increasing demand on development in cities. Although many studies have been carried out to investigate the active failure mechanism of tunnel face in sand, the study of passive failure of tunnel face is relatively rare and most of studies are analytical solutions based on the upper bound theorem. In this paper, centrifuge model tests and three-dimensional finite element analyses have been conducted to study the passive failure mechanisms of tunnel face in sand for tunnels located at cover over diameter (C/D) ratios equal to 2.2 and 4.3. Passive failure pressures of tunnel face as well as ground surface displacements were investigated in centrifuge tests. From both centrifuge and numerical investigations, it is found that for a tunnel located at C/D ratio equals to 2.2, the soil in front of the tunnel face is displaced by the advancing tunnel face while the soil further away from the tunnel face is forced upwards to the ground surface. A funnel-type failure mechanism is observed and the extent of the failure mechanism is narrower than a five-block failure mechanism commonly assumed in an existing upper bound solution. However, the calculated passive failure pressure by the upper bound solution is fairly consistent with the measured face pressure. It is observed that the funnel-type failure mechanism induces surface heaves. Both observed longitudinal and transverse heaves are well described by Gaussian distributions. For a tunnel located at C/D ratio equals to 4.3, the displacements of soil are confined around the vicinity of an advancing tunnel face and a localised failure mechanism associated with ground settlement is observed and computed. There is a large discrepancy between the localised failure mechanism and the five-block failure mechanism. The calculated failure face pressure is higher than the corresponding measured value by 50%. However, reasonable consistency can be found between measured and computed passive face pressures.

1. Introduction

In cities, tunnelling has become one of the major construction methods to sustain the increasing demand on development. When a tunnel is excavated, the tunnel face pressure shall be maintained within the minimum and maximum support pressures to prevent active or passive failure at the tunnel face. The failure may endanger human life and cause catastrophic damage to the structures within the influence zone.

Over the decades, numerous theoretical and experimental studies have been performed to investigate the active failure of tunnel face (Anagnostou and KovÃ¡ri, 1994, 1996; Chambon and Corte, 1994; Dias et al., 2008; Leca and Dormieux, 1990; Leca and Panet, 1988; Mollon et al., 2010; Soubra, 2002). But the study of passive failure of tunnel face is relatively rare and most of them are analytical solutions and numerical simulations (Dias et al., 2008; Leca and Dormieux, 1990; Mollon et al., 2010; Soubra, 2002; Soubra et al., 2008). Passive failure during drilling of the 2nd Heinenroord Tunnel (Bezuijen and Brassinga, 2005) imply that passive failure at tunnel face is not a theoretical risk. It is of important to know the passive failure pressure of tunnel face to prevent the passive failure.

Leca and Panet (1988) and Leca and Dormieux (1990) used lower and upper bound theorems to predict the passive failure pressure of tunnel face in sand. For upper bound solutions, they adopted a truncated cone as the failure mechanism. It is a planar on vertical plane of symmetry running longitudinally along centreline of tunnel. Soubra (2002) improved the upper bound solutions by introducing a log spiral instead of planar on the vertical plane of symmetry. The log spiral was idealised using multiple truncated rigid cones. But only an inscribed elliptical area to the entire circular tunnel face is involved in deriving the upper bound solutions, due to the conical shape of the rigid cones used in the derivation (Mollon et al., 2010).

While existing analytical and numerical analyses provide valuable information and knowledge on passive failure of tunnel face, the problem has not been studied systematically and fully understood. In view of this, centrifuge model tests were carried out to

* Corresponding author. Tel.: +852 9673 2276/2358 0216; fax: +852 2243 0040.
E-mail addresses: wksaa@ust.hk (K.S. Wong), charles.ng@ust.hk (C.W.W. Ng), chenyunmin@zju.edu.cn (Y.M. Chen), bianxc@zju.edu.cn (X.C. Bian).

0886-7798/$ - see front matter © 2011 Elsevier Ltd. All rights reserved.
doi:10.1016/j.tust.2011.12.004

investigate passive failure of tunnel face in sand for tunnels located at cover over diameter, C/D ratios equal to 2.2 and 4.3. In addition, finite element analyses were conducted to back-analyse the centrifuge model tests and provide further information to understand the problem. This paper presents: (a) details of centrifuge model setup and test procedures; (b) details of the finite element analyses; (c) failure mechanisms and passive failure pressure of tunnel face obtained from the centrifuge model tests and finite element analyses as well as comparisons with the existing analytical solutions; and (d) the induced ground surface displacement due to tunnel face displacement obtained from centrifuge tests.

2. Centrifuge modelling

2.1. Experimental program

The centrifuge model tests were performed in the Geotechnical Centrifuge Facility (GCF) at the Hong Kong University of Science and Technology (HKUST). The geotechnical centrifuge at HKUST (Ng et al., 2001, 2004) has a rotating arm of approximately 8.4 m in diameter. The maximum modelling capacity of the centrifuge is 400g ton. It is capable of simulating an elevating gravity field over 150 times that of the earth's gravity (g) for static model.

Three tunnelling cases with different C/D ratios were carried out in saturated sand to study the passive failure of tunnel face. Tests S2 and S4 were designed to investigate the passive failure of tunnel face for tunnels located at C/D ratios equal to 2.2 and 4.3 respectively. The performance and reliability of load cells submerged in the water deteriorated over time due to water ingress. Tunnel located at C/D ratio equals to 2.2 was repeated in Test S2R using an internal load cell as described in Section 2.2 to obtain the variation of tunnel face pressure with tunnel face displacement. Some details of the centrifuge tests are given in Table 1.

2.2. Model setup

Fig. 1 shows the plan and elevation views of the centrifuge model setup. A rectangular model container of plan dimensions 1245 × 350 mm and depth 850 mm with a perspex viewing window in the front face was used in the centrifuge model tests. A 12.7 mm thick glass, measuring 850 mm by 714 mm, was bolted to 25.4 mm thick perspex with similar dimensions to form a composite panel. The composite panel was attached to the front face of the model container with the glass side in contact with sand. The glass served the purpose for ease of PIV control marker placement while reducing the friction between the front face and the sand. The face of the glass which was in contact with the sand formed the vertical plane of symmetry. A 25.4 mm thick aluminium plate was used to separate the sand from the loading system. The aluminium plate was braced by six aluminium struts with diameter of 41.3 mm attached to the side wall of the model container.

Fig. 2 shows the model tunnel used in the Test S2R. A tunnel lining consisted of an aluminium hollow tube, 50 mm in diameter and 200 mm long with wall thickness of 2.7 mm, which was split longitudinally along the centre plane. A hollow loading piston, 20 mm in diameter and 140 mm long was screwed to the a 60 mm long tunnel face block. A 25 mm long end block was placed

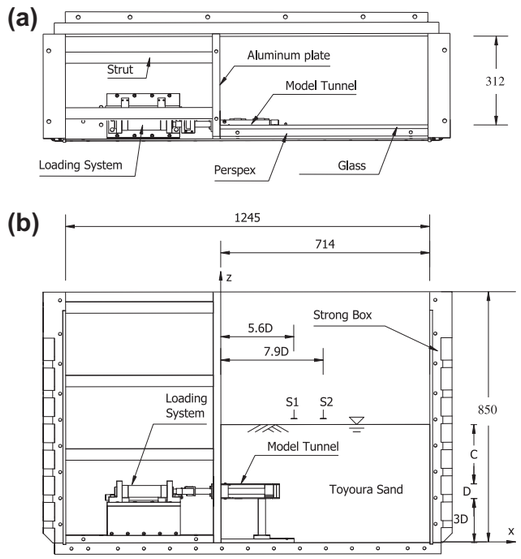

Fig. 1. Basic configuration of a centrifuge package (dimensions in mm): (a) plan view and (b) elevation view.

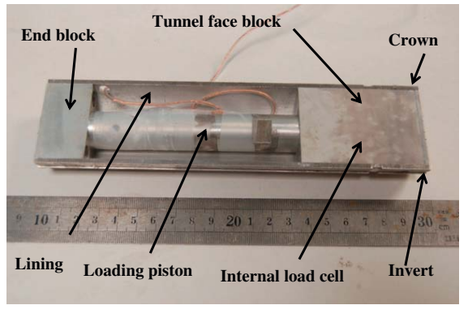

Fig. 2. Model tunnel.

at another end of the loading piston. The tunnel lining was placed on the tunnel face block and bolted to the end block.

The tunnel face block consisted of a tunnel face, an internal load cell and a sleeve. The internal load cell was made of hollow aluminium tube with semiconductor strain gauges bonded on the external surface. Epoxy coating was used to protect the strain gauges from abrasion. Full Wheatstone bridge strain gauges was arranged to compensate for temperature effects. The load cell was attached to the tunnel face and protected by the sleeve. There were two O-rings at both ends of the load cell in contact with the inner face of the sleeve. This minimised the friction between sleeve with lining/soil and glass to be transferred to the load cell. The O-rings

Table 1
Test program.

Test	C/D	Relative density (%)	Unit weight (kN/m^3)	Remarks
S2	2.2	67	19.2	Performance of load cells submerged in water deteriorated over time
S4	4.3	56	19.0	Performance of load cells submerged in water deteriorated over time
S2R	2.2	63	19.1	–

also served the purpose to isolate the load cell from water ingress. There was a ring of filler to separate the sleeve from the tunnel face to ensure load from the tunnel face was measured by the load cell only. The silica gel was squeezed into the hollow section of the load cell and isolated the strain gauges from water.

Model tunnel used in Tests S2 and S4 was similar to that used in Test S2R except the loading piston and tunnel face block also served as load cells with full Wheatstone bridge strain gauges bonded to its external surface and protected by epoxy coating. The performance and reliability of the load cells deteriorated over time due to water ingress.

Fig. 3 shows the loading system used in the centrifuge tests. The loading system consisted of a hydraulic actuator, mounted on an actuator support by using two L-shape brackets and connected to an oil supply system through two oil supply tubes. A linear variable differential transformer (LVDT) was fastened to the actuator support and its core was bolted to a fitting cap. The fitting cap was attached to the piston of the actuator. The actuator support was made of four 12.7 mm thick aluminium plates and bolted to a 25.4 mm thick base plate, which was mounted to the bottom of the model container. A connecting piston used to connect the loading system and model tunnel was slot to the fitting cap and secured by a L-shape fitting. The connecting piston also served as an external load cell with full Wheatstone bridge strain gauges bonded to its external surface and protected by epoxy coating.

The model tunnel was supported by an aluminium column at one end and bolted to the aluminium plate via two screws at another end as shown in Fig. 1. The connecting piston of the loading system passing through the aluminium plate was connected to the loading piston of the model tunnel. The hole on aluminium plate had a groove, fit with an elastomeric O-ring, which encircled the connecting piston to ensure watertight during the movement of the piston. Perforated drainage pipes wrapped with geotextiles were used to form a drainage system. The drainage system was placed on the bottom of the model container.

2.3. Instrumentation

In Tests S2 and S4, tunnel face pressure was given by an external load cell as shown in Fig. 3. In Test S2R, tunnel face pressure was given by an internal load cell in the tunnel face block as described in the previous section. Horizontal displacement of tunnel face was measured by LVDT attached to the actuator support.

Particle image velocimetry (PIV) and close-range photogrammetry originally developed by White et al. (2003) was used to monitor the subsurface soil displacement on the vertical plane of symmetry. The precision of the measurement is 0.1 mm. Digital images were captured using in flight camera mounting on the swinging platform. Each image was divided into soil patches and each patch represented

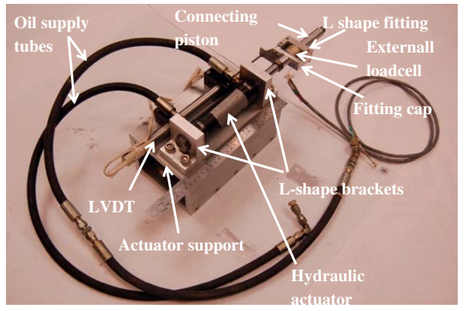

Fig. 3. Loading system.

a measurement point. The movement of soil patches between two successive images was traced based on cross-correlation. PIV can only measure the displacement in the image-space coordinates. Close range photogrammetry was used to convert the image-space coordinates to object-space coordinates. Details of PIV and close-range photogrammetry can be obtained from White et al. (2003). Longitudinal surface displacements were deduced from the PIV results. The transverse surface displacements were monitored using LVDTs at Sections S1 and S2 located at 5.6D and 7.9D respectively along the x direction as indicated in Fig. 1. For Test S2, four LVDTs were placed at Section S1. Four LVDTs were placed at Section S2 for Test S4. Four LVDTs were placed at Section S1 and three LVDTs were placed at Section S2 for Test S2R.

2.4. Model preparation

Toyoura sand used in the tests has the maximum and minimum void ratios of 0.977 and 0.597 respectively. The sand has a specific gravity of 2.65 (Verdugo and Ishihara, 1996). The sand was pluviated to the strong box through a hopper and the drop height of the sand was set as 500 mm. The relative density, D_r, of the sand sample at 100g was 67%, 56% and 63% for Tests S2, S4, and S2R respectively. The relative density and corresponding saturated unit weight of the sand sample for Tests S2, S4 and S2R are listed in Table 1.

In order to saturate the sand, aluminium cover with elastomeric O-ring was placed on top of the model container. Vacuum was applied to the sand for 2 h. Then, carbon dioxide was injected through drainage system to replace the residual air. After that, the vacuum was reapplied for another 3 h. While maintaining the vacuum, deaired water from water tank was supplied through the drainage system to the soil mass. When the water level reached required level above the ground surface of the sand sample, the saturation process was terminated. The whole saturation process required around 40 h.

2.5. Test procedures

After completion of model preparation and final check, the model container was transferred to the swinging platform. The water level was maintained at around 15 mm above the ground surface after connecting the strong box to the stand pipe on the platform. Four cameras were set up to capture photographs during centrifuge testing. Three videos were installed to monitor the test. The data logger was then set to record data at 1 Hz, and upon centrifuge spinup, photographs were taken at 150 s intervals and saved to the computer.

When the acceleration of the centrifuge reached 100g and equilibrium condition was achieved, the camera settings were changed to take photographs every 30 s. The tunnel face block was pushed toward the sand in 0.2 mm per second. The speed was chosen to ensure enough time for the water to flow into the tunnel lining so that suction was not created behind tunnel face block. The tunnel face displacement was prescribed and the corresponding face pressure was measured. After pushing the tunnel face block for a maximum displacement of 35 mm, the centrifuge was spun down. It should be noted that in actual shield tunnelling, pressure controlled is normally adopted. The measured results from centrifuge tests may not be directly applicable to the actual tunnel construction. On the other hand, pressure controlled was used in the numerical simulations described later in this paper.

3. Three-dimensional numerical modelling

3.1. Finite element mesh and boundary conditions

Three-dimensional numerical modelling were performed using Plaxis finite element code (Brinkgreve and Broere, 2004). Fig. 4

shows the finite element mesh used in the numerical modelling for tunnel located at C/D ratio equals to 2.2. The finite element mesh was 700 mm long, 300 mm high and 300 mm wide. For tunnel located at C/D ratio equals to 4.3, the finite element mesh was 700 mm long, 400 mm high and 300 mm wide. This is similar to the dimensions of the soil samples in the model container.

Only half of the tunnel was modelled, taking advantage of symmetry about $y = 0$ mm. 15-noded wedge elements and 8-noded plate elements were used to model the sand and the tunnel lining respectively. On the left and right boundaries of the mesh, the movement in the y direction was restrained. The movement in the x direction on the front and rear boundaries was restrained. Pin supports were applied to the base boundary to restrict movements in the x, y and z directions. The water table was located at the ground surface, with a hydrostatic initial pore-water pressure profiles. The tunnel lining and shield was submerged under water.

3.2. Constitutive models and model parameters

The response of the sand is modelled using a non-linear hardening-soil (H-S) constitutive model employed the Mohr–Coulomb failure criterion with a non-associated flow rule. The H-S model is a non-linear elastic–plastic formulation using multiple yield loci as a function of plastic shear strain and a cap to capture volumetric hardening as described by Schanz et al. (1999). Loading and unloading within the current yield surface, which is defined by a unloading and reloading modulus, E_{ur}, are assumed to be elastic. Critical state angle of friction, ϕ_{cs} is defined by maximum angle of dilation, ψ and peak angle of friction, ϕ' according to Eq. (1a). The mobilised dilation angle, ψ_m is related to mobilised angle of friction, ϕ'_m and ϕ_{cs} as shown in Eq. (1b).

$$\sin\phi_{cs} = (\sin\phi' - \sin\psi)/(1 - \sin\phi'\sin\psi) \tag{1a}$$

$$\sin\psi_m = (\sin\phi'_m - \sin\phi_{cs})/(1 - \sin\phi'_m\sin\phi_{cs}) \tag{1b}$$

Soil dilatancy, defined by the ratio of the plastic volumetric strain rate to the plastic shear strain rate is equal to $\sin\psi_m$. A cut-off for dilation is allowed when void ratio reaches the nominated maximum void ratio. Under triaxial condition, the model predicts a hyperbolic relationship for the drained secant Young's modulus, E, as given in Eq. (2).

$$E = 2E_{50}(1 - R_f q/q_f); \quad E_{50} = E_{50}^{ref}(\sigma'_3/p_{ref})^m \tag{2}$$

where q is the deviatoric stress; E_{50}^{ref} is the E value when q is 50% of the maximum deviatoric stress, q_f at the reference confining stress, p_{ref}; R_f is the failure ratio and m controls the stress level dependence of the stiffness; σ'_3 is the confining stress. In this study, p_{ref} was taken as 100 kPa. Beside, effective oedometer modulus, E_{oed} which control the cap of the model is also stress level dependence.

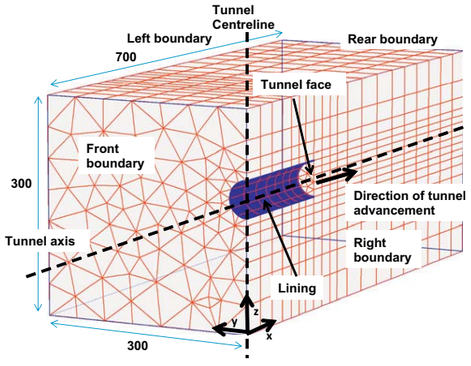

Fig. 4. Finite element mesh adopted for three-dimensional numerical modelling (dimensions in mm).

Table 2
Soil parameters used in the finite element analyses.

Parameter	Value
Saturated unit weight, γ_{sat} (kN/m^3)	19.0
Effective cohesion, c' (kPa)	1.0
Effective angle of friction, ϕ' (°)	37°
Angle of dilation, ψ (°)	7°
Effective secant modulus, E_{50} (MPa)	27
Effective unloading/reloading modulus, E_{ur} (MPa)	81
Effective oedometer modulus, E_{oed} (MPa)	27
Poisson's ratio, υ'	0.2
m	0.5
Failure ratio, R_f	0.9
At-rest earth pressure coefficient, K_o	0.5

The relative density of the sand was taken as 60%, which corresponds to a saturated unit weight, γ_{sat} of 19.0 kN/m^3. According to Verdugo and Ishihara (1996), the critical state angle of friction, ϕ_{cs} for Toyoura sand is 31° under triaxial condition. In order to obtain shear strength and stiffness parameters for numerical simulations in this study, triaxial compression tests conducted by Maeda and Miura (1999) were simulated numerically. The fitted ϕ' and ψ are 37° and 7° respectively. Small cohesion, c' of 1 kPa was assigned to the soil. In the numerical simulations, E_{50} at confining stress of 100 kPa was taken as 27 MPa. E_{oed} was set as 27 MPa (Schanz and Vermeer, 1998). The unloading and reloading modulus, E_{ur} was taken as 81 MPa, which is three times of E_{50} (Brinkgreve and Broere, 2004). The Poisson's ratio of the sand was taken as 0.2. The coefficient of earth pressure at-rest was set equal to 0.5. Soil parameters used for the numerical modelling are summarised in Table 2. The tunnel lining was modelled as linear elastic material with a Young's modulus of 70×10^6 kPa, a Poisson's ratio of 0.15, and a thickness of 2.7 mm.

3.3. Numerical modelling procedures

The analysis was started by applying an acceleration of 100g to increase the gravity of the numerical model to simulate the stress state in the centrifuge test. As tunnel was assumed to be wished-in-place and submerged under water, tunnel excavation was simulated by deactivating the soil elements within tunnel excavation zone and activated the shell elements of the lining in a single step. Such a simplified modelling approach had been adopted successfully in previous studies (Li et al., 2009). In order to ensure the sand around the vicinity of tunnel face remained at at-rest condition, a constant pressure which equal to the at-rest earth pressure at the centre of tunnel face was applied to the tunnel face. Subsequently, pressure controlled boundary was adopted at the tunnel face to investigate the passive failure of tunnel face.

4. Failure mechanism

Fig. 5a shows the measured normalised displacement vectors on the vertical plane of symmetry at normalised tunnel face displacement, S_x/D of 0.8, for tunnel located at C/D ratio equals to 2.2. The corresponding normalised tunnel face pressure, $N_{\gamma m}$ is 91. The normalised tunnel face pressure following Leca and Dormieux (1990) is given by $N_{\gamma m} = \sigma_t/\gamma D$, where σ_t = tunnel face pressure and γ = effective unit weight of sand. The displacement vectors were obtained from the centrifuge tests using PIV analyses and normalised by tunnel face displacement. The displacement vectors illustrate that the soil in front of the tunnel face is displaced by the

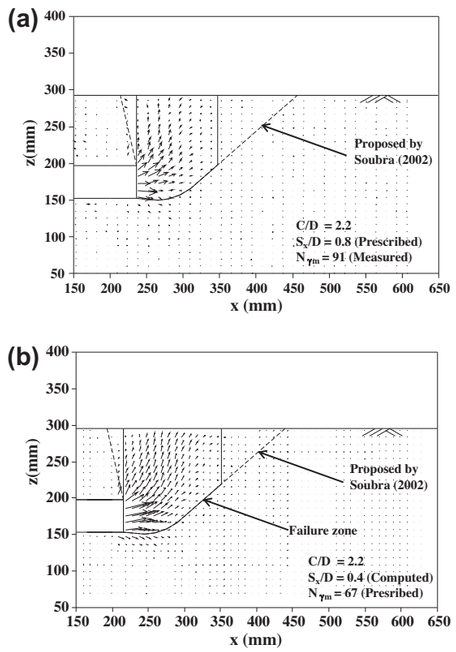

Fig. 5. Comparison of (a) measured and (b) computed normalised displacement vectors for tunnel located at C/D ratio equals to 2.2.

advancing tunnel face, while the soil further away from the tunnel face is forced upwards to the ground surface and hence the soil surface heaves. The observed failure mechanism is compared to a five-block failure mechanism (dashed lines in the figure) proposed by Soubra (2002) in obtaining upper bound solutions. The five-block failure mechanism is obtained by assuming the sand obeys normality where $\psi = \phi_{cs}$, which is rarely observed during drained failure of sand. The normality assumption may be one of the reasons that the five-block failure mechanism is wider than the observed failure mechanism. Previous studies (De Borst and Vermeer, 1984; Loukidis and Salgado, 2009; White et al., 2008) also revealed that a wider failure mechanism is obtained when the soil is more dilative. When the observed failure mechanism is idealised by solid lines, a funnel-type failure mechanism may be postulated.

Fig. 5b shows the computed normalised displacement vectors at S_x/D of 0.4 and $N_{\gamma m}$ of 67. The computed displacement vectors are obtained from numerical back-analysis and normalised by tunnel face displacement. The computed displacements vectors also show a funnel-type failure mechanism. The finite element results reveal that the soil elements in front of the tunnel face and those further away from the tunnel face at which soil is forced upwards to the ground surface. The elements reached failure are indicated by the failure zone illustrated in the figure.

Fig. 6a shows the measured normalised displacement vectors are localised around the tunnel face at S_x/D of 0.8 for tunnel located at C/D ratio equals to 4.3. The corresponding $N_{\gamma m}$ is 185. The soil in front of the tunnel face is displaced forwards, whereas the soil in regions located further away from the tunnel axis is forced outwards. Obviously, the observed failure mechanism illustrated by the displacement vectors is differed from a five-block failure mechanism (dashed lines in the figure) proposed by Soubra (2002).

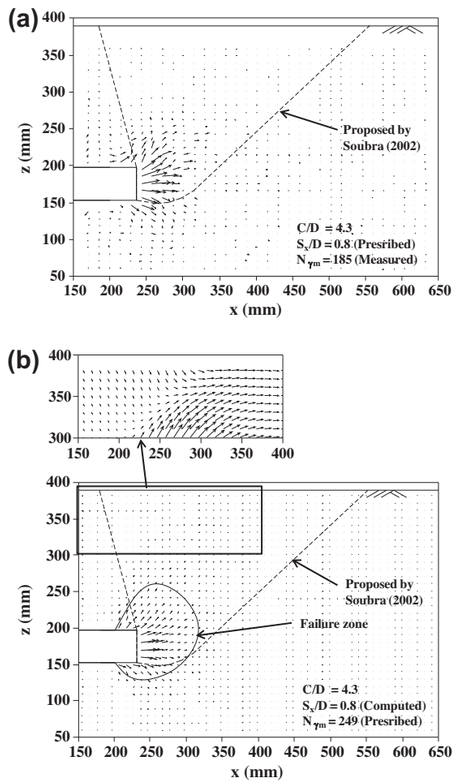

Fig. 6. Comparison of (a) measured and (b) computed normalised displacement vectors for tunnel located at C/D ratio equals to 4.3.

Fig. 6b shows the computed displacement vectors at S_x/D of 0.8 and $N_{\gamma m}$ of 249. The failure mechanism illustrated by the computed displacement vectors shows fairly close agreement with the localised failure mechanism. The finite element results reveal that the soil elements adjacent to the tunnel face reached failure. Computed failure zone is reasonably consistent with the observed displacement vectors shown in Fig. 6a. The displacement vectors at a region close to the ground surface are scaled up to 20 times for clarity. The displacement vectors illustrate surface settlements. The mobilised shear above the crown of tunnel face might drag the soil mass forwards and induce the surface settlements.

5. Passive failure pressure of tunnel face

Fig. 7 shows the variations of $N_{\gamma m}$ with S_x/D for tunnels located at C/D ratios equal to 2.2 and 4.3. For tunnels located at C/D ratio equals to 2.2, $N_{\gamma m}$ increases with S_x/D but at a reducing rate and approaches a steady state. The variation of $N_{\gamma m}$ with S_x/D for Test S2 is comparable to that obtained from Test S2R. Some of data was missing due to improper electrical gain was used in Test S2. It is observed that $N_{\gamma m}$ in Test S2 is larger than that in Test S2R. This may be reasonable as the $N_{\gamma m}$ obtained from external load cell in Test S2 was affected by the friction between tunnel face block and the lining, glass or sand. It is fortuitous that the computed pressure-displacement curve is in good agreement with the measured response. It should be noted that a displacement controlled

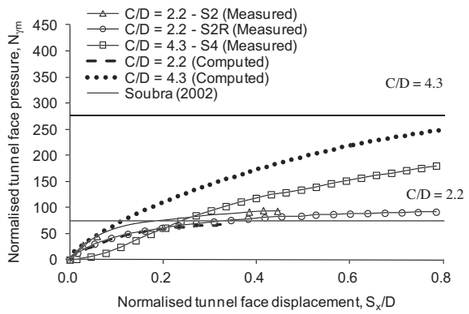

Fig. 7. Comparison of measured and computed variations of normalised tunnel face pressure with tunnel face displacement for tunnels located at C/D ratios equal to 2.2 and 4.3.

boundary was used in the centrifuge test while pressure controlled was adopted in the numerical simulation. Calculated passive failure pressure by using the upper bound solution, which were derived by Soubra (2002) are included for comparison. The calculated passive failure pressure is fairly consistent with the measured face pressure.

For tunnel located at C/D ratio equals to 4.3, the measured $N_{\gamma m}$ increases slowly when S_x/D is less than 0.1. Subsequently, $N_{\gamma m}$ increases rapidly but in a reducing rate. The computed $N_{\gamma m}$ increases in a reducing rate and a steady state value was not reached at S_x/D ratio equals to 0.8. The computed $N_{\gamma m}$ is larger than the measured one. This may be due to the presence of localised loose deposit in front of tunnel face created at 1g condition. The calculated passive failure face pressure is higher than the corresponding measured value by 50%. The discrepancy may be because the measured pressure did not reach the failure one as the pressure was still increasing. This might be also attributed to the large discrepancy between the localised failure mechanism and the five-block failure mechanism.

6. Surface displacement

It is well known that measured transverse surface settlements due to tunnelling may be represented by a Gaussian distribution as suggested by Peck (1969). The Gaussian distribution can be described by:

$$\Delta = \Delta_{\max} \exp(-s^2/2i^2) \tag{3}$$

where Δ is the transverse surface settlement; $\Delta_{\max}$ is the maximum transverse surface settlement on the tunnel centreline; s is the horizontal distance from the tunnel centreline; and i is the point of inflection of the settlement trough. The point of inflection is equal to Kz_o, whereas z_o is depth of tunnel. The relation was proposed by O'Reilly and New (1982) and validated using field data by (Lake et al., 1992; Mair and Taylor, 1997). Mair and Taylor (1997) found that the K values vary from 0.25 to 0.45 for sand and gravel. Instead of fitting settlement profiles, Gaussian distribution is attempted to fit measured heaves in this study.

Fig. 8a shows the measured normalised soil displacements, Δ/D at 0.6D below the ground surface on the vertical plane of symmetry for tunnels located at C/D ratios equal to 2.2 and 4.3. The soil displacements along the longitudinal direction were obtained from the PIV analyses. Gaussian distributions are obtained by setting K equal to 0.27 and the $\Delta_{\max}$ are deduced from the measured heaves. For tunnel located at C/D ratio equals to 2.2, heaves increase with S_x/D. This is consistent with the funnel-type failure mechanism, which extends to the ground surface. The measured heaves are

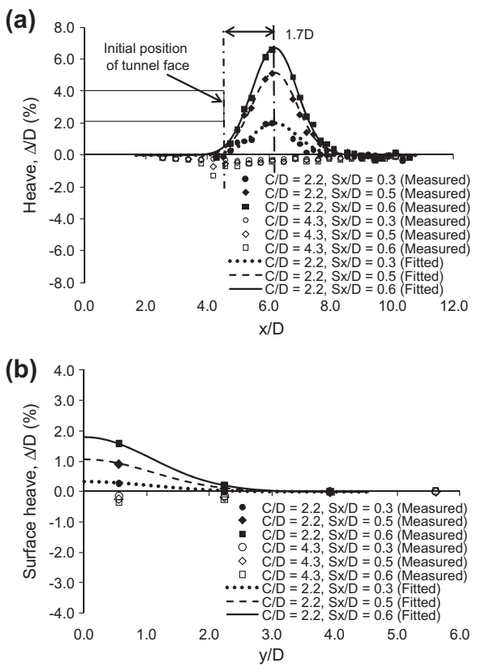

Fig. 8. Measured heaves at different tunnel face displacement for tunnels located at C/D ratios equal to 2.2 and 4.3: (a) longitudinal direction and (b) transverse direction.

well described by the Gaussian distributions. The extent of the heaves and location of the maximum heave remain around 4D and 1.7D respectively from the initial position of tunnel face for different S_x/D. For tunnel located at C/D ratio equals to 4.3, instead of heaves, settlements are induced as S_x/D is increased. This is consistent with the localised failure mechanism, which induces surface settlement as shown in Fig. 6b. The maximum settlement are located near to the initial position of tunnel face.

Fig. 8b illustrates the measured normalised transverse surface heaves induced by tunnel face displacements at a section located at 3.4D in front of the initial position of the tunnel face. The surface heaves were measured by using LVDTs. For tunnel located at C/D ratio equals to 2.2, heaves increase with S_x/D and the extent of heave remains at 3D from the longitudinal tunnel axis. Gaussian distributions are fitted to the transverse surface heaves. The fitted values of Gaussian distributions are obtained by using K equal to 0.4. The transverse surface heaves are well described by the Gaussian distributions. For tunnel located at C/D ratio equals to 4.3, settlements are induced and the extent of the settlements is around 3D from the tunnel axis.

7. Conclusions

The results of centrifuge model tests and finite element back-analyses investigating the passive failure of tunnel face in sand are reported. The soil failure mechanisms and passive failure pressures of tunnel face are described and discussed. In addition, the induced ground surface displacements due to the increase in tunnel face displacement are also reported.

For both centrifuge and numerical investigations, it is found that for tunnel located at C/D ratio equals to 2.2, the soil in front

of the tunnel face is displaced by the advancing tunnel face. The soil further away from the tunnel face is forced upwards to the ground surface and hence the soil surface heaves. A funnel-type failure mechanism is observed and the extent of the funnel-type failure mechanism is narrower than a five-block failure mechanism commonly assumed in the existing upper bound solution. However, the calculated passive failure pressure by the upper bound solution is fairly consistent with the measured face pressure. Besides, the computed pressure-displacement curve is in good agreement with the measured response. It is found that the extent of longitudinal surface heaves and the location of maximum heave remain around 4D and 1.7D respectively in front of the initial position of tunnel face at different S_x/D ratio. The extent of transverse surface heaves remains at 3D from longitudinal tunnel axis for different S_x/D ratio at a section, which is 3.4D in front of the initial position of tunnel face. Both observed longitudinal and transverse heaves are well described by Gaussian distributions.

For a tunnel located at C/D ratio equals to 4.3, the displacements of soil are confined around the vicinity of an advancing tunnel face and a localised failure mechanism associated with ground settlements is observed and computed. There is a large discrepancy between the localised failure mechanism and the five-block failure mechanism. The calculated failure face pressure is higher than the corresponding measured value by 50%. However, reasonable consistency can be found between measured and computed passive face pressures.

Acknowledgements

The authors would like to acknowledge the Research Grant 617608 from the Research Grants Council of HKSAR, the National Science Foundation of China for awarding the second author the Overseas and Hong Kong, Macau Young Scholars Collaborative Research Fund (No. 50629802) and financial support from the National Basic Research Program of China (Research Grant: 2007CB714001).

References

Anagnostou, G., KovÃ¡ri, K., 1994. The face stability of slurry-shield-driven tunnels. Tunnelling and Underground Space Technology incorporating Trenchless 9 (2), 165–174.

Anagnostou, G., KovÃ¡ri, K., 1996. Face stability conditions with earth-pressure-balanced shields. Tunnelling and Underground Space Technology 11 (2), 165–173.

Bezuijen, A., Brassinga, H.M., 2005. Blow-out pressures measured in a centrifuge model and in the field. Tunnelling: In: Bezuijen, A., Lottum, H.v. (Eds.), A Decade of Progress – GeoDelft 1995–2005. Taylor & Francis, London, pp. 143–148.

Brinkgreve, R.B.J., Broere, W., 2004. PLAXIS 3D Tunnel Version 2, PLAXIS bv, Netherlands.

Chambon, P., Corte, J.F., 1994. Shallow tunnels in cohesionless soil: stability of tunnel face. Journal of Geotechnical Engineering – ASCE 120 (7), 1148–1165.

De Borst, R., Vermeer, P.A., 1984. Possibilities and limitations of finite elements for limit analysis. Geotechnique 34 (2), 199–210.

Dias, D., Janin, J. P., Soubra, A. H., & Kastner, R., 2008. Three-dimensional face stability analysis of circular tunnels by numerical simulations. In: Proc., Geocongress 2008, ASCE, Geotechnical Special Publication vol. 179, pp. 886–893.

Lake, L.M., Rankin, W.J., Hawley, J., 1992. Prediction and Effects of Ground Movements Caused by Tunneling in Soft Ground Beneath Urban Areas. CIRIA Report 30, Construction Industry Research and Information Association, London.

Leca, E., Dormieux, L., 1990. Upper and lower bound solutions for the face stability of shallow circular tunnels in frictional material. Geotechnique 40 (4), 581–606.

Leca, E., Panet, M., 1988. Application du Calcul a la Rupture a la stabilitb du front de taille dun tunnel. Revue FranGaise de Giotechnique 43, 5–19.

Li, Y., Emeriault, F., Kastner, R., Zhang, Z.X., 2009. Stability analysis of large slurry shield-driven tunnel in soft clay. Tunnelling and Underground Space Technology 24 (4), 472–481.

Loukidis, D., Salgado, R., 2009. Bearing capacity of strip and circular footings in sand using finite elements. Computers and Geotechnics 36 (5), 871–879.

Maeda, K., Miura, K., 1999. Relative density dependency of mechanical properties of sands. Soils and Foundations 39 (1), 69–79.

Mair, R.J., Taylor, R.N., 1997. Bored tunnelling in the urban environment. In: Proc. 14th Int. Conf. Soil Mech. Found. Engng, vol. 4, pp. 2353–2385.

Mollon, G., Dias, D., Soubra, A.H., 2010. Face stability analysis of circular tunnels driven by a pressurized shield. Journal of Geotechnical and Geoenvironmental Engineering 136 (1), 215–229.

Ng, C.W.W., Van Laak, P., Tang, W.H., Li, X.S., Zhang, L.M., 2001. The Hong Kong geotechnical centrifuge. In: Proc. 3rd Int. Conf. Soft Soil Engineering, pp. 225–230.

Ng, C.W.W., Li, X.S., Van Laak, P.A., Hou, Y.J., 2004. Centrifuge modeling of loose fill embankment subjected to uni-axial and bi-axial earthquakes. Journal of Soil Dynamics and Earthquake Engineering 24 (4), 305–318.

O'Reilly, M.P., New, B.M., 1982. Settlements above tunnels in the United Kingdom – their magnitude and prediction. In: Tunnelling '82. Papers Presented at the 3rd International Symposium, pp. 173–181.

Peck, R.B., 1969. Deep excavations and tunneling in soft ground. In: Proceedings of the 7th International Conference on Soil Mechanics and Foundation Engineering, State of the Art, pp. 225–290.

Schanz, T., Vermeer, P.A., 1998. On the stiffness of sands. Pre-failure Deformation Behaviour of Geomaterials 383–387.

Schanz, T., Vermeer, P.A., Bonnier, P.G., 1999. The hardening soil model: formulation and verification. Beyond 2000 in computational geotechnics. In: Ten Years of PLAXIS International. Proceedings of the international symposium, Amsterdam, March 1999, pp. 281–296.

Soubra, A.H., 2002. Kinematical approach to the face stability analysis of shallow circular tunnels. Proceedings of the Eight International Symposium on Plasticity 443, 445.

Soubra, A.H., Dias, D., Emeriault, F., Kastner, R., 2008. Three-dimensional face stability analysis of circular tunnels by a kinematical approach. Geotechnical Special Publication 894, 901.

Verdugo, R., Ishihara, K., 1996. The steady state of sandy soils. Soils and Foundations 36 (2), 81–91.

White, D.J., Take, W.A., Bolton, M.D., 2003. Soil deformation measurement using particle image velocimetry (PIV) and photogrammetry. Geotechnique 53 (7), 619–631.

White, D.J., Cheuk, C.Y., Bolton, M.D., 2008. The uplift resistance of pipes and plate anchors buried in sand. Geotechnique 58 (10), 771–779.

本冊子由奧雅納工程顧問製作

中九龍幹線
Central Kowloon Route

路 政 署
Highways Department

ARUP Mott MacDonald
奧雅納-莫特麥克唐納顧問聯營公司
Arup-Mott MacDonald Joint Venture

Disclaimer : A person or an organization providing any comments and suggestions to the "Central Kowloon Route - Design and Construction" shall be deemed to have given consent to the Highways Department to partially or wholly publish the comments and suggestions (including the names of the individuals and organizations). If you do not agree to this arrangement, please state so when providing comments and views.